Aquifer recharge from intensively irrigated farmland. Several approaches

PhD Thesis

Department of Geotechnical Engineering and Geo-Sciences (ETCG)

Technical University of Catalonia, UPC

Joaquín Jiménez-Martínez

July 2010

Adviser: Dr. Lucila Candela Lledó

HYDROGEOLOGY GROUP
TECHNICAL UNIVERSITY OF CATALONIA

This thesis was funded by the CGL-2004-05963-C04-01 and CGL2007-66861-C04-03 research projects of the Ministry of Science and Innovation (Spain).

A mi familia, por ser como son,
por hacer lo que hacen.

“La fuerza no proviene de la capacidad física,
sino de la voluntad indomable”

Mahatma Gandhi

Agradecimientos

En primer lugar me gustaría agradecer a mi directora de tesis, Dr. Lucila Candela, la confianza depositada en mí para llevar a cabo la presente tesis. Sus consejos, con sus aciertos y con sus errores, algo común en todo proceso de investigación, han contribuido no solo a mi formación académica, sino también personal. Difícilmente podré agradecer su completa disposición.

También quiero agradecer especialmente a todos los coautores de los artículos de investigación que componen esta tesis su inestimable y estrecha colaboración: T. H. Skaggs (thanks Todd), M. Th. van Genuchten (thanks Rien), D. Hünkeler (danke Daniel), y J. Molinero (gracias Jorge). Una mención especial merece K. Tamoh (شكرا Karim), por los consejos, apoyo y dedicación en todo momento, especialmente cuando más lo necesitaba. Con todos he disfrutado y aprendido enormemente de las intensas discusiones científicas que se han generado.

Quisiera expresar mi agradecimiento a las instituciones y miembros de las mismas que han colaborado en esta investigación. Estas son U.S. Salinity Lab. ARS-USDA (thanks P. Taber), Université de Neuchâtel-Centre d'Hydrogéologie, IGME-Delegación Murcia (gracias R. Aragón y J. L. García-Aróstegui), Institut de Ciènces de la Terra Jaume Almera-CSIC (gracias I. Queralt), Universidad Politécnica de Cartagena (gracias G. García y F. Solano), Centro de Edafología y Bilogía Aplicada del Segura-CSIC.

A J. Carrera, F. J. Elorza y A. Alcolea por sus numerosos y acertados consejos. A E. Custodio y R. Aravena porque aunque los trabajos desarrollados bajo su supervisión no forman parte de esta tesis, han contribuido notablemente a mi formación.

A mis compañeros (profesores, estudiantes e investigadores asociados) del Grupo de Hidrología Subterránea y del Dpto. Ingeniería del Terreno de la Universitat Politècnica de Catalunya, por su apoyo. Gracias Francy, María, Meritxell, Pablo, Edu, Tanguy, Diogo, Victor, Benoit… A mis compañeros con los que he compartido, además de tutora, muy buenos momentos, Virginia, Wolf, Kelly, Carmen y Luis Fernando. Pero sobre todo voy a agradecer a Gloria, compañera de despacho, su paciencia por aguantar los momentos no tan buenos. También a los compañeros de la Facultad de Geología de la Universidad de Granada, Antonio Pedrera, Carlos Duque y Francisco Navarro, por haberme apoyado desde el minuto cero. Y como no, a Samu, Chema, Bermúdez, Moya, Ana… Gracias a todos por vuestra amistad y generosidad.

A mi familia paterna y materna. A mis hermanas/os Almudena, Javi, Paloma y Sergio. Pero sobre todo, quisiera expresar mi profunda gratitud a mis padres, Antonio y Angelita, por la ilusión y apoyo que siempre me han brindado, y por haberme inculcado los valores importantes de esta vida, sobre todo en los momentos difíciles ("…aquí nadie se baja del tren…"). Gracias a todos por entender mis cada vez más frecuentes ausencias en nuestra bonita tierra, una pequeña villa del Campo de Cartagena, de nombre no menos apropiado, Pozo Estrecho.

Abstract

Intensive irrigated agriculture is usually developed in arid and semi-arid regions due to the favourable weather conditions, in spite of the scarcity of water resources (e.g. Mediterranean Basin, California). Surface water resources are generally reduced and highly unreliable in these zones, as a consequence, groundwater is the primary source of water. Therefore, accurate estimation of aquifer recharge under the above mentioned conditions appears to be essential for sustainable water resource management and assessing aquifer vulnerability to contaminants.

In the past decades a large body of literature has focused on the assessment of the natural recharge and parameters of control (including climate, vegetation, soils, and topography). On the contrary, only few papers focused on aquifer recharge from intensively irrigated farmland. Although findings have improved the understanding of recharge phenomena, they still fail to characterize many features of aquifer recharge from the mentioned land use. In this context, the aims of this thesis are: (i) to improve the understanding of aquifer recharge from intensively irrigated farmland, and (ii) to provide new tools for its characterization. Also, this thesis provides a framework that can be easily used by practitioners to infer quantitative information.

Field tests, including different crop types (vegetables and fruit trees) and agricultural management (water requirements, crop rotation, drip irrigation, plastic cover), were carried out in the Campo de Cartagena area of southeast Spain, a semi-arid region where intensive irrigated agriculture is prevalent. The development of methodologies, with field observations in both saturated and unsaturated media, along with the application of numerical modelling were used to understand the processes governing the recharge from irrigated farmland. The developed approaches can be summarized as follows:

A field experiment with annual row crops (rotation lettuce and melon) and drip irrigation was carried out. Soil moisture dynamics through the root zone and below were simulated from unsaturated flow approach. Soil moisture and pressure head data at different depths were recorded along six hundred days for model calibration and prediction.

A tracer test (tritium) in the field was performed along four hundred thirty days. The test was carried out in an experimental plot with drip irrigation and annual row crops (rotation lettuce and melon). The tracer transport in soil was simulated considering a multiphase approach. Tracer concentration profiles, from a limited and sparse number of destructive samples, were used to calibrate and validate the modelling approach.

A long-term field experiment (based on nine hydrologic years) for different crop types, annual row crops (lettuce and melon), perennial vegetables (artichoke) and fruit trees (citrus), was performed. The recharge produced from each crop type was estimated from a water balance approach, including soil, vadose zone and aquifer. Water table fluctuations, recorded along the mentioned period, were used for model calibration and predictions. This long-term approach permits to evaluate recharge estimates reliability of the two previous methodologies (short-term) for the type of crop overlapped (annual row crops).

For the three approaches, ground cover and root depth are assumed as upper boundary conditions. Evapotranspiration is allocated to evaporation and transpiration as a function of leaf-area-index and is limited by soil moisture content; transpiration is distributed through the soil profile as a function of soil moisture and root depth.

Similar recharge values have been obtained from the three techniques, although the unsaturated flow approach slightly overestimates values. *Actual* evapotranspiration was always lower than *potential* evapotranspiration, because soil moisture was insufficient to sustain the potential uptake, despite high irrigation frequency. Although the agricultural practices from farmers are sound, high irrigation efficiency, high recharge values are achieved. Rainfall is unevenly distributed into a few intensive events, likewise very common in semi-arid regions, and it meaningfully contributes to deep percolation, due to consistently high soil water content and the potentially preferential flow contribution.

Resumen

La agricultura intensiva es habitualmente llevada a cabo en regiones áridas y semi-áridas debido a las favorables condiciones meteorológicas, a pesar de la escasez de recursos hídricos (Cuenca Mediterránea, California). En estas zonas los recursos hídricos superficiales son generalmente escasos, por lo que las aguas subterráneas se convierten en la principal fuente de agua. Por ello, una estimación precisa de la recarga, bajo las condiciones anteriormente mencionadas, resulta esencial para la gestión sostenible de los escasos recursos hídricos, así como para evaluar la vulnerabilidad de los acuíferos a la contaminación por agroquímicos.

En las últimas décadas la literatura se ha centrado en la estimación de la recarga natural y los parámetros que la controlan, incluyendo clima, vegetación, suelo, y topografía. Por el contrario, pocos son los trabajos centrados en la recarga de acuíferos a partir de zonas cultivadas intensamente regadas. Aunque estos han mejorado la compresión sobre el proceso de recarga, todavía resultan incompletos a la hora de estimarla a partir del mencionado uso de suelo. En este contexto, los objetivos de esta tesis son: (i) mejorar la compresión de la recarga a partir de zonas intensamente regadas, y (ii) proporcionar nuevas herramientas para su caracterización. Algunas de las metodologías proporcionadas pueden ser fácilmente reproducidas por profesionales para inferir información cuantitativa.

Ensayos en campo, incluyendo diferentes tipos de cultivo (hortícolas y árboles frutales) y prácticas agrícolas (necesidades hídricas, rotación de cultivos, riego por goteo, cubierta de plástico), son llevados a cabo en al área del Campo de Cartagena, sureste de España, una región semi-árida donde la agricultura intensiva es el principal uso de suelo. El desarrollo de metodologías con observaciones en el medio saturado y no saturado, junto con la modelación

numérica, fueron usados para mejorar la compresión de los procesos que controlan la recarga a partir de zonas intensamente regadas. Las aproximaciones desarrolladas pueden ser resumidas como sigue:

Se ha llevado a cabo un ensayo de campo a lo largo de seiscientos días bajo cultivos hortícolas anuales (rotación de lechuga y melón) y riego por goteo. La distribución del contenido de agua en la zona de raíces y bajo esta fue simulada considerando un modelo de flujo no saturado. El contenido de agua y la succión fueron medidos a diferentes profundidades y empleados para la calibración y validación del modelo.

En segundo lugar, se ha realizado un ensayo de trazador (tritio) en campo en una parcela experimental con riego por goteo y cultivos hortícolas anuales (rotación de lechuga y melón) durante cuatrocientos treinta días. El movimiento de trazador a lo largo del perfil de suelo fue simulado considerando transporte multifásico. Los perfiles de concentración de trazador, a partir de un espaciado y limitado número de muestras destructivas, fueron usados para calibrar y validar el modelo.

Por último, se ha llevado a cabo un experimento de larga duración (nueve años hidrológicos) para diferentes tipos de cultivo: cultivos hortícolas anuales (lechuga y melón), cultivos hortícolas perennes (alcachofa) y árboles frutales (cítricos). La recarga producida por cada tipo de cultivo fue estimada a partir del balance de agua en suelo, zona no saturada y acuífero. Las fluctuaciones del nivel freático registradas a lo largo del mencionado periodo fueron usadas para calibrar y validar el modelo. Esta experiencia permitió evaluar la fiabilidad de las estimaciones de recarga a partir de las otras dos metodologías previas (a corto plazo) para el tipo de cultivo coincidente (cultivos hortícolas anuales).

Para las tres aproximaciones, el cubrimiento de suelo por las plantas y el crecimiento de raíces han sido incluidos en la condición de contorno superior. La evapotranspiración se ha dividido en evaporación y transpiración como una función del índice de área de hoja, y es limitada por el contenido de agua en el suelo. La transpiración a su vez ha sido distribuida a través del perfil de suelo como una función del contenido de agua y profundidad de raíces.

Valores similares de recarga han sido obtenidos a partir de las tres técnicas, aunque el modelo de flujo no saturado la sobreestima ligeramente. La evapotranspiración real fue siempre

más baja que la potencial, ya que el contenido de agua en suelo fue insuficiente para mantener la extracción de agua por parte de las raíces, a pesar de la alta frecuencia de riego. Aunque las prácticas agrícolas por parte de los agricultores son las correctas, con una alta eficiencia de riego, se obtuvieron altos valores de recarga. La lluvia es distribuida de manera irregular en unos pocos eventos intensivos, algo por otro lado muy común en regiones semi-áridas, lo que contribuye de manera significativa a la percolación profunda, debido al constante alto contenido de humedad en el suelo y a la contribución potencial del flujo preferencial.

Table of Contents

List of Figures

List of Tables

Chapter 1

Introduction

Groundwater is estimated to make up at least 50% of potable water, 40 % of industrial water, and 20% of irrigation water in the world (*Foster and Chilton*, 2003). Arid and semi-arid regions are expanding and represent 30% of the global terrestrial surface area (*Dregne*, 1991), in these regions surface water resources are generally scarce and highly unreliable with the result that groundwater is the primary source of water. Increasing demands on limited water supplies result in a critical status of groundwater natural recharge (groundwater storage from naturally-occurring surface water supplies such as precipitation and stream flows). Estimating aquifer recharge is very important for determining water resource availability and assessing aquifer vulnerability to pollutants (*Scanlon et al.*, 2002).

Natural recharge is a critical component of the water cycle for water resources and transport of contaminants assessment to the aquifer. Estimation can be difficult, particularly in arid and semi-arid regions where water tables are typically deep and recharge is predominately focused recharge, which emanates from topological depressions such as streams and lakes. Although diffuse recharge refers to areally distributed recharge, it is believed to play a diminishing role with aridity. *Kearns and Hendrickx* (1998) point out that small diffuse recharge rates over large areas yield significant volumetric contribution to groundwater. The recharge rate is limited by the availability of water at the land surface, which is controlled by temporal and spatial climatic

factors such as precipitation and evapotranspiration (*Scanlon et al.*, 2002). In some basins recharge estimation is additionally complicated by irrigation, which may simultaneously remove water from focused recharge sources while creating new sources of diffuse recharge derived from precipitation or irrigation. In irrigated regions under arid or semi-arid conditions, accurate knowledge of recharge, evaporation, and transpiration is especially important for the sustainable management of scarce water resources (e.g. *Garatuza-Payan et al.*, 1998).

Accurate recharge estimation is not as easy task since there are many interrelated processes and factors included in the atmosphere (rainfall amount, evaporation rate), plant (root depth, transpiration rate, interception), soil and vadose zone (infiltration capacity), and aquifer (water table position). Several methods have been used to estimate natural groundwater recharge with varying degrees of success. A detailed review of the methods is beyond the scope of this chapter and the reader is referred to the existing published works (*Simmers*, 1988; *Sharma*, 1989; *Lerner et al.*, 1990; *de Vries and Simmers*, 2002; *Scanlon et al.*, 2002, can be cited among the review works). The current applied methods can be loosely grouped into three categories depending on whether the focus of the method is surface water, the vadose zone, or the saturated zone. In all of them, physical (e.g. seepage meters, lysimeters, water table fluctuation method) and tracer techniques (e.g. heat, environmental tracers) are common, as well as are numerical modelling approaches. The best choice for a particular situation depends upon the spatial and temporal scales being considered and the intended application of the recharge estimate (*Scanlon et al.*, 2002).

Regional recharge estimation for water resources evaluation has relied mostly on groundwater-based approaches, integrating over large spatial scales and generally cannot be used to estimate local variability in recharge. Areas dedicate to agriculture present a high spatial and temporal variability due to type of tillage (*Ndiaye et al*, 1997), growth stages, rotation, water requirements and irrigation methods for the different crops. A critical element of water balance and modelling approaches for recharge estimation in arid and semi-arid regions is to determine *actual* evapotranspiration rates (ET_a), which can be below *potential* rates (ET_p) for long periods of time (*Droogers*, 2000; *Haque*, 2003; *Lascano et al.*, 2007), even in irrigated systems.

Various review works focusing primarily on arid and semi-arid regions recharge have been conducted in the past (reviews include *Gee and Hillel*, 1988; *Allison et al.*, 1994; *Simmers*, 1997; *IAEA*, 2001; *Kinzelbach et al.*, 2002; *Scanlon and Cook*, 2002; *Hogan et al.*, 2004; *Scanlon*

et al., 2006). Obtained results for recharge estimates indicate that it is: higher in humid than in arid regions; the presence of vegetation markedly reduces it (*Gee et al.*, 1994); higher in areas of annual crops than in forested (*Prych*, 1998); greater in coarser than finer textured soil (*Cook and Kilty*, 1992).

The task of defining optimum methodologies to estimate recharge from cropland is still under development, although a number of papers have tried to quantify this water balance component, among them:

Ghulam and Bhutta (1996), estimated aquifer recharge for a region of Pakistan (Rechna Doab) under semi-arid climate (P = 355 mm). The main activity in this region is agriculture with a high variety of crops (cotton; rice; wheat; sugarcase; pulses; oil seed vegetables; orchards; fodder). The evapotranspiration was calculated according to *Doorenbos and Pruitt* (1977) and the modelling approach used was a cascade model, which establishes a water budget for surface, soil and aquifer. The final recharge ranged between 14–123 mm; with an average value 57 mm. No distinction between recharge from cropland and non-cultivated soils was unfortunately provided.

Dawes et al. (1997) evaluated the recharge in a cultivated area (wheat; canola; oats) of Australia along one and half year (for this period P = 1097 mm; ET = 974 mm), where the dominant soil type was structured clay loam and coarse sand. Soil moisture content at different depths was measured by means of time domain reflectrometry (TDR). To reproduce the soil moisture measurements a preliminar version of the well-know TOPOG code (*Dawes and Hatton*, 1993) was applied, based on Richards' equation to resolve the unsaturated water flow. The recharge obtained for the aforementioned period was 50 mm.

Zhang et al. (1999) developed the research in two cultivated sites located in Australia. Several crop and pasture rotation were considered involving fallow, field pea, mustard, wheat, oats, lucerne and medic pastures. The first site was located on a sandy clay soil, whereas the second one on a sandy loam soil, with a mean annual precipitation of 351 and 564 mm, respectively. Soil moisture content at different depths was measured by means of a neutron probe. The measurements were reproduced using a process-based model that simulates the dynamic interactions within the soil-vegetation-atmosphere system, which consists in sub-models to simulate the energy and water balance. The range of recharge obtained in each site was 4–13 mm and 7–26 mm, respectively.

Kendy et al. (2003) calculated recharge in an experimental site in North China Plain, where the mean annual precipitation is 366 mm. Crop rotation of wheat (winter) and maize (summer) on a loam soil was carried out. To measure soil water content at different depths neutron probe was used. Recharge was evaluated by a numerical model in which soil water flow was governed by a tipping-bucket-type mechanism and actual transpiration was computed based on the soil water status using a method introduced by *Campbell and Norman* (1998). For the range of water input (*P*+*I*) 435–816 mm, the obtained recharge range was 78–209 mm.

Brunner et al. (2004) estimated recharge by combining remotely sensed data with local values of recharge derived from the chloride method, which was used to calibrate the first method. The study was located in Botswana, specifically in the Chobe Region and Ngamiland (Kalahari Desert). The recharge ranges were -20–260 mm and -35–90 mm for each aforementioned region, respectively. Crop types, water crop requirements or irrigation methods were not specified due to the broad extension of this study. It interested to mention the presence of exfiltration phenomenon (negative values), observed in the Chad lake area (*Leblanc et al.*, 2003; 2007).

Wang et al. (2008) evaluated the impacts of different soil types (silty clay; silt; clay), land use, irrigation, and crop cultivation management on recharge. Average recharge rates were determined by tritium and bromide tracing for different sites in Hebei Plain (North China), where the mean annual precipitation is 528 mm. Average recharge rates and recharge coefficient were 0.00–1.05 mm d^{-1} (mean ± standard deviation 0.35±0.24 mm d^{-1}) and 0.0–42.5%, respectively. The results showed the following recharge rates: flood irrigation (0.42–0.58 mm d^{-1}); sprinkler irrigation (0.17–0.23 mm d^{-1}); no stalk mulch (0.56–0.80 mm d^{-1}); stalk mulch (0.44–0.60 mm d^{-1}); vegetables (0.70 mm d^{-1}); wheat-maize (0.38 mm d^{-1}); peanut (0.51 mm d^{-1}); peach (0.43 mm d^{-1}). Even, they provided a linear relationship $R = 0.21(P + I) - 47.75$. A comparison of near-ideal tritium tracer with the more common but less ideal bromide showed that bromide moved approximately 23% faster than tritiated water, maybe due to anion exclusion.

Compilation of recharge rates from studies in irrigated areas indicates that recharge rates increase as a function of precipitation plus irrigation (average 15%). Studies by *O'Connell et al.* (2003) indicate that long fallow periods potentially increase deep drainage by ≈2 mm yr^{-1} relative to fully cropped systems over a wide rainfall range (134–438 mm yr^{-1}). Similar studies have examined cropping intensification and crop rotations to reduce recharge (*Latta and O'Leary*, 2003;

Sadras and Roget, 2004). If irrigation water is derived from surface water sources or deep confined aquifers, increase in recharge can result in shallower water tables and water logging of soils (e.g. Rajasthan, India. *Ritzema et al.*, 2008). In groundwater-fed irrigation systems (shallow unconfined aquifer), increased pumping for irrigation greatly outweighs increased recharge rates, resulting in large groundwater level decline. Therefore, cultivation (irrigated and non-irrigated) has a large impact on groundwater recharge and water resources (*Scanlon et al.*, 2006).

On the other hand, with the increasing concern on Global Change forecasting of recharge predictions, generally relying on model simulations, appears to be a difficult task. Understanding the water cycle controls, such as climate, vegetation, and soils, is important in evaluating the potential impact of climate variability and land use/land cover change on the water cycle. These difficulties motivate the need for quantifying and minimizing uncertainty on recharge estimates (non-linear nature) and predictions, improved understanding of how recharge occurs in these sites today and how it could be affected in the future, which finally can facilitate groundwater resources management (*von Igel*, 2006; *Candela et al.*, 2009).

In summary this thesis aims at giving, maybe a small but indeed significant contribution, in one of the most difficult components of water cycle: aquifer recharge from irrigated farmland. A series of frameworks are developed starting from field observations in both saturated and unsaturated media. The development of methodologies and numerical model approaches are used to give insight into the processes governing the recharge from irrigated farmland.

1.1 Thesis outline

Approaches for recharge analysis were carried out in the Campo de Cartagena area, southeastern Spain, a semi-arid region where irrigated intensive agriculture is prevalent. This thesis consists of seven chapters after the introductory one. The chapters four, five and six are based on papers that have been already published or submitted to international journals.

Chapter 2 consists of a brief description of the main characteristics of the area where the different methodologies have been developed, including climate, land use and agricultural practices, as well as geology and hydrogeological framework.

In chapter 3, a common previous step for the next three chapters, characterization of the soil profile and the top of the vadose zone by means of laboratory tests, is presented. Methods used to determine physical, hydraulic, chemical and mineralogical properties along with the results obtained are shown.

In chapter 4 a field experiment carried out in a plot under drip irrigation and cultivated with annual row crops (rotation lettuce and melon) is described. Soil moisture dynamics through the root zone and below are simulated with the Richards' equation. Root water uptake and transpiration are calculated according to *Feddes et al.* (1978). Ground cover and root growth were considered also. Field data were collected, soil moisture and pressure head at different depths were in situ obtained and used to calibrate and validate the modelling approach.

Chapter 5 describes a new methodology for the interpretation of a field tracer test. This exercise was carried out under the above mentioned conditions for the first approach. The selected tracer was tritium (near-ideal) and transport in soil was simulated considering a multiphase approach, non-tritiated and tritiated water in liquid and gas phase, beyond transport of heat, ground cover, root growth and root water uptake. Tracer concentration profiles, from a limited and sparse number of measurements, were used to calibrate and validate the modelling approach.

Chapter 6 examine the recharge from three different groups of crops: annual row crops (lettuce and melon), perennial vegetables (artichoke) and fruit trees (citrus). Daily water balance in soil, vadose zone and aquifer was established. Water table fluctuations were used for model calibration and predictions. In this last technique, in contrast to the two previous techniques presented above, a long period of study was considered (1999-2008), which permitted to evaluate the recharge estimation reliability for the group crop overlapped (annual row crops).

References

Allison, G.B., Gee, G.W., Tyler, S.W., 1994. Vadose-zone techniques for estimating groundwater recharge in arid and semiarid regions. *Soil Sci. Soc. Am. J.* 58, 6-14.

Brunner, P., Bauer, P., Eugster, M., Kinzelbach, W., 2004. Using remote sensing to regionalize local precipitation recharge rates obtained from the Chloride Method. *J. Hydrol.* 294 (4), 241-250.

Campbell, G.S. and Norman, J.M., 1998. *An Introduction to Environmental Biophysics*. 2nd ed. Springer-Verlag, New York.

Candela, L., von Igel, W., Elorza, F.J., Aronica, G., 2009. Impact assessment of combined climate and management scenarios on groundwater resources and associated wetland (Majorca, Spain). *J. Hydrol.* 376, 510-527.

Cook, P.G. and Kilty, S., 1992. A helicopter-borne electromagnetic survey to delineate groundwater recharge rates. *Water Resour. Res.* 28, 2953-2961.

Dawes, W.R. and Hatton, T.J., 1993. *TOPOG_IRM. 1. Model description.* CSIRO Division of Water Resources, Technical Memorandum 93/5. Canberra, A.C.T.

Dawes, W.R., Zhang, L., Hatton, T.J., Reece, P.H., Beale, G., Packer, I., 1997. Evaluation of a distributed parameter ecohydrological model (TOPOG_IRM) on a small cropping rotation catchment. *J. Hydrol.* 191, 64-86.

de Vries, J.J. and Simmers, I., 2002. Groundwater recharge: an overview of processes and challenges. *Hydrogeol. J.*, 5-17.

Doorenbos, J. and Pruitt, W.O., 1977. *Crop water requirements*. Irrigation and Drainage. Paper No. 24 (rev.) FAO, Rome, Italy. 144 pp.

Dregne, HE., 1991. Global status of desertification. *Annals of Arid Zone* 30, 179-185.

Droogers, P., 2000. Estimating actual evapotranspiration using a detailed agro-hydrological model. *J. Hydrol.* 229, 50-58.

Feddes, R. A., Kowalik, P.J., Zaradny, H., 1978. *Simulation of Field Water Use and Crop Yield*. John Wiley and Sons, NY.

Foster, S.S.D. and Chilton, P.J., 2003. Groundwater: the processes and global significance of aquifer degradation. *Phil. Trans. R.. Soc. Lond. B*, 358, 1957-1972.

Garatuza-Payán, J., Shuttleworth, W.J., Encinas, D., McNeil, D.D., Stewart, J.B., DeBruin, H., Watts, C., 1998. Measurement and modelling evaporation for irrigated crops in Northwest Mexico. *Hydrol. Process.* 12, 1397-1418.

Gee, G.W. and Hillel, D., 1988. Groundwater recharge in arid regions: review and critique of estimation methods. *Hydrol. Process.* 2, 255-266.

Gee, G.W., Wierenga, P.J., Andraski, B.J., Young, M.H., Fayer, M.J., Rockhold, M.L., 1994. Variations in water balance and recharge potential at three western desert sites. *Soil Sci. Soc. Am. J.* 58, 63-71.

Ghulam, Z.H. and Bhutta, M.N., 1996. A water balance model to estimate groundwater recharge in Rechna Doab, Pakistan. *Irrig. Drain Syst.* 10, 297-317.

Haque, A., 2003. Estimating actual areal evapotranspiration from potential evapotranspiration using physical models based on complementary relationships and meteorological data. *Bull. Eng. Geol. Env.* 62, 57-63.

Hogan, J.F., Phillips, F.M., Scanlon, B.R., 2004. *Groundwater Recharge in a Desert Environment: The Southwestern United States: Water Science Applications Series*, Vol. 9. American Geophysical Union: Washington, DC; 294 pp.

IAEA. 2001. *Isotope Based Assessment of Groundwater Renewal in Water Scarce Regions*, IAEA TecDoc 1246. IAEA: Vienna; 273 pp.

Kearns, A.K. and Hendrickx, J.M.H., 1998. *Temporal variability of diffuse groundwater recharge in New Mexico.* Tech. Rep. No. 309, 43 pp., N.M. Water Resour. Res. Inst., Socorro.

Kendy, E., Gérard-Marchant, P., Walter, M.T., Zhang, Y., Liu, C., Steenhuis, T.S., 2003. A soil-water-balance approach to quantify groundwater recharge from irrigated cropland in the North China Plain. *Hydrol. Process.* 17, 2011-2031.

Kinzelbach, W., Aeschbach, W., Alberich, C., Goni, I.B., Beyerle, U., Brunner, P., Chiang, W-H, Rueedi, J., Zoellman, K., 2002. *A Survey of Methods for Groundwater Recharge in Arid and Semi-Arid Regions, Early Warning and Assessment Report Series, UNEP/DEWA/RS.02-2*. United Nations Environment Programme: Nairobi.

Lascano, R.J. and van Bavel, C.H.M., 2007. Explicit and recursive alculation of potencial and actual evapotranspiration. *Agron. J.* 99, 585-590.

Latta, J. and O'Leary, G.J., 2003. Long-term comparison of rotation and fallow tillage systems of wheat in Australia. *Field Crops Research* 83, 173-190.

Leblanc, M., Favreau, G., Tweed, S., Leduc, C., Razack, M., Mofor, L., 2007. Remote sensing for groundwater modelling in large semiarid areas: Lake Chad Basin, Africa. *Hydrogeol. J.* 15, 97-100.

Leblanc, M., Razack, M., Dagorne, D., Mofor, L., Jones, C., 2003. Application of Meteosat thermal data to map soil infiltrability in the central part of the Lake Chad basin, Africa., *Geophys. Res. Lett.* 30(19), 1998, doi:10.1029/2003GL018094.

Lerner, D.N., Issar, A.S., Simmers, I., 1990. *Groundwater recharge, a guide to understanding and estimating natural recharge.* International Association of Hydrogeologists, Kenilworth, Rep. 8, 345 pp.

Ndiaye, B., Molenat, J., Hallaire, V., Gascuel, C., Hamon, Y., 2007. Effects of agricultural practices on hydraulic properties and water movement in soils in Brittany (France). *Soil and Tillage Research* 93, 251-263.

O'Connell, M.G., O'Leary, G.J., Connor, D.J., 2003. Drainage and change in soil water storage below the root-zone under long fallow and continuous cropping sequences in the Victorian Mallee. *Hydrol. Process.* 54, 663-675.

Prych, E.A., 1998. *Using chloride and chlorine-36 as soil-water tracers to estimate deep percolation at selected locations on the U.S. Department of Energy Hanford Site*, Washington, U.S. Geol. Surv. Water Supply Pap., 2481, 67 pp.

Ritzema, H.P., Satyanarayana, T.V., Raman, S., Boonstra, J., 2008. Subsurface drainage to combat waterlogging and salinity in irrigated lands in India: Lessons learned in farmers' fields. *Agric. Water Manage.* 95(3), 179-189.

Sadras, V.O. and Roget, D.K. 2004. Production and environmental aspects of cropping intensification in a semiarid environment of southeastern Australia. *Agron. J.* 96, 236-246.

Scanlon, B.R. and Cook, P.G., 2002. Preface: Theme issue on groundwater recharge. *Hydrogeol. J.* 10, 3-4.

Scanlon, B.R., Healy, R.W., Cook, P.G., 2002. Choosing appropriate techniques for quantifying groundwater recharge. *Hydrogeol. J.* 10, 18-39.

Scanlon, B.R., Keese, K.E., flint, A.L., Flint, L.E., Gaye, C.B., Edmunds, W.M., Simmers, I., 2006. Global synthesis of groundwater recharge in semiarid and arid regions. *Hydrol. Proscess.* 20, 3335-3370.

Sharma, M.L., 1989. *Groundwater Recharge*. A.A. Balkema: Rotterdam, 323 pp.

Simmers, I., 1988. *Estimation of Natural Groundwater Recharge*. D. Reidel Publishing Co: Boston, MA, 510 pp.

von Igel, W., 2006. *Impactos del cambio climático y escenarios de gestión en la Unidad Hidrogeológica de Inca-Sa Pobla (Mallorca, España)*. M.Sc. Thesis, Universitat Politécnica de Catalunya, Barcelona, Spain, 126 pp.

Wang, B., Jin, M., Nimmo, J.R., Yang, L., Wang, W., 2008. Estimating groundwater recharge in Hebei Plain, China under varying land use practices using tritium and bromide tracers. *J. Hydrol.* 356, 209-222.

Zhang, L., Dawes, W.R., Hatton, T.J., Hume, I.H., O'Connell, M.G., Mitchell, D.C., Milthorp, P.L., Yee, M., 1999. Estimating episodic recharge under different crop/pasture rotations in the Mallee region. Part 2. Recharge control by agronomic practices. *Agric. Water Manage.* 42, 237-249.

Chapter 2

Study area

2.1 Geographical setting and climate

The Campo de Cartagena plain comprises an area of 1440 km^2 in the Region de Murcia, southeast of Spain. It is limited to the East by the Mediterranean Sea and Mar Menor (hypersaline coastal lagoon), and by small mountain ranges to the North, South and West, with elevations ranging between sea level and 1065 m.a.s.l. (Figure 2.1).

The region is characterised by a semi-arid Mediterranean climate, with a mean annual temperature of 18 ºC and an average annual rainfall of 300 mm, which is unevenly distributed into a few intense events highly variable in space and time. Rainfall is mainly produced during spring and autumn. Precipitation along the year only takes place during sixty raining days and half amount of the precipitation occurs in to five days, with values higher than 17 mm (Figure 2.2). Estimates of annual potential evapotranspiration (ET_P) range from 875 to 1169 mm yr^{-1}, calculated by Thornthwaite and Turc, respectively. Whereas the annual reference evapotranspiration (ET_0) values obtained by Blaney-Criddle, Hargraves and Priestley-Taylor are 1313, 1241 and 1274 mm yr^{-1}, respectively (*Sánchez et al.*, 1989). No permanent watercourse exists and the area is drained by several ephemeral streams (*ramblas*). Flash-floods are common hydrologic events during autumn.

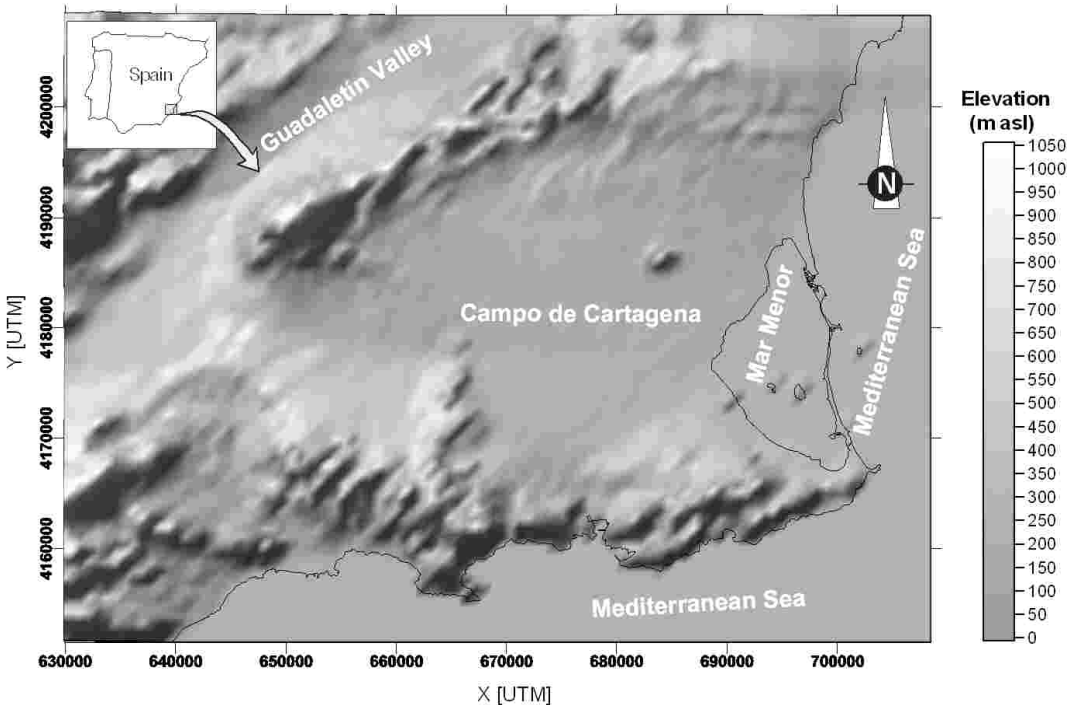

Figure 2.1: Campo de Cartagena plain and Mar Menor coastal lagoon, SE Spain.

2.2 Geology

A comprehensive geologic description of the Campo de Cartagena is beyond the scope of this chapter, having being studied by a great number of researchers (e.g. *IGME,* 2005; *Jiménez-Martínez et al.,* submitted). Only a brief summary of the geological framework is presented here.

The Campo de Cartagena constitutes a Neogene and Quaternary sedimentary basin located in the Eastern part of the Betic Cordillera. The detritic sedimentary rocks are unconformably laid over three metamorphic complexes those conform the Internal Zones of the cordillera. The metamorphic complexes are from bottom to top: (i) Nevado-Filábride, composed of marbles and mica-schists of Palaeozoic, Permian and Triassic age and outcrops in the mountain ranges to the South and West of the study area; (ii) Alpujárride, outcropping in the northern and southern mountain ranges; it is composed of schists, marbles, phyllites and quartzites of Permian

and Triassic age; (iii) Maláguide, formed by Permian and Triassic sandstones, quartzites, silts, conglomerates and limestones and outcrops in the northern part of the area (Figure 2.3a).

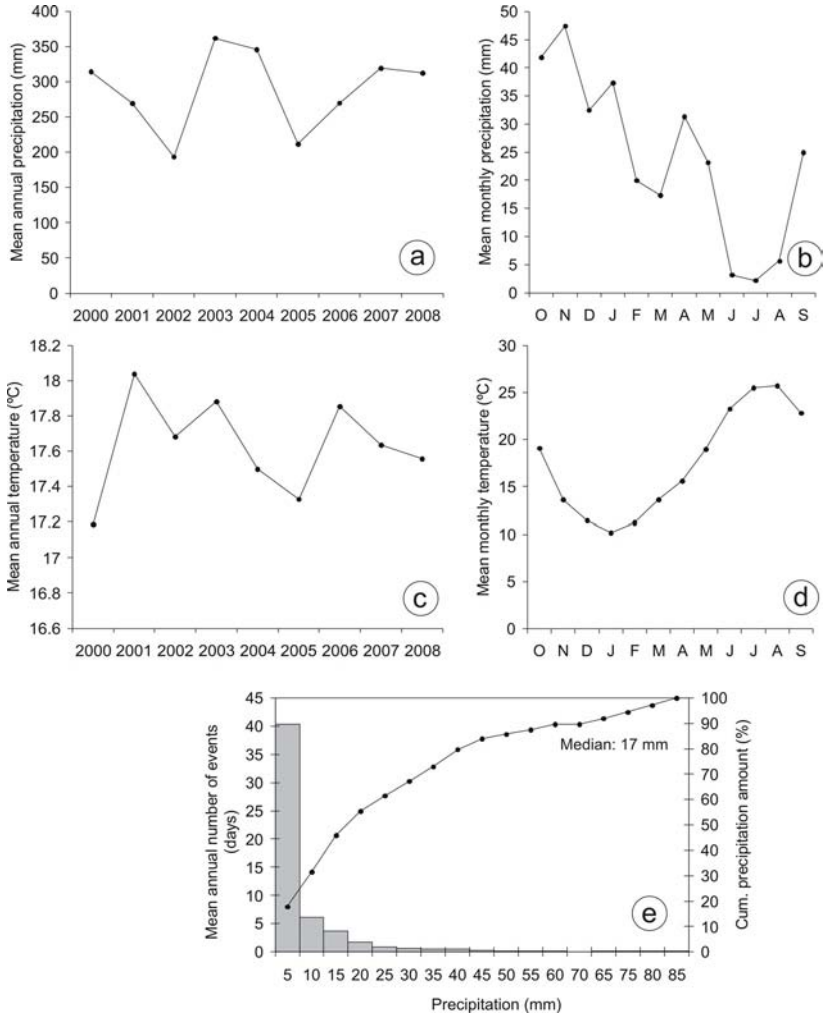

Figure 2.2: Precipitation and temperature in the Campo de Cartagena for the 2000-2008 period (eleven meteorological stations). a) mean annual precipitation. b) mean monthly precipitation. c) mean annual temperature. d) mean monthly temperature. e) mean annual number of rainfall events and cumulative precipitation.

The NE-SW to E-W normal faults break up the bedrock, developing several *horst* and *graben* structures. During the Tortonian, dacites and basalts flows result of the volcanic eruption favoured by fractures as a consequence of the tectonic activity, were deposited in the southern part of the basin. The sedimentary infill of the basin, with a maximum thickness of 2000 m, is mainly

composed by limestone, sand and conglomerate of Tortonian age, organic limestone of Messinian age and sandstone of Pliocene age, with interlayered marls and evaporites between them. Finally, overlying the Neogene sedimentary rocks, the Quaternary detritic sediments (conglomerates, sands and silts) (Figure 2.3b), covering a great part of the Campo de Cartagena (*IGME*, 1994). The observed stratigraphic variability and structural complexity of the area has important implications for the conceptual hydrogeological model establishment.

2.3 Hydrogeological framework

The multilayer hydrogeologic system is constituted by deep confined aquifers (Tortonian, Messinian and Pliocene age), which outcrops in the northern part of the study area, and a Quaternary unconfined shallow aquifer (*ITGE*, 1991; *Rodríguez Estrella*, 1995; *Jiménez-Martínez et al.*, submitted), which is objective of this thesis. The top unconfined aquifer extends over 1135 km^2 with an average thickness of 50 m (Figure 2.3b).

Whilst groundwater exploitation mainly relies on the deep confined aquifers, the shallow unconfined aquifer (Quaternary age) receives recharge from irrigation and precipitation, and is barely exploited due to its high pollution by agrochemicals. The regional groundwater flow direction in deep confined aquifers is from northwest to southeast, towards the coast, although local affections of the flow system occur due to the high density of pumping wells. With regard to the top unconfined aquifer (Quaternary), the regional groundwater flow direction is from northwest towards the coastal areas, also. The average depth of the water table is 15 m, and the hydraulic gradient of the aquifer ranges from 10^{-4} to 10^{-3} m m^{-1} (Figure 2.3a). The hydraulic conductivity ranges between 10^{-1} and 10^{1} m d^{-1}, whereas the transmissivity values vary from 10^{1} to 10^{2} m^2 d^{-1}, depending on the spatial location.

In this chapter, aquifer water balances are not provided. The last works carry out (*IGME*, 1994; *CHS*, 1997; *Albacete et al.*, 2001) do not correspond with the current situation. Moreover, several water balance components included in the mentioned works present a high uncertainty due to the employed methodology.

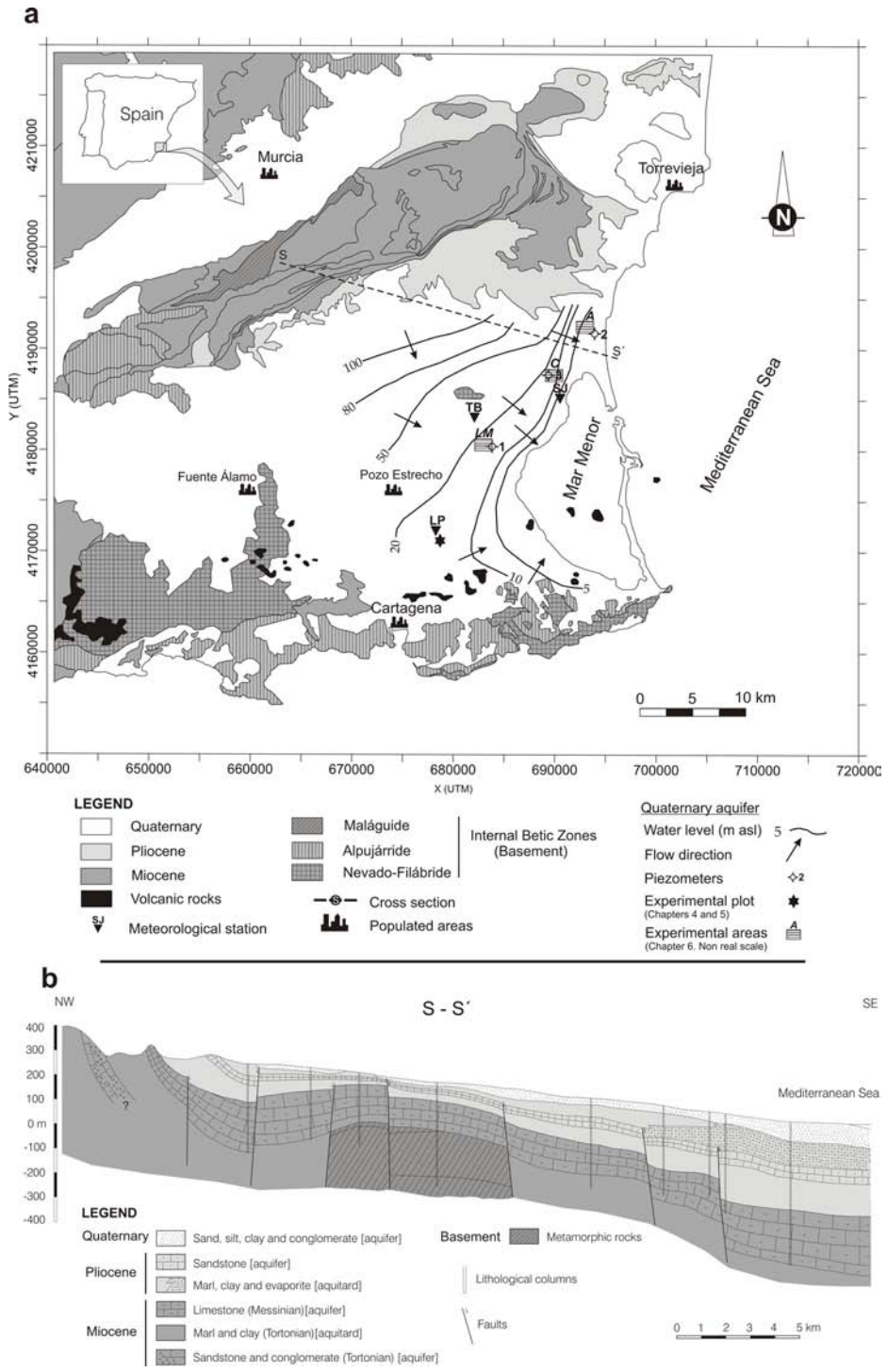

Figure 2.3: a) Location and geological sketch of the Campo de Cartagena area, Southeastern Spain. Experimental plot sites (Chapters 4, 5 and 6) are shown. b) Geological cross-section showing the aquifer system. Modified from *IGME* (1994).

A preliminary study by the Spanish Geological Survey (*IGME*, 1994) estimated that total recharge to the top unconfined aquifer, Quaternary age, was about 69 $hm^3 yr^{-1}$, distributed between 46 $hm^3 yr^{-1}$ due to natural recharge and 23 $hm^3 yr^{-1}$ due to irrigation return flow (where 1 $hm^3 = 10^6$ m^3). The *IGME* (1994) study to estimate natural recharge was based on the Thornthwaite method (*Thornthwaite*, 1948); to estimate irrigation return flows a combination of methods were applied according to existing data: (i) for areas where crop and irrigation data were available, irrigation return flows were calculated as the difference between the applied water and the potential crop water use; (ii) for other areas, where only irrigation data was available, irrigation efficiency coefficients for different irrigation methods (e.g. drip, furrow, flooding) were used to determine the fraction of water contributing to recharge. Thus return flow estimate was only based on irrigation water application and did not consider water input from precipitation. Instead, precipitation-based recharge from irrigated farmland was implicitly included in the estimate of natural recharge, which was a single value for the entire region.

2.4 Land and water uses. Agricultural practices

The dominant land use is agriculture, both irrigated and rainfed. Irrigated farmland comprises an area of approximately 299 km^2, with 128.1 km^2 of annual row crops (mainly lettuce and melon), 34.1 km^2 of perennial vegetables (mainly artichoke), and 136.8 km^2 of fruit trees (mainly citrus) (*CARM*, 2008) (Figure 2.4 and Table 2.1).

Drip irrigation (Table 2.1) is widely used in crop production due to the scarcity of water resources and the need for water conservation. An important aspect of the agricultural management in this region is the use of a plastic cover during summer crop (melon) to reduce the direct evaporation from soil surface.

Population water supply relies on surface water imported from *Canales del Taibilla*. Water for agricultural irrigation originates from deep confined aquifers, and surface *water transfer* system of the *Tajo-Segura Aqueduct* (*MIMAN*, 2000), a system which transfers water from the *Tajo basin* (central part of Spain) to the study region initiated in 1980. During the 1960's and the 1970's, the aquifers were intensively exploited. Since 1980, with the *water transfer*, the total irrigated area increased due to new available water resources. In response, an increase of induced

recharge by irrigation return flow to the top unconfined aquifer (Quaternary) was produced. As a result, two mechanisms have led to a water level rise in aquifers: irrigation return flow and decrease of pumping from wells. Since 2005 and due to the high water demand for irrigation, private desalination activities from brackish groundwater have been promoted by the farmer's community in order to increase available water resources.

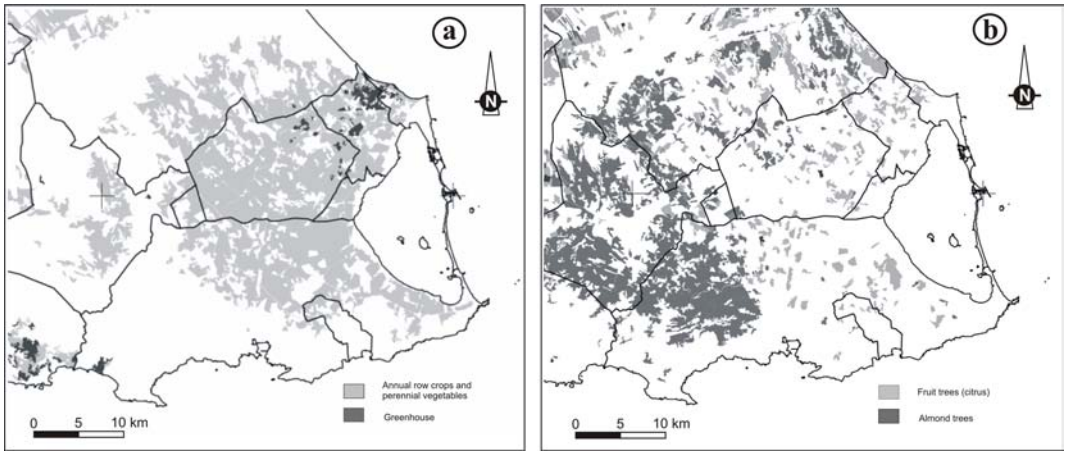

Figure 2.4: Land covered by the principal crops (*CARM*, 2008). a) vegetables and b) fruit trees.

Table 2.1: Main characteristics of the representative crops in Campo de Cartagena (source: *Allen et al.*, 1998; *CARM*, 2007; *CARM*, 2008)

Crop	Surface	Mean height crop	Maximum root depth	Furrow spacing	Drip irrigation			Crop water requirements
					Inside diameter tubing	Emitter spacing	Discharge	
	(km^2)	(cm)	(cm)	(m)	(mm)	(cm)	($l\ h^{-1}$)	($m^3\ ha^{-1}\ yr^{-1}$)
Annual row crops (principally lettuce and melon)	128.1	30 / 30	30-50 / 80-150	1	16	30	4	3287.8 / 6169.2
Perennial vegetables (artichoke)	34.1	70	60-90	1.7	16	40	4	6622.8
Fruit trees (citrus)	136.8	300	80-150	6	16	25-125	4	6407.1

Intensive agricultural practices involve, along with the irrigation return flow, the transport of mineral fertilizers, frequently exceeding crop needs (0.9-1.6 t $ha^{-1}\ yr^{-1}$), to the unconfined aquifer

(Quaternary). Discharge of this aquifer to the Mar Menor (a hypersaline coastal lagoon) is producing an important environmental impact (*Rodríguez Estrella*, 2000; *Garcia-Pintado et al.*, 2007). Elevated pumping rates in wells, pollution by agrochemicals, along with aquifers interconnection through abandoned and poorly constructed wells, enhanced by its high density (*Jiménez-Martínez et al.*, 2010), are the main impacts on the quality and quantity of groundwater resources in the region.

"The crops of Campo de Cartagena are an important source of fruits and vegetables for the European Union. Recently, however, drought conditions have worsened a deterioration that many attribute to climate change. The future of irrigated agriculture in Campo de Cartagena is in doubt; the United Nations Food and Agriculture Organization has identified current water shortage and desertification problems in southeast Spain as possibly being harbingers of what may become a global food crisis (New York Times, June 3, 2008)"

References

Albacete, M., Solís, L., Quintana, J.L., Gil, F., Gómez, A., Gómez, A., Sánchez, M., 2001. Bases para una gestión sostenible de las aguas subterráneas del Campo de Cartagena. In: VII Simposio de Hidrogeología-AEH. Murcia. Spain. Vol. XXIII, 13-24.

Allen, R.G., Pereira, L.S., Raes, D., Smith, M., 1998. *Crop evapotranspiration. Guidelines for computing crop water requirements.* Irrigation and Drainage. Paper No. 56, FAO, Rome, Italy.

CARM, 2007. *El Agua y la Agricultura en la Región de Murcia*. Un Modelo de Eficiencia. Consejería de Agricultura y Agua de la Región de Murcia. 111 pp.

CARM, 2008. Consejería de Agricultura y Agua de la Región de Murcia. Agrarian Statistics Data. Available from: <http://www.carm.es>.

CHS, 1997. Plan Hidrológico de la cuenca del Segura. Aprobado por RD 1664/1998, de 24 de julio (BOE de 11 de agosto de 1997).

García-Pintado, J., Martínez-Mena, M., Barberá, G.G., Albaladejo, J., Castillo, V., 2007. Anthropogenic nutrient sources and loads from a Mediterranean catchment into a coastal lagoon: Mar Menor, Spain. *Science of the Total Environment* 373, 220-239.

ITGE, 1991. *Estudio Hidrogeológico del Campo de Cartagena (2ª Fase)*. Volume 1/2 Memory. Volume 2/2 Annex 1, 2, 3 and 4. Tech. Rep. (unpublished).

IGME, 1994. *Las aguas subterráneas del Campo de Cartagena (Murcia)*. IGME, Madrid, Spain, 62 pp.

IGME, 2005. *Estudio de la información geológica y geofísica del subsuelo (sísmica de reflexión y sondeos) en el sector SE de la Provincia de Murcia.* Consejería de Industria y Medio Ambiente de la Región de Murcia. 37 pp. Annex 1-37. Tech. Rep. (unpublished).

Jiménez-Martínez, J., García-Aróstegui, J.L., Aragón, R., Candela, L. A quasi 3D geological model of the Campo de Cartagena, SE Spain: Hydrogeological implications (submitted to *GeologicaActa*)

Jiménez-Martínez, J., Aravena, R., Candela, L., 2010. The role of leaky boreholes on the contamination of a regional confined aquifer: A case study in the Campo de Cartagena region, Spain. *Water, Air & Soil Pollution*. doi: 10.1007/s11270-010-0480-3.

MIMAN, 2000. *Libro Blanco del Agua en España*. Spanish Ministry for the Environment.

Rodríguez Estrella, T., 1995. Funcionamiento hidrogeológico del Campo de Cartagena. *Hidrogeología* 11, 21-38.

Rodríguez Estrella, T., 2000. Physical, chemical and biological changes induced by waters from the Tage-Segura canal in the hydrogeological unit of the Campo de Carthagena and in Mar Menor laguna (Murcia Province, Spain). *Hydrogéologie* 3, 23-37.

Sánchez, M.I., López, F., Del Amor, F., Torrecillas, A., 1989. La evaporación y evapotranspiración en el Campo de Cartagena y Vega Media del Segura. Primeros resultados. *Anales de Edafología y Agrobiología*, 1239-1251.

Thornthwaite, C. W., 1948. An approach toward a rational classification of climate. *Geogr. Rev.* 38, 55-94.

Chapter 3

Soil characterization

The soil solid phase has a dominant influence on heat, water, and chemical transport and retention processes. Therefore, characterizing the physical and chemical properties of the soil solid phase is essential to understand these processes. Many processes in the soil are strongly influenced by the properties of the soil matrix, which is formed by soil particles and void spaces (*Jury and Horton*, 2004).

Soil characterization is a common previous step to estimate groundwater recharge for the three vadose zone techniques presented in this thesis. To initially characterize soil properties, disturbed and undisturbed soil samples were extracted up to a depth of 2 m before the experiments started. Disturbed samples were obtained using hand drilling, whereas for undisturbed samples (for soil matrix characterization) soil sample rings inserted by percussion were used. Subsequently, samples were immediately wrapped and transported in iceboxes to the laboratory. Obtained parameters and applied methodology are presented below.

3.1 Physical properties

Particle size distribution. Percentages of sand, silt and clay were determined according to *Gee and Or* (2002). To determine clay fraction, laser light scattering (diffraction) was used (Malvern Mastersizer E, range 0.5-600 μm)

Textural classification. The soil textural name based on the amount of sand, silt and clay was based on the USDA classification system.

Soil structure. Structural category is given from USDA Agricultural Information Bulletin 199.

Aggregate analysis. Dry-aggregate stability was characterized according to *Nimmo and Perkins* (2002), considering the fraction of soil weight that comprises stable aggregates for a defined size (A = >500 μm / <500 μm).

Particle density. Pycnometer method (constant volume container) is used for this purpose (*Flint and Flint*, 2002).

Bulk density. From the core method (undisturbed samples from rings) (*Grossman and Reinsch*, 2002).

Results of the above mentioned physical properties are shown in table 3.1.

Table 3.1: Summary table of soil physical properties (mean ± standard deviation).

Depth	Textural fractions (%)			Bulk density	Particle density	Aggregates	Textural name	Soil structure
(cm)	Sand	Silt	Clay	(g cm^{-3})	(g cm^{-3})	A		
0-30	18.7	76	3.5	1.45±0.10	2.64	0.59±0.23	silty loam	granular
30-60	13.8	80.2	6	1.52±0.11	2.65	1.05±0.23	silty loam	massive
60-90	19.5	77.2	3.3	1.58±0.05	2.67	0.59±0.40	silty loam	massive
90-150	10.8	82	6.6	1.70±0.08	2.67	0.89±0.28	silty loam	massive

3.2 Chemical and mineralogical properties

Chemical composition. Elements and oxidation states were obtained from X-Ray Fluorescence Spectrometry (XRFS) (*Jones*, 1991).

Table 3.2: Soil chemical properties (mean ± standard deviation).

	Depth (cm)			
	0-30	30-60	60-90	90-150
% by weight				
Na_2O	0.48	0.45	0.43	0.41
MgO	3.18	2.97	2.42	2.90
Al_2O_3	12.5	12.9	9.6	10.5
SiO_2	39.8	40.1	33.7	31.8
P_2O_5	0.230	0.150	0.090	0.084
SO_3	0.180	0.120	0.120	0.130
Cl	0.024	0.015	0.015	0.018
K_2O	2.39	2.40	1.64	1.90
CaO	15.36	15.85	23.99	26.68
TiO_2	0.58	0.55	0.45	0.50
MnO	0.071	0.072	0.036	0.047
Fe_2O_3	3.75	3.82	2.65	3.11
% by weight (10^{-4} ppm)				
P	0.0990	0.0660	0.0390	0.0370
S	0.0700	0.0470	0.0500	0.0510
Cr	0.0100	0.0086	0.0066	0.0065
Cu	0.0100	0.0094	0.0094	0.0090
Zn	0.0130	0.0066	0.0056	0.0055
Ga	0.0013	0.0014	0.0010	0.0008
Br	0.0010	0.0012	0.0011	0.0006
Rb	0.0064	0.0070	0.0043	0.0054
Sr	0.0371	0.0422	0.0561	0.0524
Y	0.0039	0.0037	0.0029	0.0033
Zr	0.0165	0.0150	0.0165	0.0139
Nb	0.0010	0.0010	0.0010	0.0008
Ba	0.0320	0.0390	0.0370	0.0310
Pb	0.0170	0.0034	0.0025	0.0022
Organic carbon (% by weight)	5.1±0.2	5.1±0.1	2.6±0.2	3.0±0.1
Inorganic carbon (% by weight)	29.2±0.4	30.5±0.8	40.2±1.4	46.0±0.4
Electrical conductivity, EC (μS cm^{-1})	761	949	644	655
pH	7.0±0.9	7.2±0.4	7.4±0.3	7.5±0.2

Organic Carbon. The soil organic matter content was obtained from Loss of weight On Ignition method (LOI) (*Storer*, 1984).

Inorganic Carbon. The content of inorganic carbon forms is derived from *Nelson and Sommers* (1996).

Electrical conductivity (EC) and pH. EC and pH measurements of the soil solution were carried out according to *Hanlon* (2009).

Mineralogy. X-Ray Diffraction (XRD) technique was applied to mineralogical study of clay fraction (*Brown and Brindley*, 1980). Clay minerals determined are Chlorite, Illite, Paragonite, Quartz, K-Feldspar, Plagioclase, Calcite and Dolomite.

Results of the above mentioned chemical and mineralogical properties are shown in table 3.2 and 3.3, respectively.

Table 3.3: Clay mineral identification.

Depth	Clay minerals (%)							
(cm)	Chlorite	Illite	Paragonite	Quartz	K-Feldspar	Plagioclase	Calcite	Dolomite
0-30	10	37	6	31	1	3	8	3
30-60	10	31	6	27	2	3	15	5
60-90	8	32	4	26	2	5	14	7
90-150	10	36	5	25	2	4	14	5

3.3 Hydraulic properties

Saturated hydraulic conductivity (K_s). Constant head soil core (tank) method described by *Reynolds and Elrik* (2002). Results are shown in table 3.4.

Water retention. Characteristic retention curves, pressure head (h) vs. soil water content (θ) at different depths (15, 45, 75 and 105 cm) were obtained using pressure plate extractor method (*Dane and Hopmans*, 2002). Pressure head is also commonly called matric potential. Results are shown in figure 3.1.

Table 3.4: Saturated hydraulic conductivity values.

Depth (cm)	K_s (cm d^{-1}) min / max
15	-
30	3.7 / 21.7
45	-
60	6.7 / 26.7
75	1.6 / 4.4
90	-
105	0.1 / 2.1

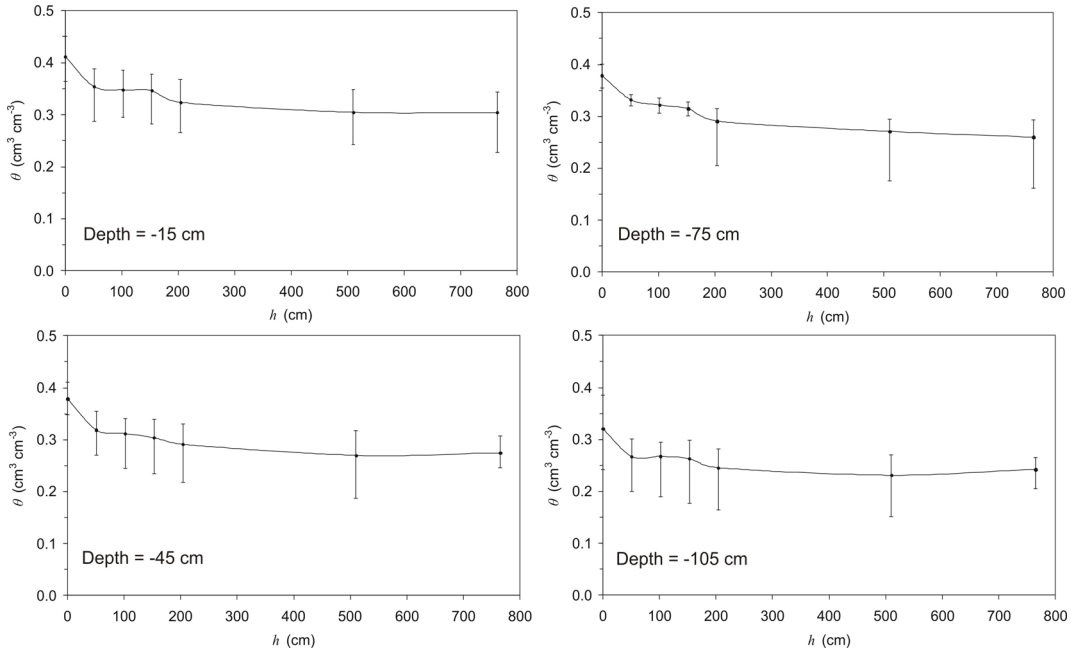

Figure 3.1: Pressure head (h)-soil water content (θ) function at different depths (15, 45, 75 and 105 cm). Vertical bars represent maximum and minimum measured water content.

References

Brown, G. and Brindley, G.W., 1980. X-ray diffraction procedures for clay mineral identification. In: G.W. Brindley and G. Brown (Eds.), Crystal Structure of Clay Minerals and their X-ray Identification. *Mineral. Soc. Monog.* 5, 305-360.

Dane, J.H. and Hopmans, J.W., 2002. Pressure Plate Extractor. In: Dane, J., Topp, C. (Eds.), Methods of soil analysis, Part 4, SSSA Book Series: 5, Am. Soc. Agron., Madison, WI. pp. 688-690.

Flint, A.L. and Flint, L.E., 2002. Particle Density. In: Dane, J., Topp, C. (Eds.), Methods of soil analysis, Part 4, SSSA Book Series: 5, Am. Soc. Agron., Madison, WI. pp. 229-240.

Gee, G.W. and Or, D., 2002. Particle Size Analysis. In: Dane, J., Topp, C. (Eds.), Methods of soil analysis, Part 4, SSSA Book Series: 5, Am. Soc. Agron., Madison, WI. pp. 255-294.

Grossman, R.B. and Reinsch, T.G., 2002. Bulk Density and Linear Extensibility. In: Dane, J., Topp, C. (Eds.), Methods of soil analysis, Part 4, SSSA Book Series: 5, Am. Soc. Agron., Madison, WI. pp. 201-228.

Hanlon, E.A., 2009. *Soil pH and Electrical Conductivity: A County Extension Soil Laboratory Manual*. Soil and Water Science Department, Florida Cooperative Extension Service, IFAS, University of Florida. CIR1081, 11 pp.

Jury, W.A. and Horton, R., 2004. *Soil physics*. 6th ed. John Wiley and Sons, Hoboken, NJ. 370 pp.

Jones, A., 1991. X-Ray Fluorescence Analysis. In: Smith, K.A. (Ed.), Soil Analysis. Modern Instrumental Techniques. 2nd ed., Marcel Dekker, New York, NY. pp. 287-324.

Nelson, D.W. and Sommers, L.E., 1996. Total carbon, organic carbon, and organic matter. In: Page, A.L. et al., (Eds.), Methods of Soil Analysis, Part 2, 2nd. ed., SSSA Book Series: 9, Am. Soc. Agron., Madison, WI. pp. 961-1010.

Nimmo, J.R. and Perkins, K.S., 2002. Aggregate Stability and Size Distribution. In: Dane, J., Topp, C. (Eds.), Methods of soil analysis, Part 4, SSSA Book Series: 5, Am. Soc. Agron., Madison, WI. pp. 317-328.

Reynolds, W.D. and Elrick, D.E., 2002. Constant Head Soil Core (Tank) Method. In: Dane, J., Topp, C. (Eds.), Methods of soil analysis, Part 4, SSSA Book Series: 5, Am. Soc. Agron., Madison, WI. pp. 804-808.

Storer, D. A., 1984. A simple high sample volume ashing procedure for determining soil organic matter. *Commun. Soil Sci. Plant Anal.* 15, 759-772.

Chapter 4

Unsaturated water flow approach*

4.1 Introduction

Groundwater recharge is water that enters into the phreatic zone. One of several ways water can enter to the aquifers is by migration (percolation) through the root zone and vadose zone. In the following chapter, a method to calculate aquifer recharge from a numerical approach, based on root and vadose zone unsaturated water flow, is presented.

To account for infiltration and evapotranspiration in many procedures, in lieu of detailed meteorological information for the upper boundary and root zone, models usually specify either a constant or time-varying flux or pressure head. It is also known that the mechanisms governing transient unsaturated flow are more complex. During drainage and water redistribution, flow mechanisms may be induced within the root zone by vegetation. Root distribution is non-uniform; roots move in the soil as the plant grows (*Brown and Scott*, 1984), so changes of water content distribution in the soil along time and space are expected. It is clear that vegetation uptake can play a dominating role in the infiltration and redistributed water that otherwise would become recharge.

* This chapter is based on the article: Jiménez-Martínez, J., Skaggs, T.H., van Genuchten, M. Th., Candela, L., 2009. A root zone modeling approach to estimating groundwater recharge from irrigated areas. *Journal of Hydrology* 367, 138-149.

Among general recharge modelling efforts, it is worth citing the works of *Kendy et al.* (2003) and *Keese et al.*, (2005). *Kendy et al.* (2003) evaluated recharge specifically for irrigated cropland using a model where soil water flow was governed by a tipping-bucket-type mechanism. They assume that gravity forces dominate over matric forces, and therefore a unit gradient exists throughout the soil profile. Thus, the modelled flux is always downward. *Steenhuis et al.* (1985) showed that these assumptions are reasonable, especially deep in the profile, where upward flux is insignificant. They consider that recharge is more dependent on evapotranspiration rates than on soil water distribution, and that errors introduced by these assumptions do not strongly influence recharge calculations. While *Keese et al.*, (2005) assessed controls on diffuse recharge (include climate, vegetation, soils, and topography) using unsaturated flow modelling based on Richards' equation. Soil hydraulic properties were estimated from soil data by means of pedotransfer functions; vegetation parameters were obtained from literature. Long-term simulations were conducted from arid to humid climates and different vegetation and soil types with successful results.

In this chapter, irrigation return flow from farmland and aquifer recharge, with non-existent hypodermic flow, is estimated using a root zone modelling approach in which irrigation, evapotranspiration, and soil moisture dynamics for specific crops and irrigation regimes were simulated with HYDRUS-1D software package (*Šimůnek et al.*, 2005). The code is a well-known computer model that simulates water, heat, and solute movement in variably saturated porous media. The model was calibrated and validated using field data collected in the experimental plot presented in section 4.2. Root zone moisture dynamics are simulated with the Richards' equation, including a sink term to account for water uptake by plants roots. Root water uptake and transpiration are calculated according to *Feddes et al.* (1978). Root growth and ground cover are also considered. To evaluate the importance of parameter uncertainty on the estimated recharge values, a sensitivity analysis is performed.

4.2 Field experiment

The study of root zone soil moisture was conducted on the experimental plot located at the Tomas Ferro Agricultural Science Center, a research facility operated by the Technical University of Cartagena. Location of the experimental plot in the study area is shown in Figure 2.3. The plot was

managed according to agricultural practices that are common in the Campo de Cartagena region, including crop rotation (melon and lettuce), drip irrigation and plastic cover for summer crops. To avoid boundary effects, the plot sides were also cultivated with the same crops and agricultural management conditions. The experiment was performed between 7 February 2007 and 21 August 2008.

An experimental plot measuring 7×2 m was established on a *silty loam* soil (USDA classification system). The groundwater level was located at a depth of 14 m below the surface. A drip irrigation system, similar to that used in Campo de Cartagena agriculture, was installed on the plot (Figure 4.1). The system featured 16 mm inside diameter tubing, 4 L h^{-1} emitters, and an emitter spacing of 30 cm. In total, 36 emitters were installed.

The plot was instrumented to monitor soil water dynamics in the root zone and below (Figure 4.1). Instrumentation consisted of two tensiometers (Soilmoisture Equipment Corp, Goleta, CA, USA), for soil water pressure head measurements, vertically installed at the 30, 45, 60, 90 and 120 cm depth (10 tensiometers total) (*Young and Sisson*, 2002). Two 44 mm diameter, 2 m deep access tubes (fibre glass) for soil moisture measurements with a TRIME-FM TDR probe (Imko GmbH, Ettlingen, Germany), which was specifically calibrated (linearly) for the mentioned soil (*Laurent et al.*, 2001; 2005). Meteorological data for the site were available from a Servicio de Información Agraria de Murcia (*SIAM*, 2008); the weather station was located 235 m from the experimental plot. The frequency of measure employed for pressure head and water content was every two days and weekly, respectively.

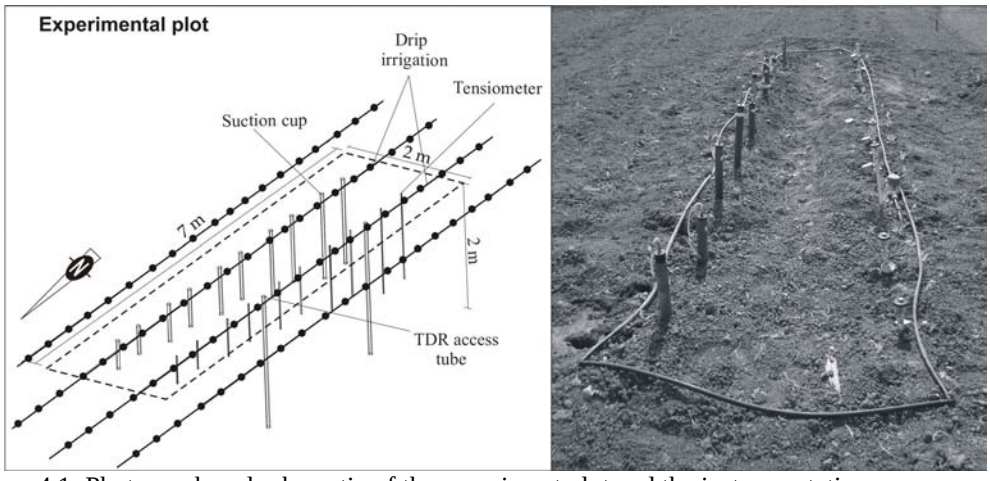

Figure 4.1: Photograph and schematic of the experiment plot and the instrumentation.

4.3 Root zone water flow approach

4.3.1 Numerical model

Water flow and root water uptake was simulated using HYDRUS-1D (*Šimůnek et al.*, 2005). Assuming that (i) the soil is homogeneous and isotropic, (ii) the air phase does not affect liquid flow processes, and (iii) water flow due to thermal gradients is negligible, the governing equation for water flow is the 1D Richards' equation:

$$\frac{\partial \theta}{\partial t} = \frac{\partial}{\partial x}\left[K\left(\frac{\partial h}{\partial x} + 1 \right) \right] - S \qquad [4.1]$$

where h = soil water pressure head; θ = volumetric water content; t = time; x = vertical space coordinate; K = unsaturated hydraulic conductivity; and S = sink term, defined as the volume of water removed from a unit volume of soil per unit time due to plant water uptake. The sink term is specified in terms of a potential uptake rate and a stress factor (*Feddes et al.*, 1978):

$$S(h) = \alpha(h) S_p \qquad [4.2]$$

where S_p is the potential water uptake rate and $\alpha(h)$ is the dimensionless water stress response function ($0 \le \alpha \le 1$) that prescribes the reduction in uptake that occurs due to drought stress. For $\alpha(h)$, we used the functional form introduced by *Feddes et al.* (1978):

$$\alpha(h) = \begin{cases} \dfrac{h - h_4}{h_3 - h_4}, & h_4 < h \le h_3 \\ 1, & h_3 < h \le h_2 \\ \dfrac{h - h_1}{h_2 - h_1}, & h_2 < h \le h_1 \\ 0, & h \le h_4 \text{ or } h > h_1 \end{cases} \qquad [4.3]$$

where h_1, h_2, h_3, and h_4 are threshold parameters such that uptake is at the potential rate when the pressure head is between h_2 and h_3, drops off linearly when $h > h_2$ or $h < h_3$, and becomes zero

when $h < h_4$ or $h > h_1$. Crop-specific values for these parameters (Table 4.1) were taken from the database contained in HYDRUS-1D (*Šimůnek et al.*, 2005).

Table 4.1: Root water uptake reduction parameters.

Crop	h_1 (cm)	h_2 (cm)	h_3 (cm)	h_4 (cm)
Melon	-10	-25	-400	-8000
Lettuce	-10	-25	-500	-8000

The soil hydraulic properties were modelled using the van Genuchten-Mualem constitutive relationships (*Mualem*, 1976; *van Genuchten*, 1980):

$$\theta(h) = \begin{cases} \theta_r + \dfrac{\theta_s - \theta_r}{\left[1 + |\alpha h|^n\right]^{1-1/n}} & h < 0 \\ \theta_s & h \geq 0 \end{cases} \quad [4.4]$$

$$K(h) = K_s S_e^{\,l} \left\{1 - \left[1 - S_e^{\,n/(n-1)}\right]^{1-1/n}\right\}^2 \quad [4.5]$$

where S_e is effective saturation:

$$S_e = \frac{\theta(h) - \theta_r}{\theta_s - \theta_r} \quad [4.6]$$

and where θ_s = saturated water content; θ_r = residual water content; K_s = saturated hydraulic conductivity; α = air entry parameter; n = pore size distribution parameter; and l = pore connectivity parameter. The parameters α, n, and l are empirical coefficients that determine the shape of the hydraulic functions. To reduce the number of free parameters, we took l = 0.5, a common assumption which is based on the work of *Mualem* (1976).

Running the model required specifying the hydraulic parameters θ_r, θ_s, α, n, K_s, and l. These parameters were estimated using Rosetta (*Schaap et al.*, 2001), a pedotransfer function

model that predicts hydraulic parameters from soil texture and related data. Rosetta contains a hierarchy of pedotransfer functions that can be used depending upon available data. The hydraulic parameters were predicted using data for bulk density and percentages of sand, silt, and clay. The data and estimated parameters are given in Table 4.2. Refinements to these parameter estimates were made subsequently based on model fitting to a subset of the measured water content and pressure head data (details given below).

Table 4.2: Measured soil textural and bulk density data, along with estimated hydraulic parameters†

Depth (cm)	Textural fractions (%)			Bulk density (g cm^{-3})	θ_r (cm^3 cm^{-3})	θ_s (cm^3 cm^{-3})	$\text{Log}_{10}(\alpha)$ (cm^{-1})	$\text{Log}_{10}(n)$	$\text{Log}_{10}(K_s)$ (cm d^{-1})
	Sand	Silt	Clay						
0-30	18.7	76.0	3.5	1.45	0.04 ±0.02	0.38 ±0.06	-2.18 ±0.51	0.21 ±0.09	1.67 ±0.49
30-60	13.8	80.2	6.0	1.52	0.05 ±0.03	0.38 ±0.06	-2.16 ±0.51	0.21 ±0.09	1.48 ±0.52
60-90	19.5	77.2	3.3	1.58	0.04 ±0.03	0.35 ±0.07	-2.01 ±0.66	0.19 ±0.11	1.48 ±0.67
90-150	10.8	82.0	6.6	1.70	0.04 ±0.03	0.38 ±0.08	-2.03 ±0.76	0.18 ±0.11	1.12 ±0.80

†Confidence intervals are two standard deviations (95%), estimated by Rosetta.

HYDRUS-1D (*Šimůnek et al.*, 2005) uses the Galerkin finite element method to solve Eqs. [4.1-4.5]. The atmospheric boundary condition (explained in the next section) was implemented at the soil surface while a free drainage condition (unit hydraulic gradient) was used at the bottom, the latter condition being appropriate due to fact that the water table was relatively far below the root zone (*Šimůnek et al.*, 2005).

4.3.2 Potential evapotranspiration and root growth

Implementing the atmospheric boundary condition required specifying daily irrigation and precipitation rates, as well as the *potential* evaporation and transpiration rates. To determine evaporation and transpiration, a reference evapotranspiration $ET_0(t)$ was calculated using the Penman-Monteith method (e.g. *Kashyap and Panda*, 2001). The *potential* evapotranspiration $ET_p(t)$ was then given by (*Allen et al.*, 1998):

$$ET_p(t) = K_c(t) \cdot ET_0(t) \qquad [4.7]$$

where $ET_0(t)$ was discretized in daily time steps and $K_c(t)$ is a crop-specific coefficient that characterizes plant water uptake and evaporation relative to the reference crop. Figure 4.2 illustrates the time variation of $K_c(t)$ in terms of annual crop growth stage (the initial, crop development, mid-season, and late season stages). *Allen et al.* (1998) provide data on the length of the growth stages and the values of K_c for various crops. *Allen et al.* (1998) method and data are considered to specify for each crop the value of K_c during each growth stage (Table 4.3, Figure 4.2).

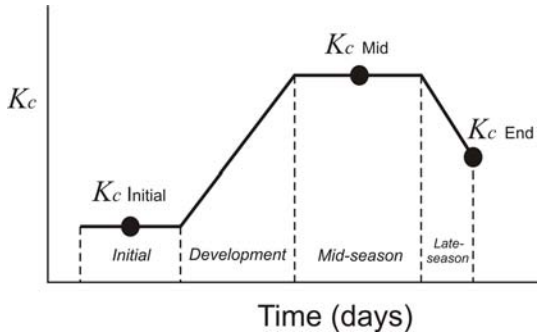

Figure 4.2: Illustration of crop growth stages and the time variation of the crop coefficient K_c.

With ET_p given by Eq. [4.7], *potential* evaporation $E_p(t)$ can be calculated according to (e.g. *Kroes and Van Dam*, 2003; *Pachepsky et al.*, 2004):

$$E_p(t) = ET_p(t) \cdot \exp^{-\beta \cdot LAI(t)} \qquad [4.8]$$

where β (≈ 0.4) is the radiation extinction coefficient and $LAI(t)$ is the leaf area index. However, $LAI(t)$ data are lacked so it instead is calculated:

$$E_p(t) = ET_p f(t) \qquad [4.9]$$

where the function $f(t)$ was specified based on the following reasoning. When a crop is first planted, ground cover is nonexistent, *potential* evaporation is maximum, transpiration is zero, and thus $f(t) = 1$. Conversely, when the crop reaches the mid-season growth stage, ground cover is complete, evaporation is effectively zero, and thereafter $f(t) = 0$. All that remains is specifying the

transition from $f(t) = 1$ at planting to $f(t) = 0$ at the beginning of the mid-season growth stage. Because crop growth typically follows an S-shaped pattern (e.g. *Overman and Scholtz*, 2002), this transition is modelled using a sigmoid curve.

Table 4.3: Growth and evapotranspiration coefficients for various crops (source: *Allen et al.*, 1998 and *CARM*, 2007)

Crop	Plant date	Growth Stage (number of days)				Crop coefficient (K_c)			Maximum root depth	Crop water requirements
		Initial	Development	Mid-season	Late-season	Initial	Mid	End	(cm)	(m^3 ha^{-1} yr^{-1})
Lettuce	Jan/Sept	35/30	50/40	45/25	10/10	0.7	1	0.95	30-50	3287.8
Broccoli	Jan/Sept	35	45	40	15	0.7	1.05	0.95	45-60	1595.7
Cauliflower	Jan/Sept	35	50	40	15	0.7	1.05	0.95	45-60	1595.7
Celery	Jan/Sept	25	40	45	15	0.7	1.05	1	45-60	2466
Endive	Jan/Sept	[a]	[a]	[a]	[a]	0.7	0.95	0.90	30-45	3474.4
Melon	May	25	35	40	20	0.5	1.05	0.75	80-150	6169.2
Watermelon	May	20	30	30	30	0.4	1	0.75	80-200	5435.1

[a]No data available, but casual observation suggests growth stages similar to those of lettuce.

With the atmospheric boundary condition, water evaporates from the soil surface at the *potential* rate E_p (a flux boundary condition) as long as the pressure head at the surface remains above a threshold value, h_{crit}. If the soil surface dries out such that the surface pressure head reaches the threshold value, the boundary switches to a constant pressure head condition (= h_{crit}), generally leading to a computed *actual* evaporation rate E_a that is well below the *potential* rate E_p. Summarizing:

$$E_a(h) = \begin{cases} E_p & h_{x=0} > h_{crit} \\ 0, & h_{x=0} \le h_{crit} \end{cases} \qquad [4.10]$$

In the simulations, h_{crit} was assumed to be -15 000 cm. The results of the simulations were not sensitive to this parameter value when specified in the range -10 000 cm to -15 000 cm because the surface soil remained relatively wet due to regular irrigation and thus remained above the h_{crit} threshold.

With ET_p and E_p given by Eqs. [4.7] and [4.9], the *potential* transpiration $T_p(t)$ was specified by:

$$T_p(t) = ET_p(t) - E_p(t) \qquad [4.11]$$

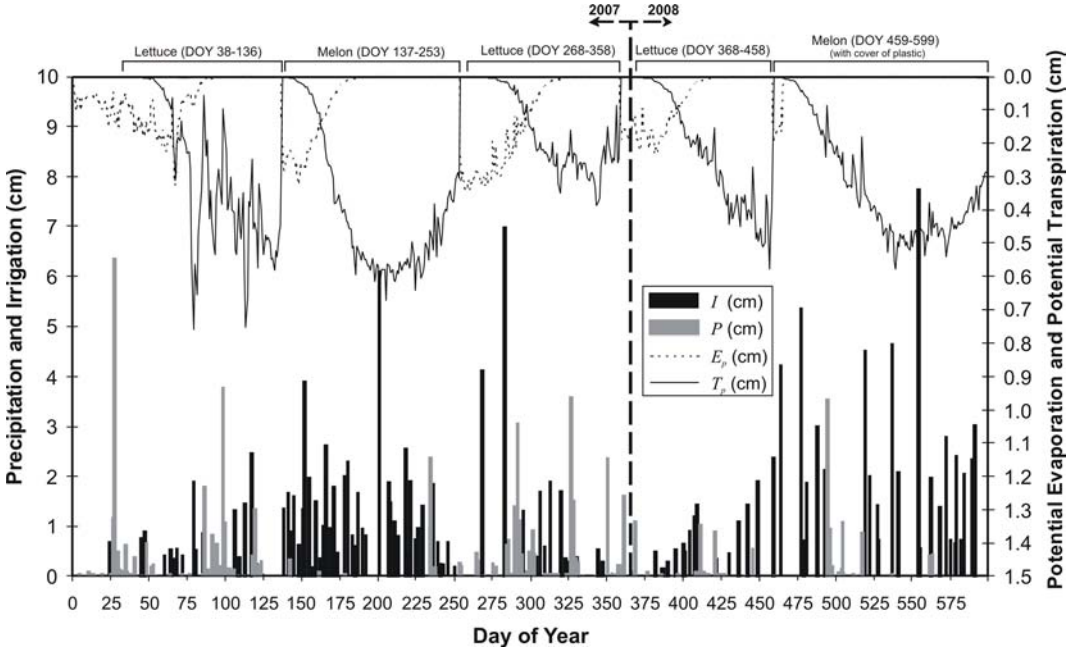

Figure 4.3: Summary of the modelled soil surface boundary conditions (I = irrigation; P = precipitation; E_p = *potential* evaporation; T_p = *potential* transpiration).

Figure 4.3 summarizes the imposed surface boundary condition, showing daily values of precipitation, irrigation, T_p, and E_p.

The modelled rooting depth was assumed to increase with time according to a logistic growth function (*Šimůnek et al.*, 2005), achieving a maximum depth at the end of the crop development stage. Values for the maximum rooting depth for particular crops (Table 4.3) were derived from *Allen et al.* (1998).

4.3.3 Uncertainty and sensitivity assessment

The modelling approach contains several potential sources of uncertainty or error. Two levels or types of uncertainty can be distinguished. From one side, uncertainty exists from the computed root zone drainage at plot or field. In this context, sources of uncertainty include the values of various model parameters such as the soil hydraulic parameters in Eqs. [4.4] and [4.5], the daily reference evapotranspiration rate ET_0(t), crop coefficients $K_c(t)$, and drought stress parameters (e.g. h_3 in Eq.[4.3], the threshold pressure head below which uptake is reduced). Quantifying the effect of these parameter uncertainties on drainage calculations requires knowledge of their statistical variability and correlation structure. In the case of the hydraulic parameters α and n, we have information in the form of 95% confidence intervals and correlation coefficients computed by HYDRUS-1D as part of the parameter optimization. For other hydraulic parameters, estimated confidence intervals are available from the Rosetta model (Table 4.2), but those estimates are unrealistically broad because they are only based on the soil separate and bulk density data and have not been conditioned on the water content and pressure head field data. The literature provides little or no information on quantifying uncertainty in other model parameters such as crop coefficients.

A second type, or uncertainty source, involves extrapolation of the field results to a larger region. Here, sources of uncertainty include data on regional irrigation practices, cropping rotation and acreages, and so forth-the type of uncertainty that exists in any modelling or water balance estimation of recharge. Additionally, it may be also consider how specific model parameters vary in the region and how those variations would affect root zone drainage calculations. Again, however, little knowledge exists on how to quantify such variability in parameters like ET_0 or $K_c(t)$. For the hydraulic parameters, the Rosetta uncertainty estimates (Table 4.2) potentially provide a good starting point for quantifying the effects of hydraulic property uncertainty. Those estimates could, for example, serve as the basis for a Monte Carlo calculation of uncertainty in the recharge estimate. However, such a calculation is more complex than it may first appear. The Rosetta uncertainty estimates are quite broad. For example, the bounds for the 95% confidence intervals for K_s span an order-of-magnitude. With that kind of variability, a problem that may be encountered is that a given irrigation regime may not be sensitive over the whole range of soil properties: a realistic regime for a medium conductivity soil may result in water logging in a low conductivity soil (a specific example is given in the sensitivity calculations discussed below, section 4.4.3). Thus, a quantitative analysis of hydraulic property uncertainty would have to

somehow account for the relationship between soil properties and irrigation regimes (i.e. surface boundary conditions).

In sum, it does not seem possible at this time to define quantitative confidence intervals on our recharge estimate owing to a lack of knowledge about parameter variability and correlation structure at multiple levels. However, it is possible to get some sense of the importance of parameter uncertainty by performing a sensitivity analysis. For this analysis, we performed a series of simulations in which individual parameters, or in one case a set of parameters, were perturbed a fixed amount while all other parameters were held at their baseline values (that is, the values used in recharge calculations). The effect of perturbation of the various parameters on the calculated recharge was then evaluated. Parameters considered for sensitivity analysis were α, n, K_s, θ_s, θ_r, l, $K_c(t)$, h_3, h_{crit} and $ET_0(t)$. Note in the following that Rosetta assumes that α, n, and K_s are lognormally distributed, such that the confidence intervals are not symmetric about the (geometric) mean parameter estimate after antilog transformation. Also note that the calibration procedure do not treat the hydraulic parameter l as adjustable, instead fixing its value at $l = 0.5$; it was included in the sensitivity analysis for completeness and because Rosetta generally estimates high levels of uncertainty for this parameter.

4.4 Results and discussion

4.4.1 Model calibration and predictions

Running HYDRUS-1D using the Rosetta hydraulic parameter estimates resulted in simulations that were in poor agreement with the field data. Therefore, the soil hydraulic property model (Eqs. 4.4 and 4.5) was attempted to calibrate using a subset of the data. The most intensive data collection at the site occurred during the cultivation of melon from 17 May to 10 September, 2007, comprising day of year (DOY 1 = 1st January 2007) 137-253. We used this data set and the parameter optimization routines of HYDRUS-1D to calibrate the soil hydraulic parameters. Several possible parameterizations were considered which differed according to the number of soil layers (from 1 to 4) and the number and type of hydraulic parameters that were fitted for each layer (different combinations of 1 to 4 parameters among α, n, K_s, and θ_s). The initial estimates for the parameters when fitted, or their fixed value when not fitted, were the Rosetta estimates given

in Table 4.2. If the results of the optimization looked promising, the fitting was repeated using different initial estimates to ensure that the same optimized parameter values were obtained. The best overall parameterization was informally determined based on diagnostic information provided by the HYDRUS-1D routines about the model fit and the convergence behaviour of the inverse algorithm, visual inspection of the model fit to the data (including laboratory water retention data, Figure 4.4), and the principle of parsimony (i.e. if two parameterizations produced a roughly equal fit to the data, the simpler of the two is taken, where "simpler" means fewer fitted parameters and/or soil layers). The best parameterization was found to involve four soil layers with two adjustable parameters, α and n, for each layer. The final fitted hydraulic parameter values are given in Table 4.4; the other parameter values are those estimated with Rosetta (Table 4.2). Fitting more

Table 4.4: Fitted hydraulic parameter values with 95% confidence intervals.

Depth (cm)	α (cm^{-1})	n (-)
0-30	0.078 ±0.010	1.16 ±0.01
30-60	0.046 ±0.005	1.23 ±0.02
60-90	0.014 ±0.004	1.27 ±0.07
90-150	0.020 ±0.002	1.46 ±0.05

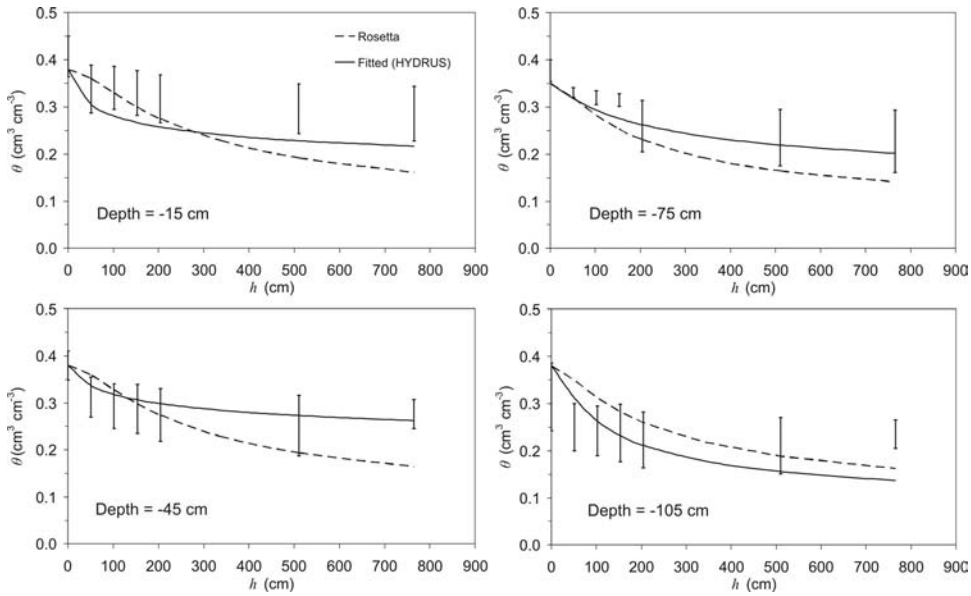

Figure 4.4: Soil water retention functions at different depths (15, 45, 75 and 105 cm) from Rosetta (dashed line) and fitted by HYDRUS (solid line). Vertical bars represent maximum and minimum θ measures in laboratory.

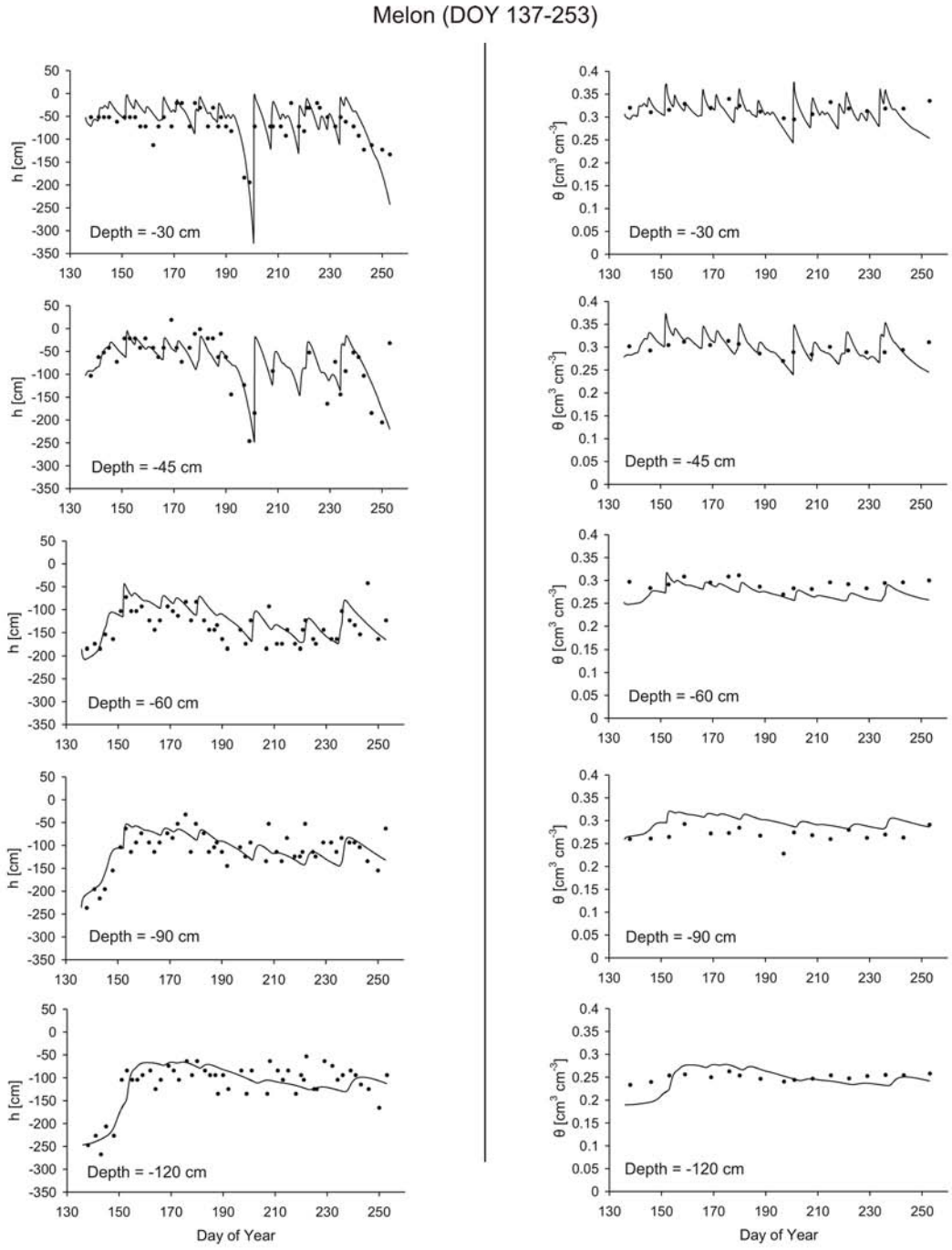

Figure 4.5: Pressure head and water content data (dots) measured at various depths in the soil profile, along with final fitted HYDRUS simulations (solid lines) for melon crop (DOY 137-253).

than two parameters per layer tended to cause the inverse algorithm to fail. Four soil layers produced a better fit to the data than was possible with fewer layers in the profile. Overall, the numerical solution with four layers and α and n fitted for each layer provided the best correlation between measured and simulated water content and pressure head values. Figure 4.5 shows water content and pressure head data for various depths in the soil profile, along with the corresponding fitted model simulation. Table 4.5 gives goodness-of-fit measures for the calibrated simulation run and data, including $R^2 = 0.90$ for the combined water content and pressure head data. Correlation coefficients $r_{x,y}$ computed by HYDRUS-1D for the eight fitted parameters were $|r_{x,y}| < 0.4$, with three exceptions: $r_{\alpha_1,\alpha_2} = -0.54$, $r_{\alpha_1,\alpha_4} = -0.55$, and $r_{\alpha_3,n_3} = -0.75$ (where numerical subscripts on α and n indicate the soil layer).

Table 4.5: Goodness-of-fit measures for simulations and experimental data.

Simulation	Data Set	*RMSE*[a]	*MAE*[b]	R^2
Melon (DOY 137-253) (calibration)	Water content (θ)	0.029	0.024	
	Pressure head (h)	33.776	27.971	
	Combined θ and h			0.90
Lettuce (DOY 38-136) (prediction)	Water content (θ)	0.024	0.022	
	Pressure head (h)	56.630	41.271	
	Combined θ and h			0.82
Lettuce (DOY 268-358) (prediction)	Water content (θ)	0.023	0.019	
	Pressure head (h)	40.013	31.279	
	Combined θ and h			0.82
Lettuce (DOY 368-458) (prediction)	Water content (θ)	0.023	0.018	
	Pressure head (h)	67.165	52.548	
	Combined θ and h			0.80
Lettuce (DOY 459-599) (prediction) (with plastic cover)	Water content (θ)	0.028	0.021	
	Pressure head (h)	72.860	56.795	
	Combined θ and h			0.67

[a] Root mean square error, $RMSE = \sqrt{\frac{1}{n}\sum_{i=1}^{n}(x_i - y_i)^2}$ [b] Mean absolute error, $MAE = \frac{1}{n}\sum_{i=1}^{n}|x_i - y_i|$

With the fitted parameterization, HYDRUS-1D was next used to predict the root zone soil moisture dynamics during the growing periods of other crops at the site: the first one grown between 7 February and 16 May 2007 (lettuce, DOY 38-136), the second one between 25 September and 24 December 2007 (lettuce, DOY 268-358), the third one between 3 January and

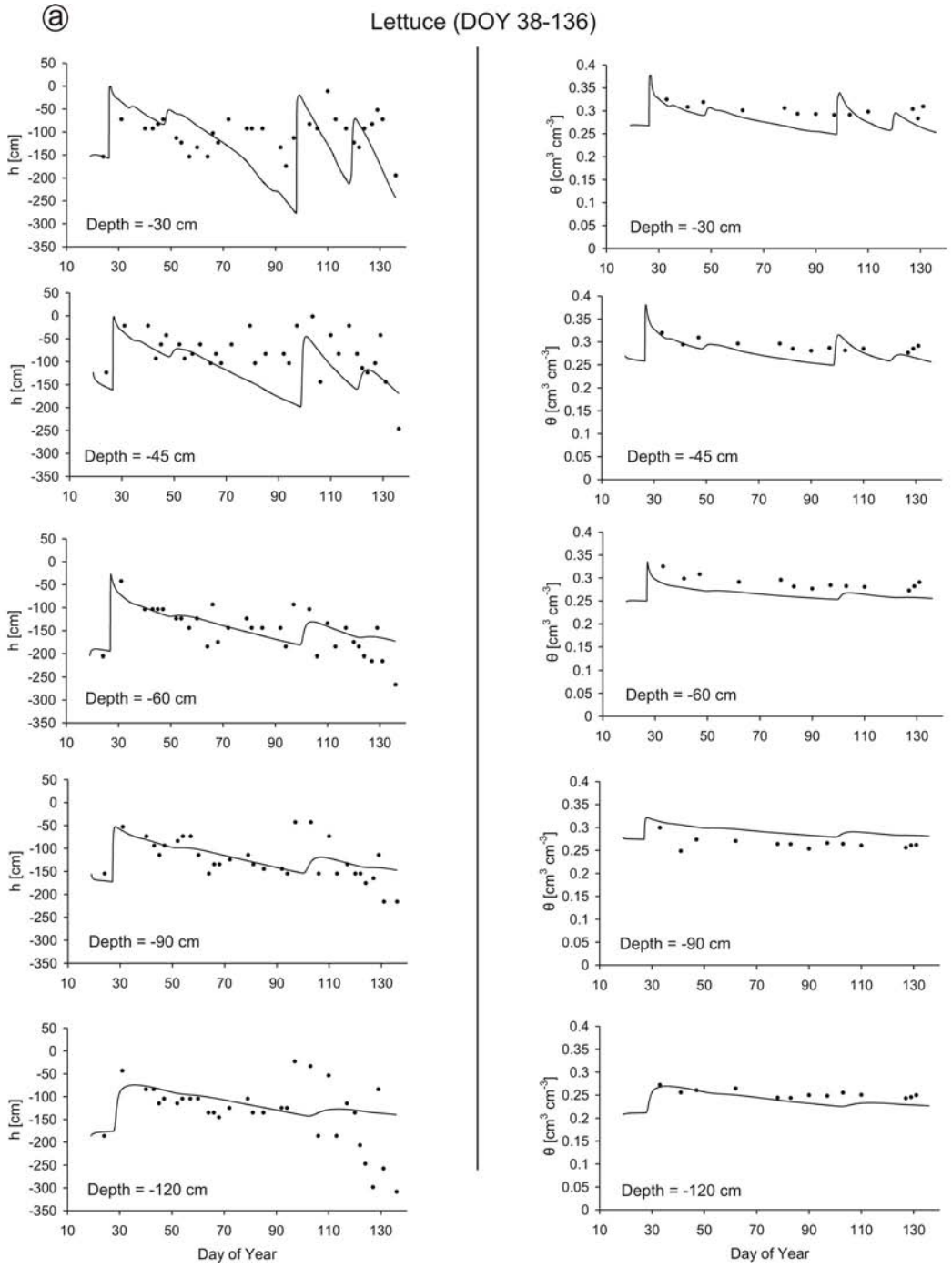

Figure 4.6: Pressure head and water content data (dots) measured at various depths in the soil profile, along with HYDRUS predictions (solid lines) for: a) lettuce (DOY 38-136), b) lettuce (DOY 268-358), c) lettuce (DOY 368-458) and d) melon with plastic cover (DOY 459-599).

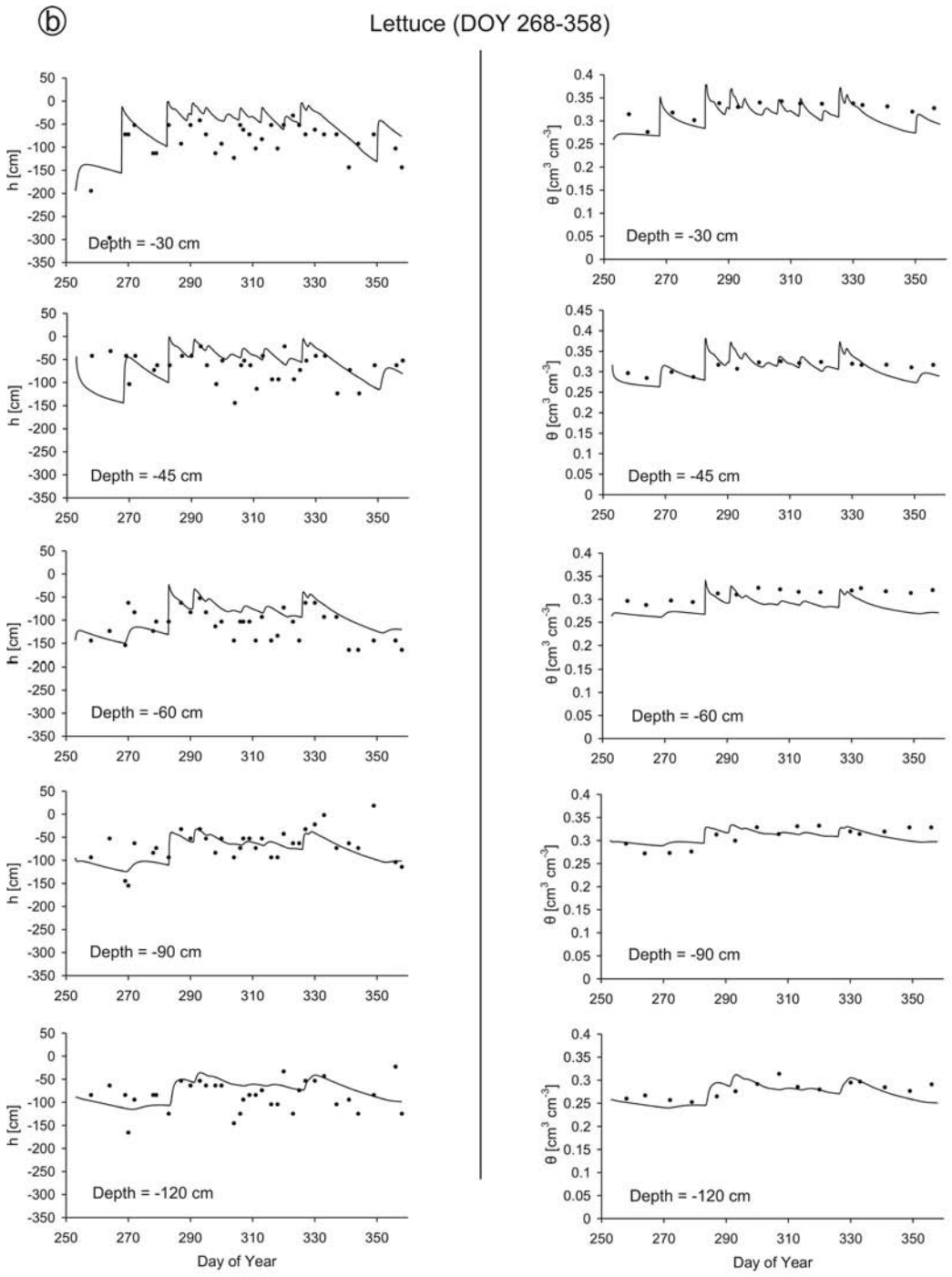

Figure 4.6 (continued)

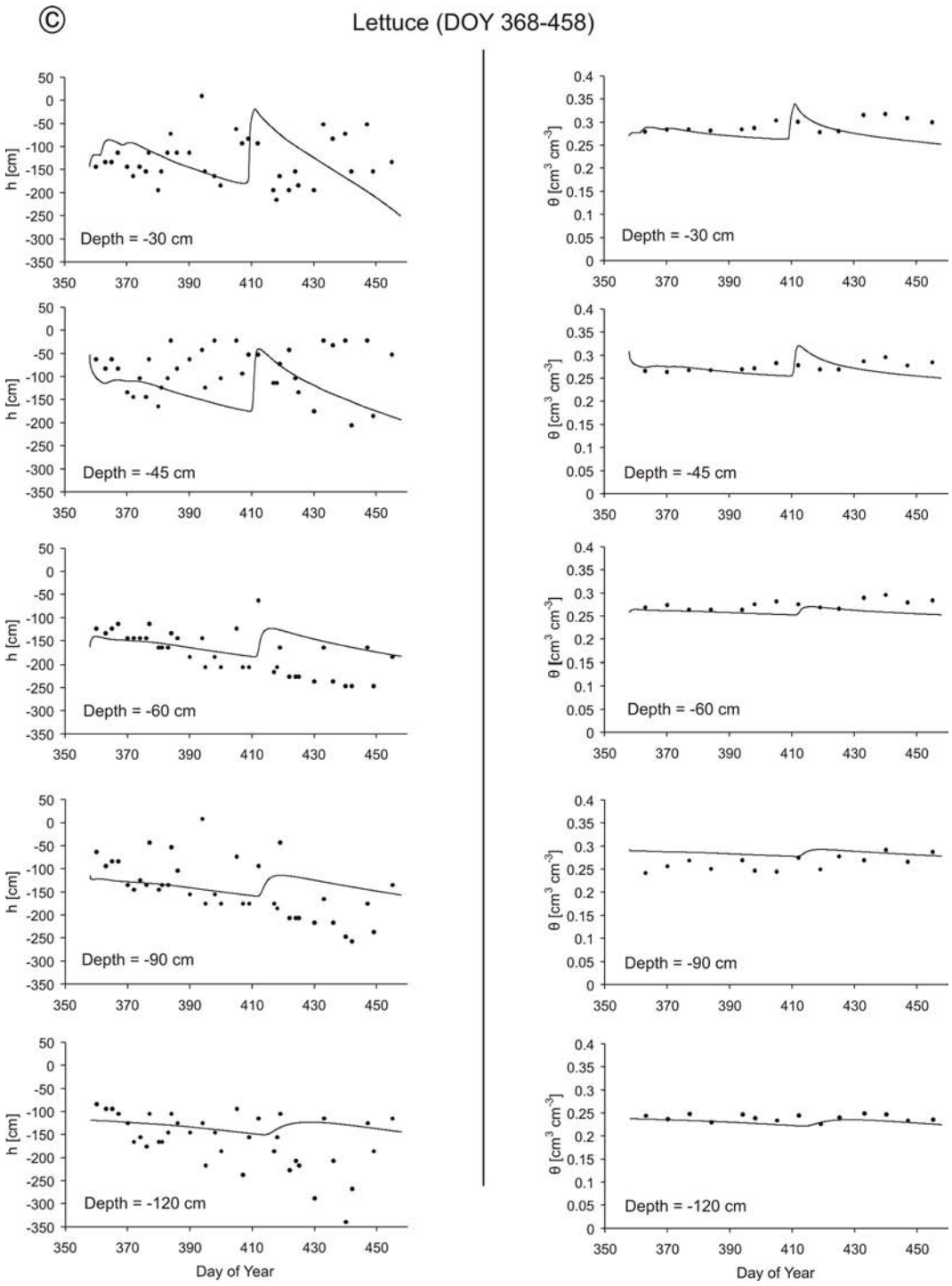

Figure 4.6 (continued)

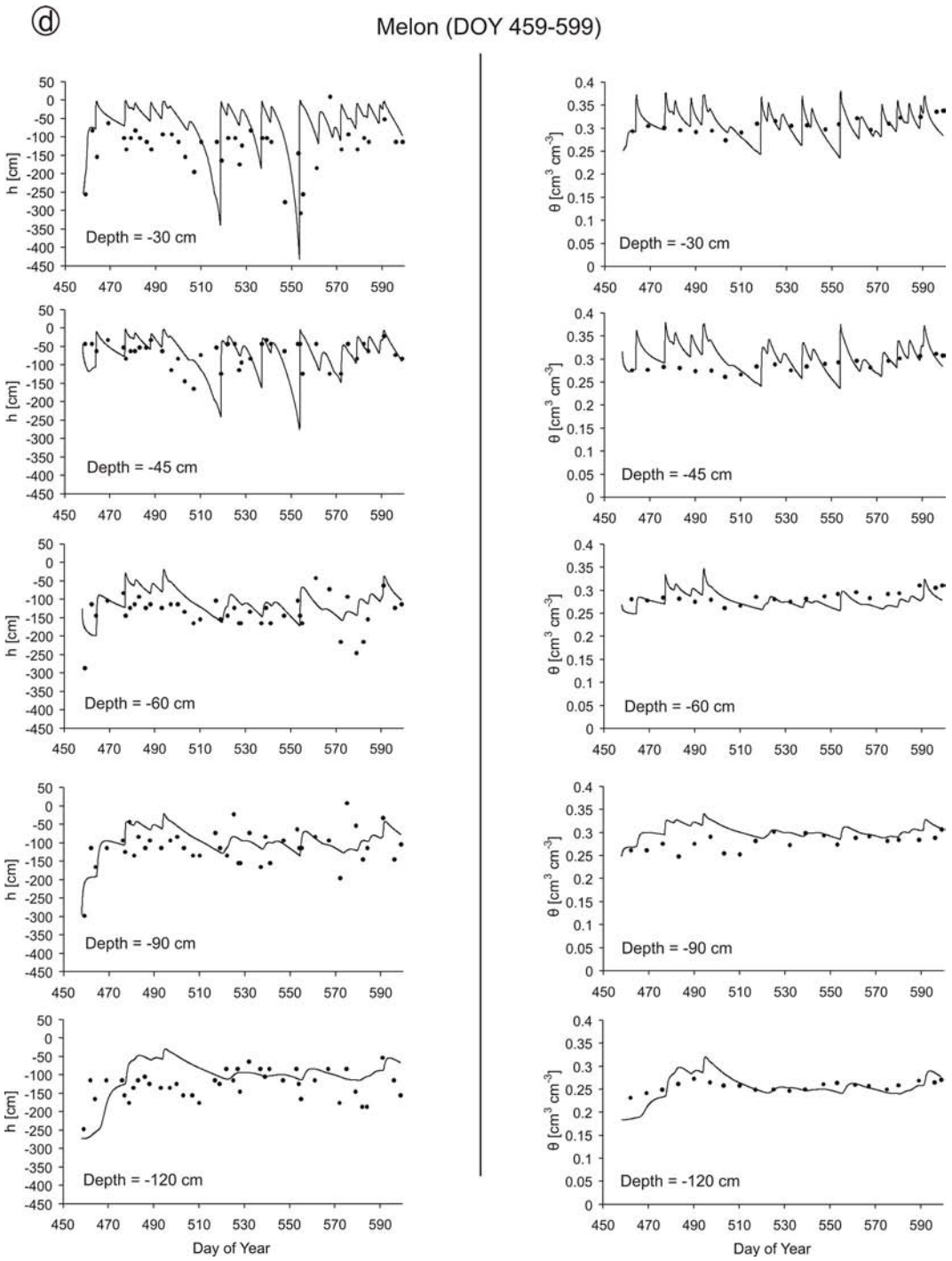

Figure 4.6 (continued)

2 April 2008 (lettuce, DOY 368-458) and finally, the last one from 3 April to 21 August 2008 (melon with plastic cover, DOY 459-599). Figure 4.6 compares the predictions with the experimental data at various depths in the soil profile. Overall, good agreement was achieved between the field measurements and the HYDRUS-1D predictions. The correlation coefficient (R^2) between measured and predicted water contents and pressure heads was around 0.80 for all the crops except for melon with plastic cover, being 0.67. Additional measures of goodness-of-fit are given in Table 4.5.

4.4.2 Recharge estimation

Subsequently, calibrated model simulations are used to evaluate the root zone soil water balance and calculate the annual recharge rate. The components of the water balance were water additions due to irrigation (I) and precipitation (P), losses due to evapotranspiration and drainage below the root zone, and changes in root zone water storage. Drainage from the bottom of the soil profile was assumed to be irrigation return flow, equal to the groundwater recharge rate. Based on the simulated drainage, the recharge rate generated during cultivation of different crops at different times of the year can be calculated. Figure 4.7 shows the cumulative drainage (recharge) as a function of time computed for all the cropping periods. The percentages of applied water (P+I) becoming recharge and irrigation efficiency for each crop are shown in Table 4.7. The higher percentage (68.2%) for the lettuce crop between September and December (DOY 254-358) was due to high precipitation and low transpiration rates (Figure 4.3), while the difference between both melon crops resulted from the use of a plastic cover in the second one, since direct evaporation from ground surface is reduced to almost zero. On the other hand, due to technical problems in the irrigation system, application of a large water volume (77 mm) on the experimental plot in the second melon crop occurred. During the year 2007 recharge was 492 mm, whereas during the hydrological year 2007-2008 was 561 mm.

Figure 4.7 also shows the cumulative *potential* and *actual* transpiration rates for all the cropping periods. *Actual* transpiration was frequently lower than the *potential* rate because soil moisture at various times was insufficient to sustain the potential uptake rate, with uptake being reduced according to Eq. [4.2]. This aspect of the root zone modelling methodology (i.e. the physically based calculation of the onset of water stress and subsequent reduced uptake) is crucial

for calculating recharge in arid and semi-arid regions where *ET* may drop below potential rates, even in irrigated systems.

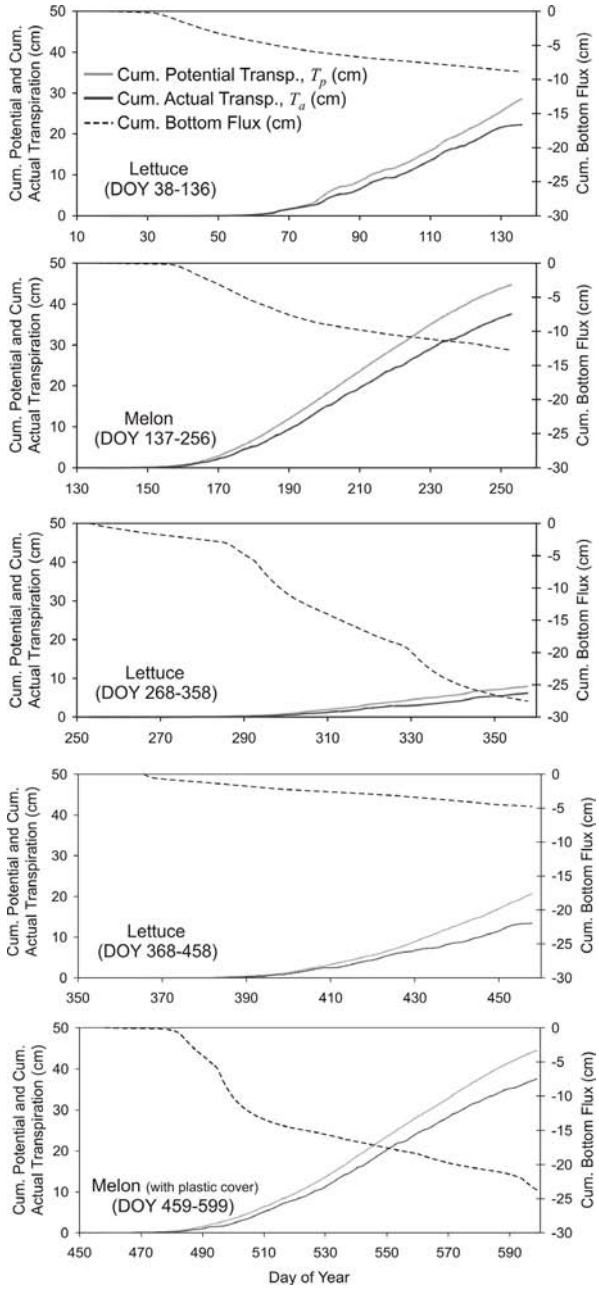

Figure 4.7: Cumulative *potential* transpiration T_p (grey line), *actual* transpiration T_a (black line), and bottom drainage (dashed line) rates computed for all the crops.

Table 4.6: Simulated bottom drainage (recharge) from applied water (*P*+*I*) for each crop. Irrigation efficiency calculated from *potential* and *actual* evaportranspiration (volume of irrigation water beneficially used).

Crop	*I* (mm)	*P* (mm)	*I*+*P* (mm)	Recharge		Irrigation Efficiency (%)†	
				(mm)	(%)	*Potential ET*	*Actual ET*
Lettuce (DOY 38-136) (prediction)	133	228	361	89	24.6	100	100
Melon (DOY 137-253) (calibration)	557	32	589	128	21.7	96	83
Lettuce (DOY 268-358) (prediction)	206	197	403	275	68.2	89	63
Lettuce (DOY 368-458) (prediction)	123	61	184	48	26	100	100
Melon (DOY 459-599) (prediction) (with plastic cover)	617	80	697	238	34.1	93	71

†Irrigation Efficiency from *Burt et al.* (1997).

4.4.3 Sensitivity analyses

The first set of sensitivity calculations involved perturbing the hydraulic parameters α, n, K_s, θ_s, θ_r, and l one at a time in individual soil layers (Table 4.7). The perturbations to the parameter values in this case were large, equal to the bounds of the 95% confidence intervals given in Table 4.2. The results for these calculations showed that among the parameters considered, recharge calculation was least sensitive to water contents θ_s and θ_r. Setting either of these parameter values to the bounds of the 95% confidence intervals in any of the four soil layers resulted in a small change to the computed recharge, considering that the 95% confidence bounds corresponded to large parameter perturbations for θ_s and θ_r (Table 4.2). Relatively low sensitivity was also found for the remaining soil hydraulic parameters (α, n, K_s, l) in the middle two soil layers. Setting α, n, K_s, or l in those layers to the 95% confidence bounds, again, the changes in computed recharge were fairly small considering the size of the parameter perturbations for n, K_s and α (recall the asymmetric confidence intervals), and greater than 1000% for l. Higher sensitivity was found for α, n, K_s, and l in the surface soil layer. Perturbations to those parameters resulted in changes to the computed recharge less than 7% with one notable exception: the lower bound for the surface saturated conductivity resulted in an increase of 58% to the calculated recharge. The reason for this large increase was that the low surface conductivity caused the surface soil to stay very close to saturation for long periods of time, such that uptake was reduced according to Eq. [4.3] and hence simulated drainage increased. *Feddes et al.* (1978) model, Eq. [4.3], specifies that uptake reduction occurs both when the soil is excessively wet and when it is too dry. The highest

sensitivity to hydraulic parameters was found in the bottom soil layer where the retention and conductivity functions directly impact the drainage of water out of the root zone. In this layer, setting individual parameters to the lower and upper bounds of the 95% confidence region led to changes of recharge between -24 and +62% for K_s, n, l and α. Although some of those changes are quite substantial, keep in mind the very large perturbations (e.g. the bounds for α corresponded to perturbations of about -83% and +474%) and the low likelihood of such a soil parameter value.

Table 4.7: Computed recharge sensitivity to the hydraulic parameter (θ_r; θ_s; α; n; K_s; l) perturbations, bounds of the 95% confidence intervals, one at time in individual soil layer.

Layer	θ_r	θ_s	α		n		K_s	l
			Rosetta	Fitted	Rosetta	Fitted		
Perturbation (%)								
1	±56	±14	-68 / 218	±13	-17 / 26	±0.9	-67 / 213	±1100
2	±54	±15	-70 / 219	±11	-17 / 23	±2	-69 / 230	±2100
3	±68	±19	-78 / 355	±30	-24 / 26	±5	-78 / 373	±1850
4	±70	±22	-83 / 474	±10	-22 / 30	±3	-84 / 533	±900
Δ Recharge (%)								
1	0.7 / 2.3	3.3 / -0.3	-11 / -12.4	-2.7 / 3.3	-11.2 / -11	1.6 / -1.1	58 / -6.6	-4.1 / 5.6
2	1 / -1.8	2.3 / 0.7	1.9 / 1.6	0.4 / -0.2	-1.6 / -5.2	0.4 / -0.3	6.9 / 3.2	2.8 / 0.7
3	1.2 / 1.7	2.2 / 0.7	1.8 / -5.1	0.7 / -0.5	0.3 / -5.2	0.5 / -0.6	-0.4 / 1.9	1.7 / 1.3
4	0.4 / 2.5	4 / -1.6	62.2 / -28.6	3.7 / -2.9	-5.7 / -2.5	0.2 / 0	-24.1 / 24.5	20.2 / -3.9

When narrower, more realistic bounds for α and n in individual soil layers were evaluated (according to Table 4.4), the changes in the calculated recharge were ±4% or less (Table 4.7). Unlike the bounds discussed in the previous paragraph, these confidence intervals incorporated measured water content and pressure head data, and thus are likely to be more reflective of the uncertainty that existed at our experimental site.

Additionally, smaller perturbations (±10%) of the hydraulic parameters (K_s, θ_s, θ_r, α, n and l) in individual soil layers were considered (Table 4.8). In these calculations, the calculated recharge was least sensitive to θ_r (~1% change in recharge), while the remaining parameter perturbations altered recharge by between 7 and -10%. The simulation for a -10% perturbation of n was not completed because the small n value caused numerical difficulties in the simulation model (a well-known problem when $n \rightarrow 1$). Lastly, the same hydraulic parameter in all soil layers was simultaneously disturbed. Using ±10% perturbations, computed recharge was insensitive to θ_r, K_s

and l (about 1% change in recharge), whereas changes in recharge for other parameters were about 4 to 10%. The lower bound calculation for n was again aborted due to numerical instability.

Table 4.8: Computed recharge sensitivity to ±10% perturbations of the hydraulic parameters (θ_r; θ_s; α; n; K_s; l) one at time in individual soil layer and one at time in all soil layers.

One at time in individual soil layer						
Layer	θ_r	θ_s	α	n	K_s	l
1	-0.5 / -0.8	-1.8 / 0.7	1.7 / -2.7	-9.6 / n.i.	-1.7 / 0.6	-0.6 / -0.8
2	-0.6 / -0.7	-1.1 / -0.2	-0.9 / -0.3	-1.7 / 7	-0.6 / -0.7	-0.7 / -0.6
3	-0.6 / -0.7	-1 / -0.3	-0.8 / -0.5	-1.6 / 0.1	-0.6 / -0.7	-0.7 / -0.7
4	-0.5 / -0.8	-1.9 / 0.5	-3.7 / 2.8	-0.5 / -2.2	0.6 / 2.1	0.9 / 0.4
One at time in all soil layers						
Layer	θ_r	θ_s	α	n	K_s	l
1-4	-0.3 / -1	-3.9 / 2.7	-1.5 / 1.4	-9.9 / n.i.	-0.3 / -0.8	-0.9 / -0.4

n.i.: numerical instability

The final sensitivity calculations involved ±10% perturbations to the parameters h_3, $K_c(t)$ and $ET_0(t)$ and ±33% to h_{crit} (Table 4.9). Note that because $K_c(t)$ and $ET_0(t)$ appear as a product in Eq. [4.7], results for a ±10% perturbation in $K_c(t)$ are identical to results that would be obtained for a ±10% perturbation in $ET_0(t)$. The recharge calculation was relatively insensitive to perturbations of h_3 and h_{crit}, with the calculated recharge changing by less than 1%. Greater sensitivity was found for $K_c(t)$ or $ET_0(t)$, where the 10% perturbations altered the recharge calculation by about ±9%.

Table 4.9: Computed recharge sensitivity to perturbations of the parameters and boundary conditions K_c, ET_0, h_{crit} and h_3.

Parameter	*Perturbation* (%)	*Δ Recharge* (%)
K_c and ET_0 (Eq. 4.7)	±10	-8.9 / 9.9
h_{crit} (Eq. 4.10)	±33	-0.5 / -0.7
h_3 (Eq. 4.3)	±10	-0.8 / -0.8

4.5 Conclusions

The root zone modelling approach described in this chapter is presented as a suitable method to estimate irrigation return flow, assumed as recharge to the aquifer under the two following assumptions: small thickness of the unsaturated zone and negligible hypodermic flow rate, as occurs on the study area. The main conclusions of this chapter can be summarized as follows:

1. Evapotranspiration and soil moisture dynamics for specific crops and irrigation regimes were successfully simulated with HYDRUS-1D. Good agreement was achieved between the HYDRUS-1D results and field measurements (h and θ at different depths) for melon and lettuce crops. Visual inspection and statistics of the model fit to the data show that agreement for θ was better than h. Soil moisture measurements with TRIME-FM TDR probe are very representative of the actual soil state, since it gives an integrated θ value for an effective influence radium of 15 cm around of the measure point, whereas the representativeness of h measurements from tensiometers is more limited. Numerical solution for four layers, being α and n fitted for each layer, provided the best correlation between h and θ measured and simulated. A better agreement was found between simulations and field measurements at higher depths due to a minor influence of plant-atmosphere processes.

2. Simulations showed that *actual* transpiration was always lower than *potential* transpiration because soil moisture was insufficient to sustain the potential uptake rate, despite regular irrigation.

3. The recharge during the 2007 year was 492 mm for a water input $P+I$ = 1353 mm, whereas during the 2007-2008 hydrological year was 561 mm for a water input $P+I$ = 1284 mm. Results indicated a high amount of recharge late in the year when *potential* evapotranspiration is lower and main precipitation events occur, between October and December, and in summer due to the plastic cover.

4. Models as Rosetta, also called pedotransfer functions, permit to translate easily measured data such as soil texture and bulk density into unsaturated hydraulic properties. Direct measurements permit the most exact determination of soil hydraulic properties, but they often require a substantial investment in both time and money. Rosetta permits to reduce the investment in soil hydraulic parameter estimation; however, the main problem is that the uncertainty of estimates can

be quiet broad. The confidence intervals bounds for some parameters span several orders of magnitude. Therefore, a sensitivity analysis over the whole range of soil properties used in a model results essential to determine the reliability of the results.

5. The highest sensitivity was found for the α, n, K_s, and l hydraulic parameters in the top and bottom soil layers, where the retention and conductivity functions directly impact on the drainage. Moreover, in the top soil, K_s strongly impacts on *Feddes et al.* (1978) model that supposes root uptake reduction.

6. Root zone modelling approach shows a promising method for estimating recharge in irrigated semi-arid regions. Compared with other techniques, the modelling approach is relatively data intensive, involving several of crop- and soil-specific parameters. However, often these parameters can be approximated from existing databases and estimation tools. For example, maps of soil texture and related soil physical properties are available at many locations; soil hydraulic parameters can be easily estimated from those data using pedotransfer functions or related approaches. Likewise, water stress parameters for many important crops have been tabulated (e.g. *Kroes and van Dam*, 2003).

Notation

α	air entry (cm^{-1})
$\alpha(h)$	dimensionless water stress response function-uptake reduction (-)
β	extinction radiation coefficient (-)
E_a	actual evaporation (cm)
E_p	potential evaporation (cm)
ET_p	potential evepotranspiration (cm)
ET_0	reference evapotranspiration (cm)
f	ground cover sigmoid function (-)
h	soil water pressure head (cm)
h_{crit}	pressure head threshold value for evaporation (cm)
I	irrigation (cm)
K	unsaturated hydraulic conductivity ($cm\ day^{-1}$)
K_c	crop-specific coefficient (-)
K_s	saturated hydraulic conductivity ($cm\ day^{-1}$)
l	pore connectivity (-)
LAI	leaf area index ($m^2\ m^{-2}$)
n	pore size distribution (-)
P	precipitation (cm)
S	sink term ($cm\ cm^{-3}\ day^{-1}$)
S_e	effective saturation (-)
S_p	potential water uptake rate ($cm\ cm^{-3}\ day^{-1}$)
t	time (day)
T_p	potential transpiration (cm)
θ	volumetric water content ($cm^3\ cm^{-3}$)
θ_r	residual volumetric water content ($cm^3\ cm^{-3}$)
θ_s	saturated volumetric water content ($cm^3\ cm^{-3}$)
x	vertical space coordinate (cm)

References

Allen, R.G., Pereira, L.S., Raes, D., Smith, M., 1998. *Crop evapotranspiration. Guidelines for computing crop water requirements.* Irrigation and Drainage. Paper No. 56, FAO, Rome, Italy.

Brown, D.A. and Scott, H.D., 1984. Dependence of crop growth and yield on root development and activity. In: Barber, S.A., Bouldin, D.R. (Eds.), Roots, Nutrient and Water Influx, and Plant Growth, ASA Spec. Pub. No. 49. SSSA, SCA, ASA, Madison, WI. pp. 101-136.

Burt, C.M., Clemmens, A.J., Strelkoff, T.S., Solomon, K.H., Hardy, L., Howell, T., Eisenhauer, D., Bleisner, R., 1997. Irrigation performance measures – Efficiency and uniformity. *J. Irrigation and Drainage Engineering* 123(6), 423-442.

Campbell, G.S. and Norman., J.M., 1998. *An Introduction to Environmental Biophysics*. 2nd ed. Springer-Verlag, New York.

CARM, 2007. *El Agua y la Agricultura en la Región de Murcia. Un Modelo de Eficiencia.* Consejería de Agricultura y Agua de la Región de Murcia. 111 pp.

Feddes, R. A., Kowalik, P.J., Zaradny, H., 1978. *Simulation of Field Water Use and Crop Yield*. John Wiley and Sons, NY.

Kashyap, P.S. and Panda, R.K., 2001. Evaluation of evapotranspiration estimation methods and development of crop-coefficients for potato crop in a sub-humid region. *Agric. Water Manage.* 50, 9-25.

Keese, K.E., Scanlon, B.R., Reedy, R.C., 2005. Assessing controls on diffuse groundwater recharge using unsaturated flow modeling. *Water Resour. Res.*, 41, W06010, doi:10.1029/2004WR003841.

Kendy, E., Gérard-Marchant, P., Walter, M.T., Zhang, Y., Liu, C., Steenhuis, T.S., 2003. A soil-water-balance approach to quantify groundwater recharge from irrigated cropland in the North China Plain. *Hydrol. Process.* 17, 2011–2031.

Kroes, J.G. and Van Damm, J.C., 2003. *Reference manual SWAP: Version 3.0.3.* Rep. 773. Alterra Green World Res., Wageningen, the Netherlands.

Laurent, J.P., Ruelle, P., Delage, L., Bréda, N., Chanzy, A., Chevallier, C., 2001. On the use of the TDR Trime-Tube system for profiling water content in soil. Proceedings TDR´01, Evanston-Illinois, USA 5-2 Sept. 2001, 1–10.

Laurent, J.P., Ruelle, P., Delage, L., Zaïri, A., Ben Nouna, B., Adjmi, T., 2005. Monitoring Soil Water Content Profiles with a Commercial TDR System: Comparative Field Tests and Laboratory Calibration. *Vadose Zone J.* 4, 1030–1036.

Mualem, Y., 1976. A new model predicting the hydraulic conductivity of unsaturated porous media. *Water Resour. Res.* 12, 513-522.

Overman, A.R. and Scholtz, R.V., 2002. *Mathematical Models of Crop Growth and Yield.* Marcel Dekker, Inc. New York.

Pachepsky, Y.A., Smettem, K.R.J., Vanderborght, J., Herbst, M., Vereecken, H., Wosten, J.H.M., 2004. Reality and fiction of models and data in soil hydrology. In: Feddes R.A. et al. (Eds.), Unsaturated-zone modeling. Kluwer Academic Publishers, Dordrecht, the Netherlands.

Ramírez, I., Vicente, M., García, J., Vaquero, A., 1999. *Mapa digital de suelos de la Región de Murcia.* Consejería de Agricultura, Agua y Medio Ambiente. Handbook and CD-ROM. 78 pp.

Schaap, M.G., Leij, F.J., van Genuchten, M.Th., 2001. ROSETTA: a computer program for estimating soil hydraulic parameters with hierarchical pedotransfer functions. *J. Hydrol.* 251, 163-176.

SIAM, 2008. Servicio de Información Agraria de Murcia. Climatology Data. Available from: <http://siam.imida.es>.

Šimůnek, J., van Genuchten, M.Th., Šejna, M., 2005. *The HYDRUS-1D Software Package for Simulating the Movement of Water, Heat, and Multiple Solutes in Variability Saturated Media, Version 3.0.* Department of Environmetal Sciences University of California Riverside, Riverside, California, USA. 270 pp.

Steenhuis, T.S., Jackson, C., Kung, K.J.S., Brutsaert, W.H., 1985. Measurement of groundwater recharge on eastern Long Island. *J. Hydrol.* 79 (1-2), 145-169.

van Genuchten, M. Th., 1980. A closed-form equation for predicting the hydraulic conductivity of unsaturated soils. *Soil Sci. Soc. Am. J.* 44, 892-898.

Young, M.H., Sisson, J.Y., 2002. Tensiometry. In: Dane, J., Topp, C. (Eds.), Methods of soil analysis, Part 4, SSSA Book Series: 5, Am. Soc. Agron., Madison, WI. pp. 575-609.

Chapter 5

Tritium tracer test. Multiphase transport approach*

5.1 Introduction

Among the available methodologies, isotopic methods integrate all of the processes that jointly affect water flow in the vadose zone, such as infiltration, evapotranspiration and recharge (*Allison et al.*, 1994; *Dunger*, 1995). Moreover, they allow direct measurement of water movement. An additional advantage is that tracer diffusivity shows less variability to changes in water content and soil type than soil water diffusivity (*Allison*, 1987). Thus, tracer behaviour represents a very robust indicator of water movement in soil and has been used to obtain quantitative estimates of water flux. In (semi-)arid regions, the main process of solute transport through the vadose zone may be solute diffusion in the aqueous phase or solute diffusion in the aqueous and gas phase when the solute is volatile (*Barnes et al.*, 1994; *Joshi et al.*, 1997).

Tritium (^{3}H half-life 12.33 yr) is almost an ideal tracer, as it is chemically identical to hydrogen and thus directly interacts with water and organic substances. In addition, its behaviour

* This chapter is based on the article: Jiménez-Martínez, J., Tamoh, K., Hunkeler, D., Candela, L. Vadose zone tritium tracer test to estimate aquifer recharge from irrigated areas. Multiphase transport approach (submitted to *Water Resources Research*)

differs considerably from other radionuclides in the environment (*Raskob*, 1995) and from other more commonly used tracers, such as bromide, which can move faster as a result of anion exclusion (*Wang et al.*, 2008). Tritium is frequently used to trace the movement of water in natural systems. Tritiated water (HTO_l) has a volatile character, gas phase, named HTO_g for simplicity. Tritiated water can easily diffuse in ordinary water and move with it, either in liquid phase or in vapour phase (see Figure 5.1). If soil is covered with vegetation, root water uptake and the subsequent loss of HTO_l by vapour exchange with the atmosphere through stomata (*Kline and Stewart*, 1974) constitutes an important sink of the HTO_l stored in the soil.

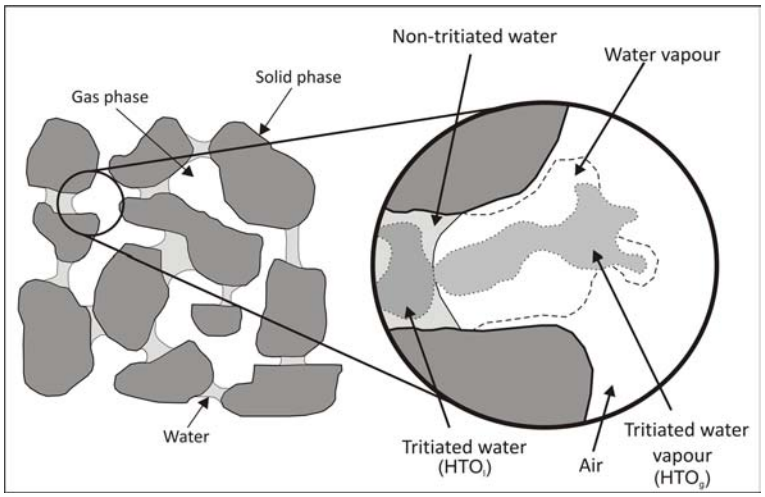

Figure 5.1: Conceptual scheme for tritiated and non-tritiated water behaviour in liquid and gas phase within an unsaturated porous media.

Several studies using tritiated water to establish the soil water balance for different ground covers and weather conditions have been undertaken, among them *Araguás-Araguás et al.* (1995) and *Scanlon* (1992) can be cited. In the first one, the authors compared the effective infiltration rate in forested soil and grassland in humid tropical climate. The water infiltration was 1465 and 1850 mm yr^{-1}, respectively. In the second study, ^{36}Cl and tritium were used to evaluate liquid and vapour water flow in a desert climate (bare soils); non-isothermal simulations showed that annual net downward vapour flux was consistent with the tracers experimental data. In arid regions a deeper penetration of tritium than ^{36}Cl was observed, which is attributed to enhanced downward movement of tritium in vapour phase, fact being negligible in humid regions. The infiltration rate calculated from ^{36}Cl was 1.4 mm yr^{-1}, whereas the one tritium based was 7 mm yr^{-1}. The difference of infiltration between the two tracers suggested a vapour flux presence of

approximately 6 mm yr^{-1}. Good agreement was achieved between simulations and field measurements in both studies, with the exception of forested soil, which could not be properly reproduced by the model.

Modelling the alternate upward and downward transport of tritium close to the ground surface generally requires rather complex models and detailed input, as tritium concentration varies sharply and is very sensitive to many interrelated factors, including rainfall amount, evapotranspiration rate or root depth. Many numerical models exist to predict tritium migration throughout the unsaturated zone. Such models, which have been generally developed by atomic energy agencies, can be used to predict the effect of tritiated rain or the reemission of tritium from polluted groundwater to the atmosphere throughout the vadose zone (*Täschner et al.*, 1995; *Garcia et al.*, 2009). They can also be used to calculate the absorbed mass by plants and food (organically bound tritium, OBT) (*BIOMOVS II*, 1996). A comparison of various existing codes has been presented by *Barry et al.* (1999) and *Belot et al.* (2005). In other research papers (*Logsdon et al., 2002*; *Mayers et al.*, 2005) common numerical models for hydrological studies, such as MACRO (*Larsbo and Jarvis*, 2003) or TOUGH2 (*Pruess et al.*, 1999), have been applied to simulate tritium transport in unsaturated porous media. Most of the existing models have been defined under isothermal and monophasic conditions or hardly consider the role of the plant.

In this chapter, an experimental method for a tritium tracer test in the field and a numerical model approach to estimate aquifer recharge from irrigated farmland are described. The present study was carried out in the study site. The modelling approach utilized was SOLVEG (*Yamazawa and Nagai*, 1997; *Yamazawa*, 2001), a one-dimensional numerical model for simulating transport of heat, water and tritiated water in liquid and gas phase through a bare soil. The code was modified and adapted for this study to include ground cover, root growth and root water uptake. The main objective of the study was to estimate aquifer recharge from farmland, taking into account the fact that tritium is a very effective tracer for investigating water movement through the unsaturated zone. The aim was to establish an accurate water balance under the aforementioned conditions, from of an accurate tritium mass balance obtained in a field experiment with relatively low sampling density (from soil drilling).

5.2 Materials and methods

5.2.1 Field site and experiment

The test was conducted in a neighbouring experimental plot (Figure 5.2) to the previously described in chapter 4.2. The plot was managed under the same condition including crop rotation (lettuce and melon), drip irrigation and plastic cover for summer crops. To avoid boundary effects, the plot sides were also cultivated under the same agricultural management and crops.

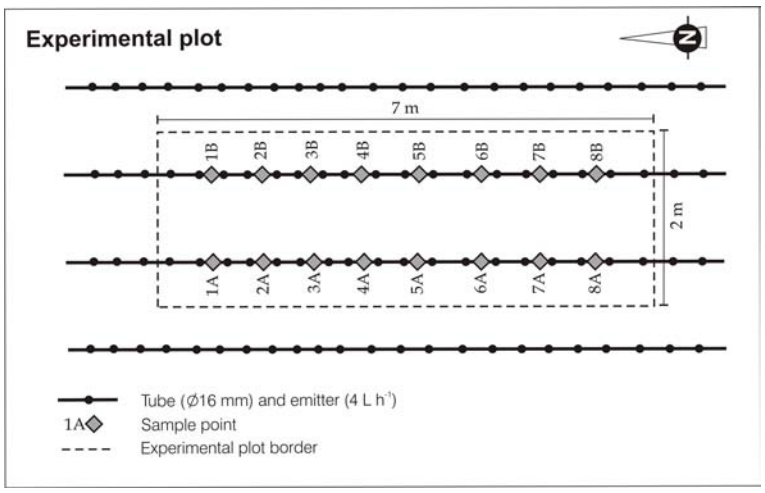

Figure 5.2: Experimental plot and sample points.

Isotope content (deuterium ^{2}H; oxygen ^{18}O) in precipitation, including tritium (^{3}H), was obtained from a station that belongs to the Global Network Isotopes in Precipitation (*GNIP/IAEA*, 2009), located 15 km NE to experimental plot.

In June 2007, a solution of tritiated water (12 L) at a concentration of $7.3 \cdot 10^{8}$ Bq m^{-3} was sprinkled (simulated rainfall) over the plot. Subsequently, 250.2 L of tracer-free water was applied to the soil surface to push down the labelled water and to reduce tracer losses due to evaporation. The solution was prepared at the study site before application. Soil profile monitoring for tritium transport was performed by destructive sampling.

Soil cores were obtained by hand drilling and the maximum depth was 180 cm. Soil samples from cores, representative for a depth interval of 10 cm, were taken at regular depth intervals and given times, and the sampled length was determined from the expected tracer concentration profile. To prevent possible contamination from overlying layers, soil samples were taken from the inner part of the core and immediately stored in leak proof bottles and transported in iceboxes to avoid tritium loss by evaporation.

The experiment took place from 17 May 2007 to 21 August 2008, during four crop periods. The most intensive data collection for model calibration took place during the first crop (melon) from 17 May to 10 September, noted as day of year (DOY) 137-253 (DOY 1 = 1st January 2007), between the tracer injection day and the harvest of this crop (DOY 170-253). To validate the model the following sampling surveys, included in the rest of crops, were used: the first one (lettuce) was between 25 September and 24 December 2007 (DOY 268-358), the second (lettuce) was between 3 January and 2 April 2008 (DOY 368-458) and finally, the last one (melon with plastic cover) was from 3 April to 21 August 2008 (DOY 459-599).

5.2.2 Analytical methods

A volume of 0.07 L deionized water was added to 450 g of soil samples from the cores to obtain the needed water volume for tritium analysis. Subsequently, samples were centrifuged and the resulting pore water was subjected to a process of simple distillation to eliminate coloration, organic matter, and salts that might interfere with the analysis. The distilled samples were then mixed with a scintillation solution (Ultima Gold LLT). The samples were analyzed at the CEDEX-Isotopic Technique Lab., using a liquid scintillation alpha-beta spectrometer (Tri-Carb 2560 TR/XL, Packard Instruments), which enables the measurement of very low-level radioactivity ($2 \cdot 10^{-3}$ Bq m^{-3}). Finally, pore water tritium concentration of each soil sample was recalculated.

5.3 Numerical model

The field tritium tracer test was simulated using SOLVEG (*Yamazawa and Nagai*, 1997; *Yamazawa*, 2001), a one-dimensional finite-difference numerical model for simulating transport of

heat, water in liquid and gas phase, and tritiated water in liquid (HTO_l) and gas (HTO_g) phase through unsaturated bare soil, as well as soil-atmosphere exchange. Radioactive decay is also considered. In SOLVEG advection and diffusion terms are resolved with an explicit and semi-implicit scheme, respectively. The code was adapted to the current experiment by including the tritium processes related to ground cover, root growth and root water uptake. The boundary conditions were also modified. Hourly data values were used to solve the aforementioned items.

Although isotopically different, HTO_l and H_2O molecules behave in a similar way. For example, no exiting fractionation processes are produced as a result of evaporation and transpiration. However, differences between reemission and evaporation processes exist. Reemission is a mechanism that generally acts during nighttime and depends on HTO_l content in the uppermost soil layer and the concentration of HTO_g in the air adjacent to the soil surface (*Ingraham and Criss*, 1993; *Slattery and Ingraham*, 1994; *Ingraham and Criss*, 1998). During daytime, reemission is coupled to the evaporation process (*Täschner et al.*, 1997). The differences between reemission and evaporation are shown in the numerical model that is presented below.

5.3.1 Water flow and vapour

A table containing parameters definition and the symbols used in the numerical model has been included at the end of the chapter for the sake of clarity.

The model simulates water content θ and the specific humidity of soil air W_a along the soil profile. The classical Richard's equation is used for the liquid water movement, being the volumetric water content the dependent variable. The equation has additional terms concerning transpiration (via root water uptake) and evaporation-condensation, sinks/sources of water:

$$\frac{\partial \theta}{\partial t} = -\frac{1}{\rho_w}\left[\frac{\partial q}{\partial z} + (E_e + E_t)\right] \qquad [5.1]$$

where the vertical flow of water is expressed as:

$$q = -\rho_w \left[D(\theta) \frac{\partial \theta}{\partial z} + K(\theta) \right] \qquad [5.2]$$

The equation for water vapour contains a diffusion term and an evaporation-condensation term:

$$\frac{\partial (\theta_s - \theta) W_a}{\partial t} = \frac{\partial}{\partial z} \left[D_{wa} \tau_a(\theta) \frac{\partial W_a}{\partial z} \right] + \frac{E_e}{\rho_a} \qquad [5.3]$$

The model does not consider the advection of soil air, which might be caused by air pressure variations at the ground surface or by the infiltration of water. $\tau_a(\theta)$ is the tortuosity for soil air at volumetric water content θ. As in *Jackson et al.* (1974), the model uses $\tau_a(\theta) = (\theta_s - \theta)/1.5$.

Regarding sink/source terms of water, E_t represents the root water uptake due to transpiration, whereas the evaporation-condensation of water in soil is expressed as:

$$E_e = \frac{\rho_a}{r_e(\theta)} \left[W_{sat}(T_s) - W_a \right] \qquad \text{when} \qquad W_{sat}(T_s) > W_a \qquad [5.4]$$

Eq. [5.4] is based on the concept that the driving force of evaporation-condensation in soil is the difference of specific humidity between the evaporation site (the surface of the soil water) and the pore air. Moreover, evaporation is regulated by the density of moist air ρ_a, as a function of the temperature, and the evaporation resistance r_e, experimentally determined for the main soil types (loam, silt, sand, clay loam, silty sand or silty loam, among others) as a function of θ (*Kondo and Saigusa*, 1994; *Kondo and Xu*, 1997). It is assumed that water condensation occurs in a very short time to keep the specific humidity of soil air lower than or equal to the saturation specific humidity at the soil temperature.

The upper boundary condition of Eq. [5.1] is determined by the continuity of liquid water flux at the ground surface:

$$q_0 = \begin{cases} q_{s0} = -\rho_w K_s & \theta_0 \geq \theta_{s0} \\ -(P + I) + E_r & \theta_0 < \theta_{s0} \end{cases} \qquad [5.5]$$

where E_r is the amount of runoff and q_{s0} the maximum infiltration flux when the soil is saturated. When soil water exceeds the saturated soil water content (θ_{s0}), the model assumes that excess water is stored at the ground surface, therefore $E_r = 0$. The lower boundary condition corresponds to free drainage.

The boundary condition for the specific humidity (W_a) in Eq. [5.3] can be determined by the following equation:

$$E_0 = -\rho_a D_{wa} \tau_a(\theta) \left. \frac{\partial W_a}{\partial z} \right|_{z=0} + E_{e0} \qquad [5.6]$$

where

$$E_{e0} = \int_{-\delta z_0}^{0} E_e dz \qquad [5.7]$$

and

$$E_0 = \rho_a c_E \left| u_r \right| (W_{a0} - W_r) f(t) \qquad [5.8]$$

This boundary condition assumes that water vapour flux from the ground surface to the atmosphere is composed by the sum of diffused water vapour flux from inside the uppermost soil layer and by direct evaporation from the surface (δ_{z0}-thick) in contact with the atmosphere. c_E is the bulk transfer coefficient, a thermodynamic coefficient dependent on wind velocity among other meteorological variables (*Matsushima and Kondo*, 1995), which enables us to estimate the evaporation efficiency from bare soil. As natural crop growth typically follows an S-shaped pattern (e.g. *Overman and Scholtz*, 2002), a sigmoid curve $f(t)$ has been used to represent the ground cover in the model. When a crop is first planted, the ground cover is non-existent, the *potential* evaporation is maximal, and thus $f(t) = 1$. Conversely, when the crop reaches the mid-season growth stage, ground cover is complete, evaporation is zero, and thereafter $f(t) = 0$. All that remains is to specify the transition from $f(t) = 1$ at planting to $f(t) = 0$ at the beginning of the mid-

season growth stage. Table 4.3 provides data on the length (days) of the growth stages (*Allen et al.*, 1998).

5.3.2 Soil hydraulic properties

The water retention $h(\theta)$ and hydraulic conductivity $K(\theta)$ curves were estimated using the power law equations of *Campbell* (1974). This type of formulation was originally used in the first version of SOLVEG (*Yamazawa and Nagai*, 1997; *Yamazawa*, 2001), due to its numerical simplicity. It is given by:

$$h(\theta) = h_s \left(\frac{\theta}{\theta_s} \right)^{-b} \quad [5.9]$$

$$K(\theta) = K_s \left(\frac{\theta}{\theta_s} \right)^{2b+3} \quad [5.10]$$

where b is the pore size distribution index and $2b+3$ is the pore disconnectedness index.

The soil water diffusivity is expressed by:

$$D(\theta) = K(\theta) \frac{\partial h}{\partial \theta} \quad [5.11]$$

Table 5.1 lists soil parameters that are used in the model obtained in laboratory (θ_s) and from the literature (K_s, h_s and b) (*Clapp and Hornberger*, 1978 and *Cosby et al.*, 1984).

5.3.3 Tritiated water (HTO_l) flow and vapour (HTO_g)

The two equations of the one-dimensional form for the transport of tritium in liquid (HTO_l) and gas (HTO_g) phases respectively are:

$$\frac{\partial \theta C_w}{\partial t} = -\frac{1}{\rho_w}\frac{\partial q C_w}{\partial z} + \frac{\partial}{\partial z}\left[D_T \frac{\partial C_w}{\partial z} \right] - (e_e + e_t) \qquad [5.12]$$

$$\frac{\partial (\theta_s - \theta) C_a}{\partial t} = \frac{\partial}{\partial z}\left[D_{Ta} \tau_a(\theta) \frac{\partial C_a}{\partial z} \right] + e_e \qquad [5.13]$$

Both equations are linked by the evaporation-condensation term inside the soil, e_e:

$$e_e = \frac{\rho_a}{r_e(\theta)}\left[\frac{W_{sat}(T_s) C_w}{\rho_w} - \frac{C_a}{\rho_a} \right] \qquad [5.14]$$

As for the non-tritiated water, this term is controlled by the evaporation resistance r_e. The mass of tritium extracted by root water uptake corresponds to the product of root water uptake and HTO_l concentration at each depth.

The gas phase equation (Eq. 5.13) only includes a diffusion term, whereas the liquid phase equation (Eq. 5.12) includes the advection and hydrodynamic dispersion (effective diffusion-dispersion) terms. The latter includes molecular diffusion and mechanical dispersion, which is a function of the velocity of water flow in soil (Table 5.1):

$$D_T = \tau_w(\theta) D_{Tw} + \frac{\lambda q}{\rho_w} \qquad [5.15]$$

The surface boundary condition for the liquid phase (HTO_l) equation (Eq. 5.12) is specified by an additional term for the top layer only (the ground surface), and expresses a gain in HTO_l, due to precipitation plus irrigation. Mass dilution due to precipitation plus irrigation is indirectly accounted for by the increase in water content on the left hand side of Eq. [5.12]. HTO_l evaporation from the ground surface to the atmosphere is expressed in a similar manner as that of non-tritiated water, but independently:

$$e_0 = -D_{Ta}\tau_a(\theta)\left.\frac{\partial C_a}{\partial z}\right|_{z=0} + e_{e0} \qquad [5.16]$$

where

$$e_{e0} = \int_{-\delta z_0}^{0} e_e dz \qquad [5.17]$$

and

$$e_0 = c_E \left|u_r\right| (C_{a0} - C_r) f(t) \qquad [5.18]$$

5.3.4 Heat conduction and thermal characteristics

The heat conductivity of soil is obtained according to the *McCumber and Pielke* (1981) formulation, which states that the relationship between soil thermal conductivity, $\lambda_t(\theta)$, and soil water potential is nearly independent of the soil type. This relation comes from fitting *Al Nakshabandi and Kohnke's* (1965) data.

Soil temperature, T_s, is expressed as a one-dimensional heat conduction equation:

$$\frac{\partial T_s}{\partial t} = \frac{\partial}{\partial z}\left(k_s \frac{\partial T_s}{\partial z}\right) + \frac{H_b}{M_s \rho_s} - \frac{M_w q}{M_s \rho_s}\frac{\partial T_s}{\partial z} \qquad [5.19]$$

The equation is composed of three terms from left to right: a conduction term, where k_s is the thermal diffusivity $\left(k_s = \lambda_t(\theta)/M_s\rho_s\right)$ and $M_s\ \rho_s$ is the volumetric heat capacity of soil as a function of θ and the specific heat for both solid and water along with their respective densities (*Campbell and Norman*, 1998); a latent heat exchange term (sink/source of heat) for soil water evaporation-condensation ($H_b = l\ E_e$; l is the latent heat of vaporization of water as function of temperature); and an advection (convection) heat transport term, due to liquid water movement. The heat conduction through plant root is assumed to be negligible.

Table 5.1: Summary of input parameter values.

Parameter			Value	Unit
Soil physical properties				
		Sand	15.79	%
	Textural fractions	Silt	79.32	%
		Clay	4.89	%
	Bulk density	ρ_s	1560±120	kg m^{-3}
Soil hydraulic properties				
	Saturated water content	θ_s	0.372	m^3 m^{-3}
	Saturated pressure head	h_s	-0.759 [a b]	m
	Saturated hydraulic conductivity	K_s	0.281 10^{-5} [a b]	m s^{-1}
	Pore size distribution index	b	5.33 [a b]	-
Flow and transport				
(liquid and gas phase)	Water density	ρ_w	1000	kg m^{-3}
	Water vapour diffusion coeff. in air	D_{wa}	2.60 10^{-5} [c]	m^2 s^{-1}
	Molecular HTO_g diffusion coeff. in air	D_{Ta}	2.47 10^{-5} [d]	m^2 s^{-1}
	Molecular HTO_l diffusion coeff. in water	D_{Tw}	2.24 10^{-9} [e]	m^2 s^{-1}
	Dispersivity of HTO_l	λ	0.05 [f]	m
Thermal properties				
	Specific heat of solids	M_{solid}	733 [g]	J kg^{-1} K^{-1}
	Specific heat of water	M_w	4186 [g]	J kg^{-1} K^{-1}

[a] *Clapp and Hornberger* (1978); [b] *Cosby et al.* (1984); [c] *Cussler* (1997); [d] *Mayers et al.* (2005); [e] *Mills* (1973); [f] *Yamazawa* (2001); [g] *Farouki* (1986)

The upper boundary condition for soil temperature equation (Eq. 5.19) is a ground surface heat budget equation; although the latent heat exchange term is not included in it since the water vapour flux is resolved in Eq. [5.3] (*Yamazawa and Nagai*, 1997; *Yamazawa*, 2001). Constant soil temperature is assumed as lower boundary condition.

5.3.5 Root water uptake and root growth

Root water uptake due to transpiration is considered a water and HTO_l sink term. To estimate transpiration, reference evapotranspiration, ET_0, at hourly time steps, obtained through Penman-

Monteith method, is used (e.g. *Kashyap and Panda*, 2001). The *potential* evapotranspiration ET_p was then given by (*Allen et al.*, 1998):

$$ET_p = K_c ET_0 \quad [5.20]$$

where K_c is a crop-specific coefficient that characterizes plant water uptake and evaporation relative to the reference crop. Figure 4.2 illustrates the time variation of K_c in terms of annual crop growth stage. The *Allen et al.* (1998) method and K_c data for each specific crop and growth stage (Table 4.3, Figure 4.2) were used. *Allen et al.* (1998) provide data on the length of the growth stages and the values of K_c for various crops.

Potential evaporation E_p can be calculated according to (e.g. *Kroes and Van Dam*, 2003; *Pachepsky et al.*, 2004):

$$E_p = ET_p \exp^{-\beta \cdot LAI(t)} \quad [5.21]$$

where β (≈ 0.4) is the radiation extinction coefficient and $LAI(t)$ is the leaf area index. However, $LAI(t)$ data were not available, so instead E_p was calculated:

$$E_p = ET_p f(t) \quad [5.22]$$

Where $f(t)$ is the function specified above (Chapter 5.3.1).

Given ET_p and E_p according to Eqs. [5.20] and [5.22], the *potential* transpiration T_p was obtained as:

$$T_p = ET_p - E_p \quad [5.23]$$

The *potential* transpiration, defined as the water removed from the soil due to plant water uptake, is equally distributed over the root zone. This sink term was computed by a method introduced by *Campbell and Norman* (1998), which is based on soil water status. *Actual* transpiration, E_t, is calculated according to *Feddes et al.* (1978):

$$E_t(\theta) = \alpha(\theta)\frac{T_p}{z_{root}} \qquad [5.24]$$

where $\alpha(\theta)$ is the dimensionless water stress response function ($0 \leq \alpha \leq 1$) describing water uptake reduction due to drought stress. For $\alpha(\theta)$, a modified functional form introduced by *Feddes et al.* (1978) was applied:

$$\alpha(\theta) = \begin{cases} 1, & \theta_3 \leq \theta < \theta_s \\ \dfrac{h(\theta) - h_4}{h_3 - h_4}, & \theta_4 \leq \theta < \theta_3 \\ 0, & \theta \leq \theta_4 \text{ or } \theta = \theta_s \end{cases} \qquad [5.25]$$

where h_3 and h_4 are threshold parameters, in a sense that uptake is at the potential rate when the water content is between θ_3 and θ_s. This drops off when $\theta < \theta_3$ and becomes zero for $\theta < \theta_4$ or $\theta = \theta_s$. Crop-specific values for the parameters (Table 5.2) were taken from *Wesseling* (1991) and *Taylor and Ashcroft* (1972).

Table 5.2: Root water uptake reduction parameters for Eq. [5.25] (source: *Wesseling*, 1991; *Taylor and Ashcroft*, 1972).

Crop	h_3 (m)	θ_3 (m^3 m^{-3}) (Eq. 5.9)	h_4 (m)	θ_4* (m^3 m^{-3}) (Eq. 5.9)
Melon	-4	0.270	-80	0.154
Lettuce	-5	0.259	-80	0.154

*wilting point

A root growth model is required to simulate the change in rooting depth with time for annual crops. The model assumes the classical Verhulst-Pearl logistic growth function, and attains a maximum depth at the end of the crop development stage. Values for the maximum rooting depth for particular crops (Table 4.3) were derived from *Allen et al.* (1998).

The surface boundary condition, which shows daily values of precipitation, irrigation and T_p, are summarized in Figure 5.3.

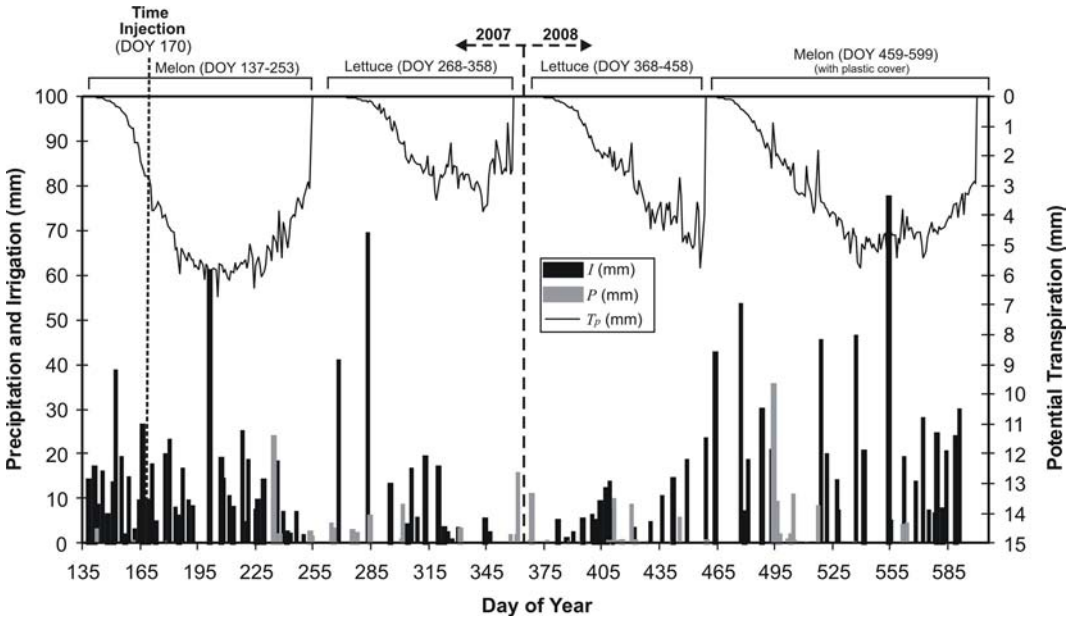

Figure 5.3: Summary of the soil surface boundary conditions (I = irrigation; P = precipitation; T_p = *potential* transpiration).

5.4 Results and discussion

5.4.1 Field data

Figure 5.4 shows the HTO_l soil water concentration measured along the soil profile in the four sampling surveys developed during the initial part of the experiment (DOY 170-253), which was carried out during the first crop (melon). For this period, rainfall accounted for 28 mm, irrigation for 358 mm and *potential* evapotranspiration was 426 mm. At the end of this first period, HTO_l migration attained a maximum depth of 60 cm after 73 days. In Figure 5.5, the HTO_l profiles for

the following three cropping periods (DOY 254-599) are shown. Background HTO_l concentration in the soil profile was 925 Bq m^{-3} and the movement of the tracer's peak centre of mass through the soil profile is clearly observed in the sampling campaigns. In general, the relative standard deviation (%) from laboratory samples analyses was lower for high HTO_l concentration values. The HTO_l concentration decreased exponentially due to plant transpiration, evaporation and *"night-reemission"*, which was a result of the high soil and atmosphere tritium concentration gradient during the first days of the experiment.

5.4.2 Model calibration and predictions

The period between tracer injection day and the harvest of the first crop (170-253 DOY) was used for model calibration. The initial input parameters for modelling (Table 5.1) resulted in simulations that were in poor agreement with the field data. Therefore manual calibration process was carried out. Several parameterizations were considered by varying the number and type of parameters and following the principle of parsimony (i.e. fewer fitted parameters). The best parameterization was found for two parameters: saturated hydraulic conductivity of soil, K_s, and dispersivity, λ. θ_s and ρ_s were obtained in the laboratory, some parameters of Table 5.1 were considered fixed (ρ_w; D_{wa}; D_{Ta}; D_{Tw}; M_w; M_{solid}) and the rest of them were taken from literature, according to a given soil type (h_s; b).

Several statistics to assess goodness-of-fit between the observed and simulated values were used: the root mean square error (*RMSE*), the mean absolute error (*MAE*), and the mean relative error (*MRE*). Final fitted parameters were obtained by minimizing the objective function (*MRE*) and by visual inspection of the model fit to the data. *MRE* was selected as objective function because trirtium mass decay in soil occurred in an exponential way. The final fitted parameter values are given in Table 5.3.

Figure 5.4 shows measured and calibrated HTO_l concentration soil profiles. The most prominent feature for the calibrated period (DOY 170-253) is the strong decrease of HTO_l concentration in soil. Although experimental data are relatively sparse and the maximum concentration decreases by three orders of magnitude after seventy days, the predicted pattern of HTO_l concentration is generally in good agreement with data. Table 5.4 gives goodness-of-fit results for calibrated data.

Table 5.3: Initial and fitted parameter values.

Parameter	Initial value	Fitted value
Saturated hydraulic conductivity, K_s (m s^{-1})	0.281 10^{-5}	0.868 10^{-5}
Dispersivity of HTO_l, λ (m)	0.05	0.10

After calibration, the model was used to predict HTO_l and HTO_g transport during the growing periods of three more crops (DOY 254-599) and results are presented in Figure 5.5. The agreement between field observations and simulations appears to be better than *MRE* results, probably due to the gradual decrease of HTO_l in the soil and the lower influence of soil-atmosphere processes. Goodness-of-fit results are given in Table 5.4.

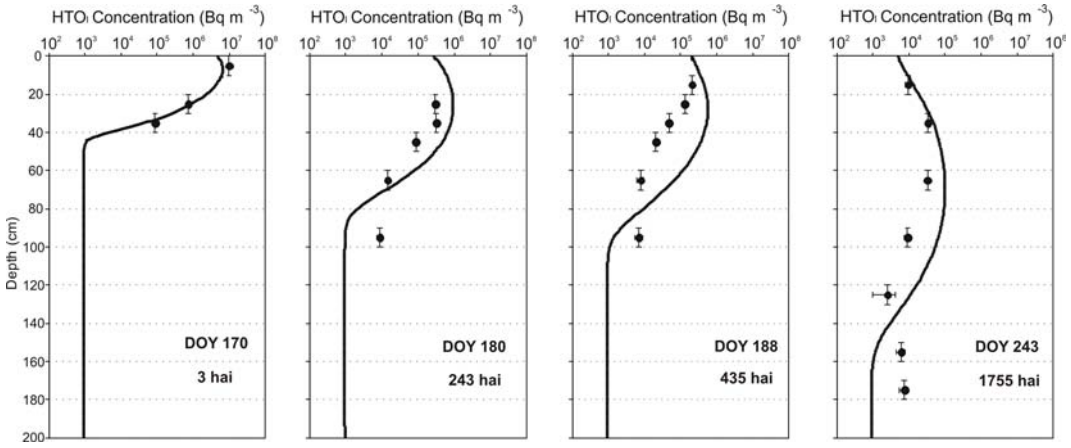

Figure 5.4: Measured (dots) and simulated (solid lines) tritium content (HTO_l) profiles for the calibration period (DOY 170-253, during melon crop). Mean and standard deviation (horizontal bars), and sampled interval (vertical bars) are shown for the experimental values. hai: hours after injection.

Presence of HTO_l in sampled profiles at higher depths than simulated can be explained by preferential flow generation through roots and cracks within the first centimetres of the soil surface (tilled soil). In addition, only one water retention $h(\theta)$ and hydraulic conductivity $K(\theta)$ curve were considered for the total soil profile, they could also account for the difference.

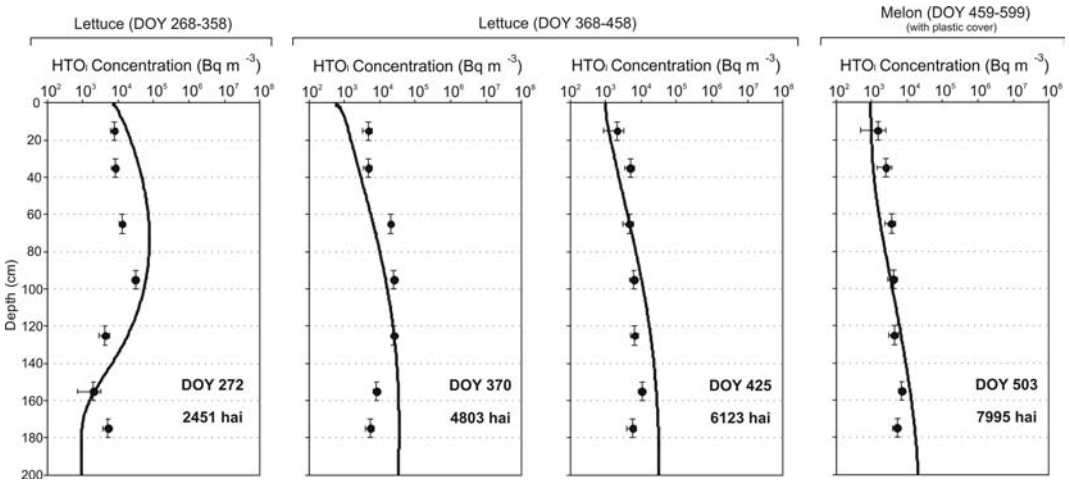

Figure 5.5: Measured (dots) and simulated (solid lines) tritium content (HTO_l) profiles for the predicted period (DOY 254-599, during three cropping periods). Mean and standard deviation (horizontal bars), and sampled interval (vertical bars) are shown for the experimental values. hai: hours after injection.

Table 5.4: Goodness-of-fit for simulated and experimental values.

Simulation	*RMSE*[a]	*MAE*[b]	*MRE*[c]
Melon (DOY 137-253) (calibration)	785158.1	326002.7	0.580
Lettuce (DOY 268-358) (prediction)	29031.6	21505.1	0.706
Lettuce (DOY 368-458) (prediction)	14238.8	10375.3	0.686
Melon (DOY 549-599) (prediction) (with plastic cover)	4634.8	3224.3	0.530
Total prediction period (DOY 254-599)	17817.2	11370	0.681

[a] Root mean square error, $RMSE = \sqrt{\frac{1}{n}\sum_{i=1}^{n}(x_i - y_i)^2}$ [b] Mean absolute error, $MAE = \frac{1}{n}\sum_{i=1}^{n}|x_i - y_i|$

[c] Mean relative error, $MRE = \frac{\frac{1}{n}\sum_{i=1}^{n}|x_i - y_i|}{\frac{1}{n}\sum_{i=1}^{n}|y_i|}$

5.4.3 Temperature soil profiles

Simulated soil temperature following diurnal variations is illustrated in Figure 5.6. For the sake of simplicity, only temperature (ºC) at 1, 10, 30, 50 and 100 cm depth along with the air temperature for a one summer day (Figure 5.6a) and one winter day (Figure 5.6b) have been presented. The predicted summer temperatures decrease with depth during the day, while the opposite behaviour was observed during winter. For both seasons, the maximum temperature at the ground surface was between 12 and 18 pm.

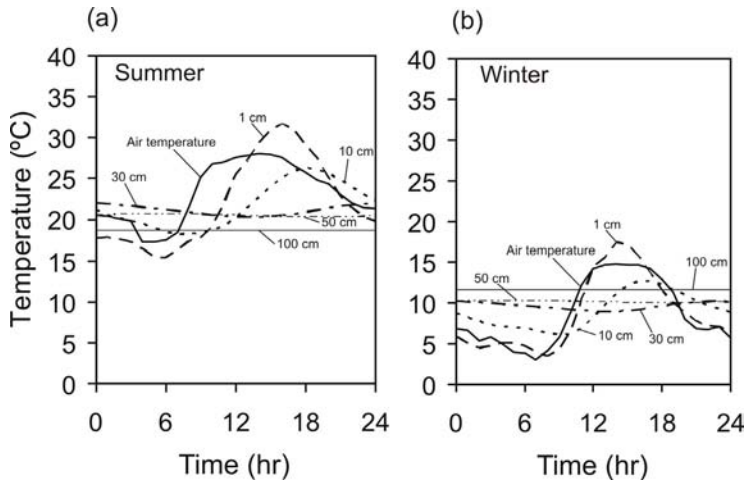

Figure 5.6: Diurnal variation of predicted soil temperature for (a) June 22, 2007 (DOY 173), and (b) January 22, 2008 (DOY 387).

5.4.4 Tritium transport and mass balance

The transport of HTO_l includes the advection and hydrodynamic dispersion terms (Eq. 5.15). Hydrodynamic dispersion (D_T) is defined as the sum of effective molecular diffusion (D_p) and mechanical dispersion (D_d). D_p, also called *pore diffusion*, is a function of molecular diffusion coefficient in free solution (D_{Tw}) and the tortuosity of the medium as function of water content (τ_w), $D_p = \tau_w(\theta) D_{Tw}$. D_{Tw} was taken directly from the literature (*Mills*, 1973) and was used to determine the range of possible values of D_p. Previous research on clay soils (bentonite, kaolinite, montmorillonite) reported D_p values for tritium between $4.5 \cdot 10^{-4}$ mm^2 s^{-1} and $17 \cdot 10^{-4}$ mm^2 s^{-1} (*Phillips and Brown*, 1968; *Gillham et al.*, 1984). *Young and Ball* (1998) found D_p in the range of

3.8-5.9·10^{-4} mm^2 s^{-1} for a soil with 35% clay, 38% silt, and 27% sand. *Toupiol et al.* (2002) reported a value of D_p ranges between 4 and 8·10^{-4} mm^2 s^{-1} for a compacted soil with 30% clay, 33% silt, and 37% sand. For this study (silty loam) D_p was estimated between 2.4·10^{-4} mm^2 s^{-1} and 4.7·10^{-4} mm^2 s^{-1} (10^{-10} m^2 s^{-1}). On the other hand, mechanical dispersion is equal to the product of the seepage velocity v_s ($v_s = q/\theta$) and the dispersivity λ ($D_d = \theta\, v_s\, \lambda$), as shown in Eq. [5.15]. While advection controls the transport of HTO_l in all soil profile, mechanical dispersion (D_d) decrease with depth and effective molecular diffusion (D_p) stay more or less constant along the profile (Eq. 5.12).

Transport of HTO_g only includes the diffusion term, effective molecular diffusion or *pore diffusion* (Eq. 5.13). The model was run including in the Eq. [5.13] the advection term for HTO_g that supposes diffusion of non-tritiated vapour in air (Eq. 5.3). The obtained results with the included change were equal that those obtained considering only effective molecular diffusion. This fact supports that the main transport process of HTO_g is molecular diffusion.

Hourly tritium concentration in the soil vapour (HTO_g) at different depths is shown in Figure 5.7 for the calibration period (first crop experiment, DOY 170-253). A seasonal diurnal variation in HTO_g concentration, which was directly related to meteorological parameters (Figure 5.6), along with a trend to decrease with depth, is observed. Soil heat storage in the daytime favours HTO_l evaporation to HTO_g in the soil media. Subsequently, at sunset, condensation begins (Eq. 5.14). Within the first centimetres of soil (the surface), the decline of HTO_g concentration during the night time is reinforced by *"night-reemission"*. After application of a large volume of water (precipitation or irrigation), the increase in HTO_g concentration at greater depths is due not only by the downward flux of HTO_l, but also by downward molecular HTO_g diffusion, D_{Ta} (Eq. 5.13).

Tritium mass balance for the total studied period (DOY 170-599) is presented in Figure 5.8. Tritium mass for each water balance component and states have been considered: tritium mass in liquid and gas phase; evaporated and transpirated tritium mass; deep drainage of tritium mass; and radioactive decay. The tritium mass decay after 83 days (1992 hours), between the day of tracer injection and the harvest of the first crop (melon), was 95%. After 429 days, which was the total duration of the field test, the background HTO_l concentration in the soil was practically recovered.

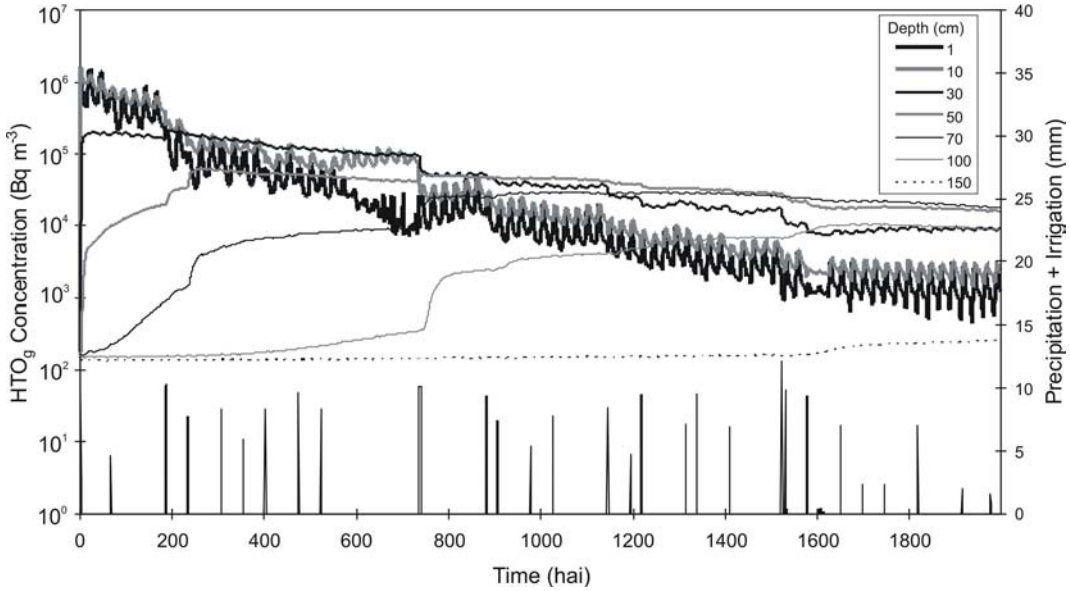

Figure 5.7: Simulated tritium gas concentration (HTO_g) in soil vapour at different depth for the calibrated period (DOY 170-253, during melon crop). (hai): hours after injection.

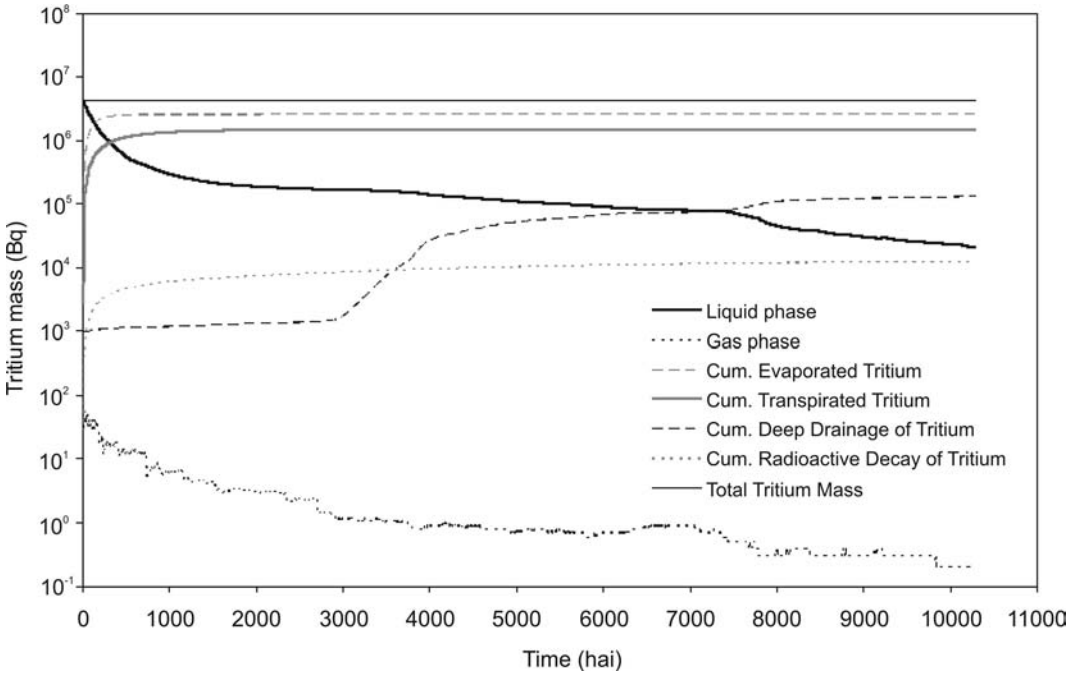

Figure 5.8: Tritium mass included in each water balance components and states, it involves: tritium mass in liquid and gas phase, evaporated and transpirated tritium mass, deep drainage of tritium mass, and radioactive decay. (hai): hours after injection.

5.4.5 Water balance and recharge

One of the objectives of the modelling exercise was to evaluate soil water balance and to calculate recharge rate. The components of the water balance included water addition due to irrigation and precipitation; losses by transpiration, evaporation and drainage; and changes in soil water storage. Potential recharge to the aquifer is made up the drained volume of water from the bottom of the soil profile or irrigation return flow. Simulated drainage permits to determine the recharge rate generated by each crop at different times of the year under two assumptions: small thickness of the unsaturated zone and negligible hypodermic flow rate, as occurs in the study area.

Percentages of applied water ($P + I$) that constitute recharge for each crop are shown in Table 5.5. The high percentage of recharge (48%) generated during the second crop (lettuce, DOY 268-358) was due to high precipitation (197 mm) and lower transpiration between September and December. Differences between the first (14.9%) and fourth (32.3%) crop (melon) are the result of the plastic crop cover, since this type of agricultural management reduces direct evaporation from the ground surface to almost zero (Figure 5.3). The important irrigation dose (77 mm) applied to the experimental plot could also explain this difference. Total recharge for the 2007-2008 hydrological year was 476 mm.

Table 5.5: Simulated bottom drainage (recharge) following applied water ($P+I$) for each crop. Irrigation efficiency calculated from *potential* and *actual* evaportranspiration (volume of irrigation water beneficially used).

Crop	*I* (mm)	*P* (mm)	*I+P* (mm)	Recharge		Irrigation Efficiency (%)†	
				(mm)	(%)	*Potential ET*	*Actual ET*
Melon (DOY 137-253) (calibration)	557	32	589	88	14.9	96	100
Lettuce (DOY 268-358) (prediction)	206	197	403	194	48.1	89	61
Lettuce (DOY 368-458) (prediction)	123	61	184	57	30.9	100	100
Melon (DOY 459-599) (prediction) (with plastic cover)	617	80	697	225	32.3	93	60

†Irrigation Efficiency from *Burt et al.* (1997).

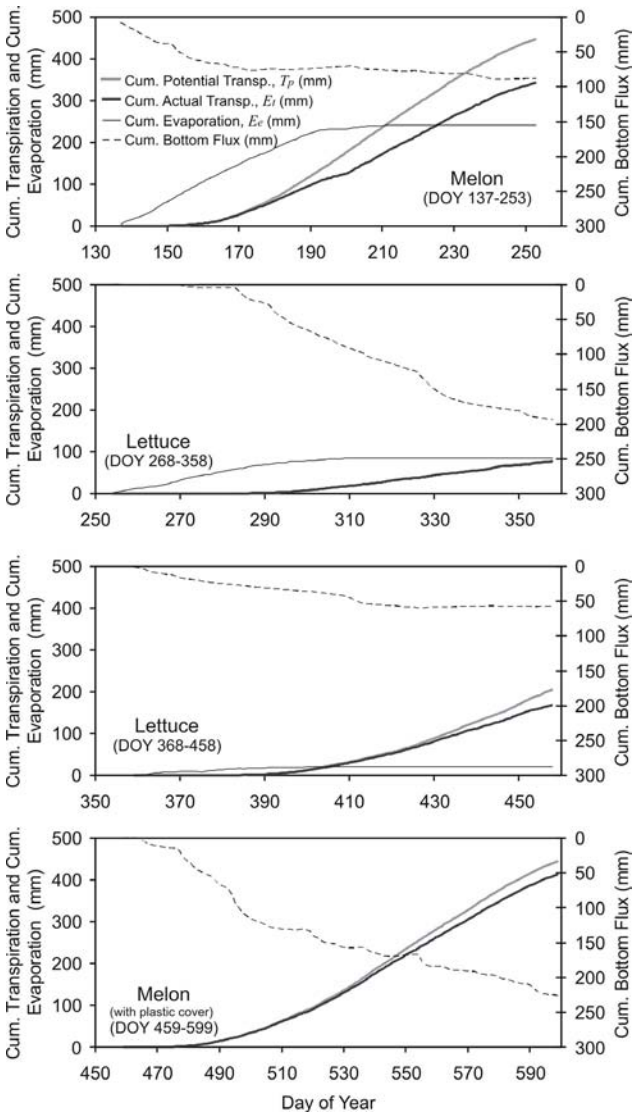

Figure 5.9: Cumulative *potential* transpiration (T_p), *actual* transpiration (E_t), evaporation (E_e) and drainage (recharge) rates computed for the four crops.

Figure 5.9 shows cumulative recharge values along with some water balance components (T_p; E_t; E_e) for the four cropping periods. *Actual* transpiration was lower than the *potential* values in all cases, because soil moisture content was not enough to sustain potential root water uptake (Eqs. 5.24 and 5.25) at several periods of time. This is crucial for recharge calculation in semi-arid regions, in which *actual* evapotranspiration may drop below *potential* rates, even for irrigated systems.

5.5 Conclusions

The defined field experiment and modelling approach appears to be highly suitable for estimating aquifer recharge by irrigation return flow, when small thickness of the unsaturated zone and negligible hypodermic flow rate exist, as occurs in the study area. The main conclusions from this chapter are:

1. Tritium downward movement is clearly observed in the sampling campaigns. The relative standard deviation from laboratory analyses was lower for high tritium concentration value. Numerical solution with two parameters K_s and λ fitted for the soil provided a good agreement between simulations and field measurements, in spite of the relatively low sampling density. The presence of tritium at higher depths than simulated can be explained by several reasons: (i) preferential flow in top soil (roots and cracks); (ii) only one water retention $h(\theta)$ and hydraulic conductivity $K(\theta)$ curve defined for the total soil profile; (iii) water retention $h(\theta)$ (power law) from *Campbell* (1974) do not work well close to saturation.

2. The effective molecular diffusion (D_p) of tritium in liquid phase obtained from this study (silty loam) was estimated between $2.4 \cdot 10^{-4}$ mm^2 s^{-1} and $4.7 \cdot 10^{-4}$ mm^2 s^{-1}. Advection and mechanical dispersion controlled the transport of liquid tritium, whereas molecular diffusion (*pore diffusion*) was the main process for tritium in vapour phase. Diffusion of non-tritiated vapour in air does not meaningfully contribute to the final results for tritium gas transport.

3. Seasonal diurnal variation in tritium gas concentration directly related to seasonal variation of meteorological parameters was observed. The decline of tritium gas concentrations in the top soil during night time is reinforced by *"night-reemission"*.

4. The sink terms of tritium evaporation, transpiration, deep drainage and radioactive decay account for 61.51%, 34.65%, 3.13% and 0.29% tritium losses, respectively. According to modeling, tritium mass balance error was 0.5%. Evaporation and transpiration contribute meaningfully to the decontamination process. After 83 days tritium mass decay was 95 %, and tritium background concentration in soil is practically recovered after 429 days.

5. During the 2007-2008 hydrological year recharge was 476 mm for a water input $P+I$ = 1284 mm. Intensive precipitation events (between September and December) greatly contribute to natural recharge, as high water content prevails in the soil profile due to irrigation.

6. *Actual* transpiration was lower than *potential* values in all cases, despite high irrigation frequency, as soil moisture content was not enough to sustain potential root water uptake at several periods of time.

7. Field investigation and monitoring of tritium present the complexity of profiling tritium concentration in soil and the difficulty of sampling tritium migration through preferential flow. Compared with other available techniques, this methodological approach requires relatively low sampling density.

8. If tritium is used as a tracer, multiphase transport has to be considered for accurate recharge predictions.

Notation

$( )_0$	values at the ground surface
α	dimensionless water stress response function (-)
b	pore size distribution index (-)
β	extinction radiation coefficient (-)
c_E	bulk transfer coefficient for evaporation (-)
C_r	HTO_g concentration at reference height (Bq m^{-3} air)
C_a	HTO_g concentration of soil air (Bq m^{-3} air)
C_w	HTO_l concentration of soil water (Bq m^{-3} water)
D	soil water diffusivity function (m^2 s^{-1})
D_p	effective HTO_l molecular diffusion (pore diffusion) (m^2 s^{-1})
D_d	HTO_l mechanical dispersion (m^2 s^{-1})
D_T	effective HTO_l diffusion-dispersion in water (m^2 s^{-1})
D_{Ta}	molecular HTO_g diffusion coefficient in air (m^2 s^{-1})
D_{Tw}	molecular HTO_l diffusion coefficient in water (m^2 s^{-1})
D_{wa}	water vapor diffusion coefficient in air (m^2 s^{-1})
e_e	evaporation-condensation of HTO_l in soil (kg m^{-3} s^{-1})
e_t	transpiration of HTO_l in soil (kg m^{-3} s^{-1})
E_e	evaporation-condensation of water in soil (kg m^{-3} s^{-1})
E_r	amount of runoff (kg m^{-2} s^{-1})
E_t	actual transpiration due to root water uptake (kg m^{-3} s^{-1})
E_p	potential evaporation (kg m^{-2} s^{-1})
ET_p	potential evapotranspiration (kg m^{-2} s^{-1})
ET_0	reference evapotranspiration (kg m^{-2} s^{-1})
f	ground cover sigmoid function (-)
τ_a	tortuosity for soil air (-)
τ_w	tortuosity for soil water (-)
h	pressure head (m)
h_s	saturated pressure head (m)
H_b	latent heat of evaporation in soil (J m^{-3} s^{-1})
I	irrigation (kg m^{-2} s^{-1})
K	unsaturated hydraulic conductivity of soil (m s^{-1})
K_c	crop-specific coefficient (-)
K_s	saturated hydraulic conductivity of soil (m s^{-1})
k_s	thermal diffusivity of soil (m^2 s^{-1})
l	latent heat of vaporization of water as function of temperature (J kg^{-1})
LAI	leaf area index (m^2 m^{-2})
λ	dispersivity of HTO_l (m)
λ_t	thermal conductivity of soil as function of water content (J s^{-1} m^{-1} K^{-1})
M_s	specific heat of soil (J kg^{-1} K^{-1})
M_{solid}	specific heat of solids (J kg^{-1} K^{-1})
M_w	specific heat of water (J kg^{-1} K^{-1})

P	precipitation (kg m^{-2} s^{-1})
q	vertical liquid water flux (kg m^{-2} s^{-1})
r_e	resistance of evaporation in soil as function of water content (s)
ρ_a	density of moist air as function of temperature (kg m^{-3})
ρ_s	bulk density of soil (kg m^{-3})
ρ_w	density of liquid water (kg m^{-3})
T_p	potential transpiration (kg m^{-2} s^{-1})
T_s	soil temperature (K)
θ	volumetric soil water content (m^3 m^{-3})
θ_s	saturated volumetric soil water content (m^3 m^{-3})
u_r	wind speed at reference height (m s^{-1})
v_s	seepage velocity (kg m^{-2} s^{-1} = 10^{-3} m s^{-1})
W_r	specific humidity of air at reference height (kg kg^{-1})
W_a	specific humidity of soil air (kg kg^{-1})
W_{sat}	saturation specific humidity (kg kg^{-1})
z_{root}	root depth (m)

References

Allen, R.G., Pereira, L.S., Raes, D., Smith, M., 1998. *Crop evapotranspiration. Guidelines for computing crop water requirements.* Irrigation and Drainage. Paper No. 56, FAO, Rome, Italy.

Allison, G.N., 1987. A review of some physical, chemical and isotopic techniques available for estimating groundwater recharge. In: Estimation of Natural Groundwater Recharge, D. Reidel Pub. Co: Norwell Ma, USA. NATO Series C: 222, 49-72.

Allison, G.B., Gee, G.W., Tyler, S. W., 1994. Vadose zone techniques for estimating groundwater recharge in arid and semi-arid regions. *Soil Sci. Soc. Am. J.* 58(1), 6-14.

Al Nakshabandi, G. and Kohnke, H., 1965. Thermal conductivity and diffusivity of soils as related to moisture tension and other physical properties. *Agricultural Meteorology* 2, 271–279.

Araguás-Araguás, L., Rozanski, K., Plata Bedmar, A., Tundis Vital, A. R., Tancredi, A. C., Franken, W., 1995. Changes of soil balance due to forest clearing in the central Amazon region. Proceedings Solutions' 95, Managing the Effects of Man's Activities on Groundwater, International Association of Hydrology International Congress XXVI, June 4–10, Edmonton, Canada.

Barnes, C.J., Jacobson, G., Smith, G.D., 1994. The distributed recharge mechanism in the Australian arid zone. *Soil Sci. Soc. Am. J.* 58(1), 31-40.

Barry, P.J., Watkins, B.M., Belot, Y., Davis, P.A., Edlund, O., Galeriu, D., Raskob, W., Rusell, S., Togawa, O., 1999. Intercomparison of the model predictions of tritium concentrations in

soil and foods following acute airborne HTO exposure. *J. Environ. Radioactivity* 42, 191-207.

Belot, Y., Watkins, B.M., Edlund, O., Galeriu, D., Guinois, G., Golubev, A.V., Meruville, C., Raskob, W., Täschner, M., Yamazawa, H., 2005. Upward movement of tritium from contaminated groundwaters: a numerical analysis. *J. Environ. Radioactivity* 84, 259-270.

BIOMOVS II, 1996. *Tritium in the food chain: comparison of predicted and observed behaviour. A. Re-emission from soil and vegetation. B. Formation of organically bound tritium in grain of spring wheat.* Technical Report No. 13. Swedish Radiation Protection Institute, 171 16 Stockholm, Sweden.

Burt, C.M., Clemmens, A.J., Strelkoff, T.S., Solomon, K.H., Hardy, L., Howell, T., Eisenhauer, D., Bleisner, R., 1997. Irrigation performance measures – Efficiency and uniformity. *J. Irrigation and Drainage Engineering*, 123(6), 423-442.

Campbell, G.S., 1974. A simple method for determining unsaturated conductivity from moisture retention data. *Soil Sci.* 117, 311-314.

Campbell, G.S. and Norman, J.M., 1998. *An Introduction to Environmental Biophysics*. 2nd ed. Springer-Verlag, New York.

Clapp, R. and Hornberger, G., 1978. Empirical equations for some soil hydraulic properties. *Water Resour. Res.* 20, 601-604.

Cosby, B. J., Hornberger, G.M., Clapp, R.B., Ginn, T.R., 1984. A Statistical Exploration of the Relationships of Soil Moisture Characteristics to the Physical Properties of Soils. *Water Resour. Res.* 20(6), 682-690.

Cussler, E.L., 1997. *Diffusion: Mass transfer in fluid systems*. Cambridge Univ. Press, New York.

Dunger, V., 1995. Methodical aspects of modelling the water and tritium balance of the unsaturated zone. Isotopes Environ. *Health Stud.* 31, 29-46.

Farouki, O.T., 1986. Thermal properties of soils. Series on Rock and Soil Mechanics 11 (Trans Tech, 136 pp.).

Feddes, R. A., Kowalik, P.J., Zaradny, H., 1978. *Simulation of Field Water Use and Crop Yield*. John Wiley and Sons, NY.

Garcia, C.A., Andraski, B.J., Stonestrom, D.A., Cooper, C.A., M. J. Johnson, M.J., Michel, R.L., Wheatcraft, S. W., 2009. Transport of tritium contamination to the atmosphere in an arid environment. *Vadose Zone J.* 8, 450-461.

Gillham, R.W., Robin, M.J.L., Dytynyshyn, D.J., Johnston, H.M., 1984. Diffusion of non-reactive and reactive solutes through fine-grained barrier materials. *Can. Geotech. J.* 21,541-550.

GNIP/IAEA, 2009. International Atomic Energy Agency. Isotopes Hydrology Information System. The ISOHIS Database, <http://isohis.iaea.org/>.

Ingraham, N.L. and Criss, R.E., 1993. Effects of surface area and volume on the rate of isotopic exchange between water and water vapor. *JGR* 98 (D11), 20547-20553.

Ingraham, N.L. and Criss, R.E., 1998. The effect of vapor pressure on the rate of isotopic exchange between water and water vapor. *Chemical Geology* 150, 287-292.

Jackson, D.R., Reginato, R.J., Kimball, B.A., Nakayama, F.S., 1974. Diurnal soil water evaporation. Comparison of measured and calculated soil water fluxes. *Soil Sci. Soc. Amer. J.* 38, 861-866.

Joshi, B., Maule, C., De Jong, C., 1997. Subsurface hydrologic regime and estimation of diffuse soil water flux in a semi arid region. Electronic *Journal of Geotechnical Engineering*. http:/geotech.cive.okstate.edu/ejge/ppr9702/index.htm.

Kashyap, P.S. and Panda, R.K., 2001. Evaluation of evapotranspiration estimation methods and development of crop-coefficients for potato crop in a sub-humid region. *Agric. Water Manage.* 50, 9-25.

Kline, J.R. and Stewart, M.L., 1974. Tritium uptake and loss in grass vegetation which has been exposed to an atmospheric source of tritiated water. *Health Physics* 26, 567-573.

Kondo, J. and Saigusa, N., 1994. Modeling the evaporation from bare soil with a formula for vaporization in the soil pores. *JMSJ* 72(3), 413-421.

Kondo, J. and Xu, J., 1997. Seasonal variations in the heat and water balance for nonvegetated surfaces. *Journal of Applied Meteorology* 36(12), 1676-1695.

Kroes, J.G. and Van Damm, J.C., 2003. *Reference manual SWAP: Version 3.0.3.* Rep. 773. Alterra Green World Res., Wageningen, the Netherlands.

Larsbo, M. and Jarvis, N.J., 2003. *MACRO 5.0. A model of water flow and solute transport in macroporous soil.* Technical description. Emergo 2003: 6, Studies in the Biogeophysical Environment, Department of Soil Sciences, Swedish University of Agricultural Sciences, Uppsala, Sweden, pp. 47.

Logsdon, S.D., Keller, K.E., Moorman, T.B., 2002. Measured and predicted solute leaching from multiple undisturbed soil columns. *Soil Sci. Soc. Am. J.* 66, 686-695.

Matsushima, D. and Kondo, J., 1995. An estimation of the bulk transfer coefficients for a bare soil surface using a linear model. *Journal of Applied Meteorology* 34(4), 927-940.

Mayers, C.J., Andraski, B.J., Cooper, C.A., Wheatcraft, S.W., Stonestrom, D.A., Michel, R.L., 2005. Modeling tritium transport through a deep unsaturated zone in arid environment. *Vadose Zone J.* 4, 967-976.

McCumber, M.C. and Pielke, R.A., 1981. Simulations of the effects of surface fluxes of heat and moisture in a mesoscale numerical model 1 soil layer. *JGR* 86 (C10), 9929-9938.

Mills, R., 1973. Self-diffusion in normal and heavy water in the range 1-45º. *J. Phys. Chem.* 77, 685-688.

Overman, A.R. and Scholtz, R.V., 2002. *Mathematical Models of Crop Growth and Yield*. Marcel Dekker, Inc. New York.

Pachepsky, Y.A., Smettem, K.R.J., Vanderborght, J., Herbst, M., Vereecken, H., Wosten, J.H.M., 2004. Reality and fiction of models and data in soil hydrology. In: Feddes R.A. et al. (Eds.), Unsaturated-zone modeling. Kluwer Academic Publishers, Dordrecht, the Netherlands.

Phillips, R.R. and Brown, D.A., 1968. Self diffduion of tritiated water in montmorillonite and kaolinite clay. *Soil Sci. Soc. Am. J.* 32, 302-306.

Pruess, K.A., Oldenburg C., Moridis, G., 1999. *THOUGH2 user's guide. Version 2.0.* LBNL-43134. Lawrence Berkeley Natl. Lab., Berkeley, CA.

Raskob, W., 1995. Assessment of the environmental-impact from tritium releases under normal operation conditions and after accidents. *Fusion Technology* 28, 934-939.

Scanlon, B.R., 1992. Evaluation of Liquid and Vapor Water Flow in Desert Soils Based on Chlorine 36 and Tritium Tracers and Nonisothermal Flow Simulations. *Water Resour. Res.* 28(1), 285-297.

Slattery, M.W. and Ingraham, N.L., 1994. Detritiation of water by isotopic exchange: experimental results. *Environ. Sci. Technol.* 28 (8), 1417-1421.

Täschner, M., Bunnenberg, C., Camus, H., Belot, Y., 1995. Investigations and modelling of tritium re-emissions from soil. *Fusion Technology* 28, 976-981.

Täschner, M., Bunnenberg, C., Raskob, W., 1997. Measurements and modeling of tritium reemission rates after HTO depositions at sunrise and at sunset. *J. Environ. Radioactivity* 36, 219-235.

Taylor, S.A. and Ashcroft, G.M., 1972. *Physical Edaphology*. Freeman and Co., San Francisco, California, 434-435.

Toupiol, C., Willingham, T.W., Valocchi, A.J., Werth, C.J., Krapac, I.G., Stark, T.D., Daniel, D.E., 2002. Long-term tritium transport through field-scale compacted soil liner. *J. Geotech. Geoenviron. Eng.* 128(8), 640-650.

Wang, B., Jin, M., Nimmo, J.R., Yang, L., Wang, W., 2008. Estimating groundwater recharge in Hebei Plain, China under varying land use practices using tritium and bromide tracers. *J. Hydrol.* 356, 209-222.

Wesseling, J.G., Elbers, J.A., Kabat, P., van den Broek, B.J., 1991. SWATRE: instructions for input, Internal Note, Winand Staring Centre, Wageningen, Netherlands.

Yamazawa, H., 2001. A one-dimensional dynamical soil atmosphere tritiated water transport model. *Environmental Modelling and Software* 16, 739-751.

Yamazawa, H. and Nagai, H., 1997. *Development of one-dimensional atmosphere-bare soil model.* JAERI-Data/Code 97-401.

Young, D.F. and Ball, W.P., 1998. Estimating diffusion coefficients in low permeability porous media using a macropore column. *Environ. Sci. Technol.* 32, 2587-2584.

Chapter 6

Water balance approach. Soil, vadose zone and aquifer*

6.1 Introduction

Water table fluctuation method (WTF) to estimate aquifer recharge is a groundwater-based approach founded on groundwater level data. Its application requires knowledge of specific yield and changes in water level over time. Although simplicity is one of the method advantages, uncertainties associated to the limited accuracy of some parameters determination (e.g. specific yield) may restrict its applicability. Techniques based on groundwater level are among the most widely applied methods for estimating recharge rates. This is likely due to the availability of groundwater level records and the simplicity of estimating recharge rates from temporal fluctuations or spatial patterns of groundwater levels (*Healy and Cook*, 2002).

The WTF approach can be only applied to unconfined aquifers. It is based on the premise that rise of groundwater level is due to recharge water arriving to water table. The time lag span between the water application (from irrigation or precipitation) and the water arriving to the

* This chapter is based on the article: Jiménez-Martínez, J., Molinero, J., Tamoh, K., Candela, L. Groundwater recharge in irrigated semi-arid areas with different crops. Quantitative hydrological modelling and sensitivity analysis (submitted to *Hydrogeology Journal*)

aquifer during a recharge event is critical for this approach. It is valid over short periods of time (hours or a few days). If water is abstracted from the water table at a rate that is not significantly slower than the rate at which recharge water arrives at the water table, then the method is of little value.

Modelling aquifer water balance is not a new undertaking and several numerical codes are applied, generally. For codes describing balance processes, the reader is referred to SAHYSMOD (*ILRI*, 2005), VisualBALAN v. 2.0 *(Samper et al.*, 2005), TOPOG (*CSIRO*, 2008), and INFIL (*USGS*, 2008), among others.

This chapter presents a method to estimate aquifer recharge from different crop types based on water table fluctuations. The current work concerns the application of a computer code, VisualBALAN v. 2.0 (*Samper et al.*, 2005), to simulate water balance in the soil, vadose zone and aquifer. The boundary conditions were detailed for each crop and according to the agricultural practices. The chapter starts with the field experiment description. Next, the numerical modelling approach is described. Finally, a critical discussion of the recharge results from irrigation return flow obtained for each crop is undertaken. A comprehensive sensitivity analysis is performed to evaluate the reliability and uncertainty of the estimated recharge values.

6.2 Field experiment

Three experimental plots with different types of crops (*LM*, *A* and *C* in Figure 2.3) were selected to assess the water balance: *LM*, with annual row crops (rotation of lettuce and melon); *A*, with perennial vegetables (artichoke); and *C*, with fruit trees (citrus). The main criteria for selecting the sites were prior long-term cultivation of the crops in the experimental area (1999-2008), the existence of piezometric records (piezometers 1, 2 and 3) and a nearby meteorological station (TB and SJ), as shown in Figure 2.3.

Each experimental plot had an area of 10 000 m^2 and the soil is a *silty loam* (USDA soil textural classification), which is relatively uniform throughout the Campo de Cartagena region (*Ramírez et al.*, 1999). Daily meteorological data for the study period were provided by SIAM and the water level data, recorded every two months, were obtained from the CHS database.

The plots (*LM*, *A* and *C*) were managed according to agricultural practices that are common in the Campo de Cartagena region (Table 6.1), including crop rotation for annual row crops (lettuce and melon), drip irrigation and water requirements (Figure 6.1). For summer row crops (melon) cultivation is carried out under plastic to increase irrigation efficiency. For simulation purposes and to avoid boundary effects, the same agricultural management practices were conducted in the neighbouring areas of experimental plots.

Table 6.1: Main characteristics of the experimental plots (source: *Allen et al.*, 1998 and *CARM*, 2007).

Exp. plot	Mete. station	Piezometer	Crop	Mean height crop	Maximum root depth	Furrow spacing	Drip irrigation			Crop water requirements
							Inside diameter tubing	Emitter spacing	Discharge	
				(cm)	(cm)	(m)	(mm)	(cm)	(l h^{-1})	(m^3 ha^{-1} yr^{-1})
LM	TB	1	lett. / melon	30 / 30	30-50 / 80-150	1	16	30	4	3287.8 / 6169.2
A	SJ	2	artichoke	70	60-90	1.7	16	40	4	6622.8
C	SJ	3	citrus	300	80-150	6	16	25-125	4	6407.1

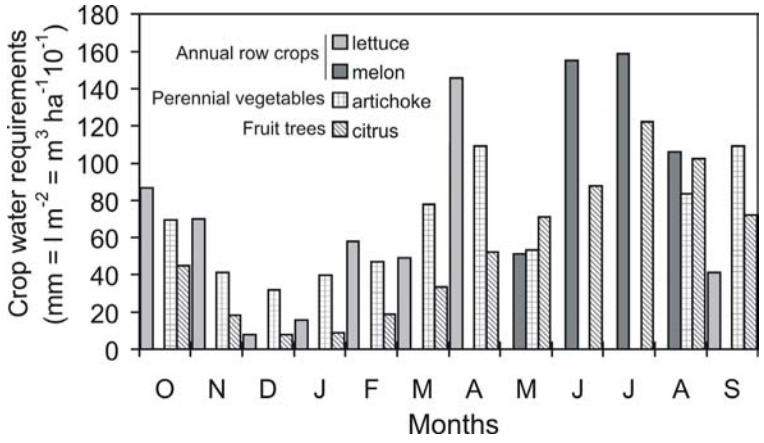

Figure 6.1: Monthly water requirements for the three types of crop studied.

6.3 Estimation of recharge using water balance modelling

6.3.1 Water balance modelling description: equations and parameters used

Water recharge was calculated with VisualBALAN v. 2.0 (*Samper et al.*, 2005), a computer code suitable for long-term simulation of water balance in the soil, vadose zone and aquifer. VisualBALAN has been applied successfully at many Spanish and South American case studies, as for example *Carrica and Lexow*, 2004; *García-Santos et al.*, 2005; *Samper et al.*, 2007; *Castañeda and García-Vera*, 2008; *Candela et al.*, 2009; *Sena and Molinero*, 2009, among many others. The experiment was performed for the October 1999 and September 2008 period, nine hydrological years. Calibration and prediction were accomplished for annual row crops (lettuce and melon), perennial vegetables (artichoke) and fruit trees (citrus).

In comparison to other mentioned codes (INFIL, SAHYSMOD, TOPOG), VisualBALAN aims at using generally available input data, that can be estimated with reasonable accuracy, or easily measured. For example, INFIL (*ILRI*, 2005) focusses in the root zone, whereas SAHYSMOD (*USGS*, 2008) was designed for long-term management applications and output results are based on weighted seasonal averages. Moreover, the latter requires runoff like input data.

The code used in this investigation comprises three sub-models that take into account processes in a) the upper part of the soil (root zone), b) the vadose or unsaturated zone (lower soil) and c) the saturated zone (aquifer). A schematic representation of the balance components is represented in Figure 6.2.

The state variable in each of the three zones is water volume, expressed as volume per surface unit (e.g. l m^{-2}) or equivalent height of water (e.g. mm). The water volume in soil (V_s) is the product of water content (θ) and soil thickness (b_s), $V_s = \theta\, b_s$. The amount of water in the vadose zone is $V_h = \Phi_e\, y_h$, where Φ_e is the drainable porosity and y_h the thickness of the waterfront. In the saturated zone, the relationship between water volume (V_a) and height of the groundwater level (h) are related by the specific yield S_y by $V_a = S_y\, h$ (for unconfined aquifer is assumed $S = S_y$, where S is storage coefficient or storativity). Model parameters are automatically

calibrated by means of the comparison between measured and estimated water levels, and are optimized by minimizing the objective function through the Powell Method or multidimensional minimization (*Press et al.*, 1989).

The water balance for **vegetated soil** is represented by:

$$P + Ir - In - E_s - ET_a - P_e = \Delta\theta \qquad [6.1]$$

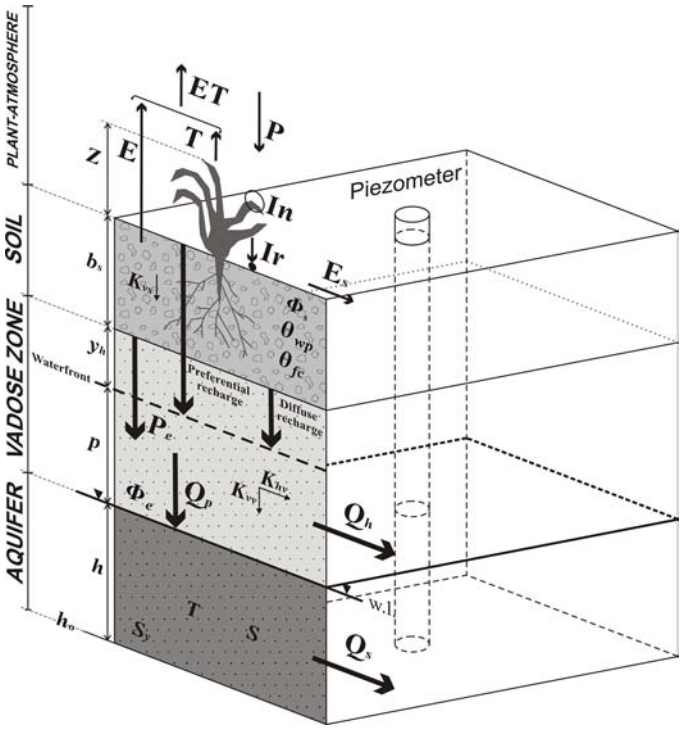

Figure 6.2: Scheme of the water balance components in soil, vadose zone and aquifer as defined in the VisualBALAN computer code (*Samper et al.*, 2005). Notation can be found in the text and at the end of this chapter.

where P is precipitation, Ir irrigation, In canopy interception, E_s runoff, ET_a represents the *actual* evapotranspiration, P_e is the potential recharge to the vadose zone and $\Delta\theta_s$ is the variation of soil water storage. The approach assumes a cascade model for precipitation, interception, runoff, evapotranspiration and the recharge process. In the aforementioned model, water balance in soil is

attained by usinging rainfall and daily irrigation data. The model simulates temporal differences (between t_i and t_f, $\Delta t = t_f - t_i$) of *actual* evapotranspiration and groundwater recharge.

As infiltrated water is the residual water after evapotranspiration, the infiltration term, *I*, can be introduced in the water balance equation as:

$$I - (ET_a - P_e) = \Delta\theta \quad [6.2]$$

$$P + Ir - In - E_s = I \quad [6.3]$$

Eq. [6.1] is the sum of Eq. [6.2] and [6.3].

Canopy interception, *In*, is the fraction of precipitation intercepted by the vegetation (leafs, branches and trunk), which involves loss of water by evaporation and runoff decrease. Canopy interception was derived from the empirical model of *Horton* (1919), which describes a linear relationship between intercepted volume *In* and total precipitation on vegetation P_d in a rainfall event:

$$In = S_d + \gamma P_d \quad [6.4]$$

being S_d and γ empirical parameters related to the type of vegetation and plant height (Table 6.2). As *In* is a fraction of precipitation, it cannot exceed the P_d value, therefore Eq. [6.4] is valid only when P_d exceeds a threshold defined by:

$$P_d > \frac{S_d}{1-\gamma} \quad [6.5]$$

For values lower than threshold, $In = P_d$.

The surface runoff estimation, E_s, is derived from the curve number method (*Soil Conservation Service*, 1975), which is based on the relations between losses by canopy interception and precipitation. Before runoff occurs, there is a precipitation threshold, P_o, due to

interception and infiltration. If this is taken into account, precipitation is P-P_o. For dry conditions

Table 6.2: Applied S_d and γ parameters (Horton method) and crop height (from *López and Giráldez*, 1997).

Crop	S_d	γ	Mean height crop Z (m)
Annual row crops (lettuce and melon)	1.67·Z	0.49·Z	0.3
Perennial vegetables (artichoke)	1.67·Z	0.49·Z	0.7
Fruit trees (citrus)	1.02	0.18	3

and intensive rainfall events, as in our specific study area, E_s can be empirically calculated according to:

$$E_s = \frac{(P - P_o)^2}{P + 4P_o} \qquad [6.6]$$

A critical element for recharge estimation is to determine *actual* evapotranspiration $ET_a(t)$ rates, which can be below *potential* rates $ET_p(t)$ for long periods of time in arid and semi-arid regions, even for irrigated systems. An exponential method to relate $ET_a(t)$ with $ET_p(t)$ was used (e.g. *Poulovassilis et al.*, 2001). The method works with hydric deficits θ_{hd} at time t:

$$ET_a(t) = \begin{cases} 1.9\ ET_p(t)\ e^{\{-0.6523[\theta_{hd}(t) - W(t)]/\theta_{ceme}\}} & \theta_{hd}(t) - W(t) > \theta_{ceme} \\ ET_p(t) & \theta_{hd}(t) - W(t) < \theta_{ceme} \end{cases} \qquad [6.7]$$

where $W(t)$ represents the input water along time (available water), being $\theta_{hd}(t) = \theta_{fc} - \theta(t)$, θ_{fc} is field capacity and $\theta(t)$ soil water content. θ_{ceme} constitutes the hydric deficit limit value and ranges between field capacity (θ_{fc}) and wilting point (θ_{wp}). All parameters are expressed as equivalent height of water.

The potential diffuse recharge to the vadose zone P_e was estimated assuming that the soil is homogeneous and isotropic. To solve this aspect, a linear function was applied (e.g. *Castañeda and García-Vera*, 2008), defined as:

$$P_e(t) = \begin{cases} 0 & \theta(t) < \theta_{fc} \\ \theta(t) - \theta_{fc} & \theta_{fc} \le \theta(t) < \theta_{fc} + K_{vs}\Delta t \\ K_{vs}\Delta t & \theta(t) \ge \theta_{fc} + K_{vs}\Delta t \end{cases} \quad [6.8]$$

where K_{vs} is the soil vertical hydraulic conductivity and θ_{fc} and $\theta(t)$ are expressed as equivalent height of water.

In the **vadose zone,** potential recharge P_e, constitutes the entry of water, which can be divided into hypodermic Q_h, and vertical flow or percolation to the aquifer Q_p, defined by the following expressions:

$$Q_h(t) = \alpha_h V_h(t) \quad [6.9]$$

$$Q_p(t) = K_{vv} + \alpha_p V_h(t) \quad [6.10]$$

being V_h water volume stored in the vadose zone, α_h and α_p are depletion coefficients for hypodermic flow and vertical flow or percolation, respectively, and K_{vv} the vertical hydraulic conductivity in the vadose zone. The α_h parameter is proportional to the horizontal hydraulic conductivity K_{hv}, drainable porosity Φ_e, mean slope i and length in the hypodermic flow direction L, according to:

$$\alpha_h = \frac{2K_{hv}i}{L\ \Phi_e} \quad [6.11]$$

As in Eq. [6.10], α_p is obtained by considering that V_h and y_h are related by means of $V_h = \Phi_e\ y_h$, where y_h is the thickness of the waterfront, taking into account the distance between the waterfront and the regional groundwater level p:

$$\alpha_p = \frac{K_{vv}}{p\ \Phi_e} \quad [6.12]$$

In this study, an explicit scheme was applied for solving water balance in the vadose zone.

Water balance in the **aquifer**, VisualBALAN (*Samper et al.*, 2005), was obtained by estimating the groundwater level in the aquifer at each Δt. The code enables solving the water balance by treating the region as a mono-cell or multi-cell pattern. For this exercise, the experimental plot (10 000 m^2) was considered as only one cell. The water volume in the aquifer, V_a, and the groundwater level, h, are related to a reference value, h_o (base value), which corresponds to a volume V_{ao}. The water volume stored over the reference value, $\Delta V_a = (V_a - V_{ao})$, is related to the change of level $\Delta h = (h - h_o)$ through the specific yield S_y by means of $\Delta V_a = S_y\ \Delta h$. Balance in the aquifer is carried out considering the entry of water by vertical flow or percolation Q_p and the groundwater discharge Q_s:

$$Q_s(t) = \alpha_s \Delta V_a \quad [6.13]$$

where α_s is the discharge depletion coefficient,

$$\alpha_s = a\frac{T}{S\lambda^2} \quad [6.14]$$

which is related to hydraulic diffusivity (T/S) by means of the transmissivity, T, and storage coefficient, S ($S = S_y$ for unconfined aquifer), a characteristic length λ and a dimensionless constant α (common range between 1/3 and 1/1.5). The stored volume in the aquifer at time t, $V_a(t)$, is obtained from:

$$V_a(t) = V_a(t-1) + (Q_p - Q_s)\Delta t \quad [6.15]$$

Once the final volume is known, the water level is calculated, $h(t)$:

$$h(t) = h_o + \frac{V_a(t) - V_{ao}}{S} \quad [6.16]$$

which allows an estimation of the water level in the aquifer.

Goodness of fit between measured and simulated water levels was assessed by the root mean square error (*RMSE*) and mean absolute error (*MAE*).

6.3.2 Atmospheric boundary conditions

Daily irrigation, *Ir*, and precipitation, *P*, rates are the only input to the system. In order to determine evaporation and transpiration rates, reference evapotranspiration, $ET_0(t)$, was calculated according to Penman-Monteith method. The *potential* evapotranspiration, $ET_p(t)$, was derived from (*Allen et al.*, 1998):

$$ET_p(t) = K_c(t) \cdot ET_0(t) \quad [6.17]$$

where $K_c(t)$ is a crop-specific coefficient that characterizes plant water uptake and evaporation relative to the reference crop. $ET_0(t)$ was obtained at daily time steps. Values for $K_c(t)$ are shown in Table 4.3 and Figure 4.3 for annual row crops, along with growth stages and length (days). An annual mean value of K_c = 0.95 (*Allen et al.*, 1998) for perennial vegetables (artichoke) and a monthly mean value (*Castel*, 2001) for fruit trees (citrus) respectively was applied, although for the last case the annual mean value is K_c = 0.68 for a ground cover ≥ 64%.

Potential evaporation $E_p(t)$ was calculated according to (e.g. *Kroes and Van Dam*, 2003; *Pachepsky et al.*, 2004):

$$E_p(t) = ET_p(t) \cdot \exp^{-\beta \cdot LAI(t)} \quad [6.18]$$

being β (≈ 0.4) the radiation extinction coefficient and $LAI(t)$ is the leaf area index. Data on $LAI(t)$ was not available and it was estimated as:

$$E_p(t) = ET_p\, f(t) \quad [6.19]$$

The $f(t)$ function was defined on the basis of the following reasoning: when a crop is planted for the first time, ground cover is nonexistent, *potential* evaporation is maximal, transpiration is zero, and thus $f(t) = 1$. Conversely, when the crop reaches the mid-season growth stage, ground cover is complete, evaporation is effectively zero, and thereafter $f(t) = 0$. The transition from $f(t) = 1$ at planting to $f(t) = 0$ at the beginning of the mid-season growth stage was modelled using a sigmoid curve (*Jiménez-Martínez et al.*, 2009).

Therefore, *potential* transpiration $T_p(t)$ was determined as:

$$T_p(t) = ET_p(t) - E_p(t) \quad [6.20]$$

According to agricultural practices in the area, the $ET_p(t)$ for winter crops (lettuce) is given by Eq. [6.17], while for summer crops (melon) only $T_p(t)$ from Eq. [6.20] was taken into consideration. Selection was based on the fact that the plastic cover reduces $E_p(t)$ to zero (Figure 6.3). For perennial vegetables and fruit trees, the $ET_p(t)$ given by Eq. [6.17] was applied considering that a complete growth development occurs.

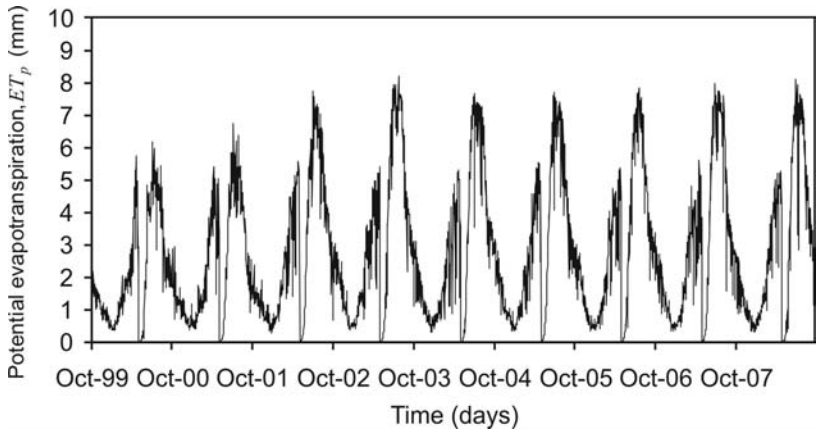

Figure 6.3: Estimated *potential* evapotranspiration ET_p (Eqs. 6.17-6.20) as a soil input boundary condition for annual row crops (set lettuce and melon).

6.3.3 Uncertainty and sensitivity analysis

The modelling approach contains several potential sources of uncertainty, which are either related to model parameters (P_o; α_h; α_s; S; h_d; K_{vv}; α_p; θ_{ceme}; b_s; Φ_s; θ_{wp}; θ_{fc}; Curve Number; K_{vs}), initial conditions (initial water content in the soil and vadose zone; initial water level in the single-cell aquifer) or the boundary conditions (precipitation; crop coefficient; reference evapotranspiration; irrigation; height of the crop). Quantifying the effect of uncertainties on the recharge calculation requires knowledge of the abovementioned model parameters and of their statistical variability and correlation structure. To our knowledge, the literature provides little or no information on quantifying uncertainty for some of the parameters. However, it is possible to evaluate the importance of the parameter uncertainties on recharge as objective function by means of sensitivity analysis.

To involve a cascade model, the parameters and initial conditions that potentially concern the recharge are included in soil and vadose zone (P_o; α_h; K_{vv}; α_p; θ_{ceme}; b_s; Φ_s; θ_{wp}; θ_{fc}; Curve Number; K_{vs}; initial water content in soil and vadose zone), whereas parameters and initial conditions of the aquifer (α_s; S; h_d) have a impact on water level but no on the objective function, recharge. A series of simulations were performed on individual parameters by a given amount of perturbation and by estimating water balance.

The uncertainties associated with the boundary conditions were evaluated by computing a defined relative sensitivity as AS/CP. Parameter CP is the relative change of a given variable or parameter, defined as $\left|P_s - P_b\right| / P_b \cdot 100$, and AS is the relative change in the output (recharge) value, defined as $\left|C_s - C_b\right| / C_b \cdot 100$. P_s and P_b are variable values used for sensitivity and calibrated base runs, respectively, and C_s and C_b are output data (recharge) computed in sensitivity and calibrated base runs, respectively. The magnitude of the perturbation (CP) was ±10% with respect to the original data. However, for the height crop this figure stood at ±30%.

6.4 Results and discussion

6.4.1 Model calibration and predictions

As could be expected, initial simulations using guessed parameters were in poor agreement with measured data. We therefore attempted to calibrate model parameters in the three zones (soil, vadose zone and aquifer) by parameter optimization routines and field data (water level data). Several possible parameterizations were considered, according to the number and type of parameters that were fitted. The best overall parameterization was determined on the basis of diagnostic information from the computer program, a visual inspection of the model fit to the data and the principle of parsimony (i.e. if two parameterizations produce equal fit, the simpler of two

Table 6.3: Initial value and final fitted parameter estimates. Prescribed values when not fitted parameters.

Parameter	Annual row crops (lettuce and melon)		Perennial vegetables (artichoke)		Fruit trees (citrus)	
	Initial value	Fitted value	Initial value	Fitted value	Initial value	Fitted value
Calibration period		99-02		99-05		99-03
Fitted						
Rainfall threshold to downpour, P_o (mm)	2	2	2	2	2	2
Hypodermic flow depletion coefficient, α_h (day^{-1})	0.01	0.01	0.01	0.01	0.01	0.01
Groundwater discharge depletion coefficient, α_s (day^{-1})	0.0173	0.0050050	0.0173	0.0009812	0.0173	0.0009812
Storage coefficient, S	0.2	0.2098	0.2	0.2065	0.2	0.2
Discharge single-cell aquifer water level, h_d (m)	15.80	15.78	1.50	1.50	13.55	13.57
Vadose zone vertical hydraulic conductivity, K_{vv} (mm day^{-1})	432	432	432	432	432	432
Vertical flow depletion coefficient, α_p (day^{-1})	0.6931	0.6931	0.6931	0.6931	0.6931	0.6931
θ_{ceme} (mm) [hydric deficit limit value, between θ_{wp} and θ_{fc}]	20	1.549	20	0.965	20	1.006
Prescribed[a]						
Soil thickness, b_s (m)	0.5		1		1.50	
Soil total porosity, Φ_s (m^3 m^{-3})	0.4		0.4		0.4	
Wilting point, θ_{wp} (m^3 m^{-3})	0.1		0.1		0.1	
Field capacity, θ_{fc} (m^3 m^{-3})	0.2		0.2		0.2	
Curve Number[b]	58		58		25	
Soil vertical hydraulic conductivity, K_{vs} (mm day^{-1})	382		382		382	

Source: [a] *Jiménez et al.*, 2007 and *Jiménez-Martínez et al.*, 2009 ; [b] *Soil Conservation Service*, 1975.

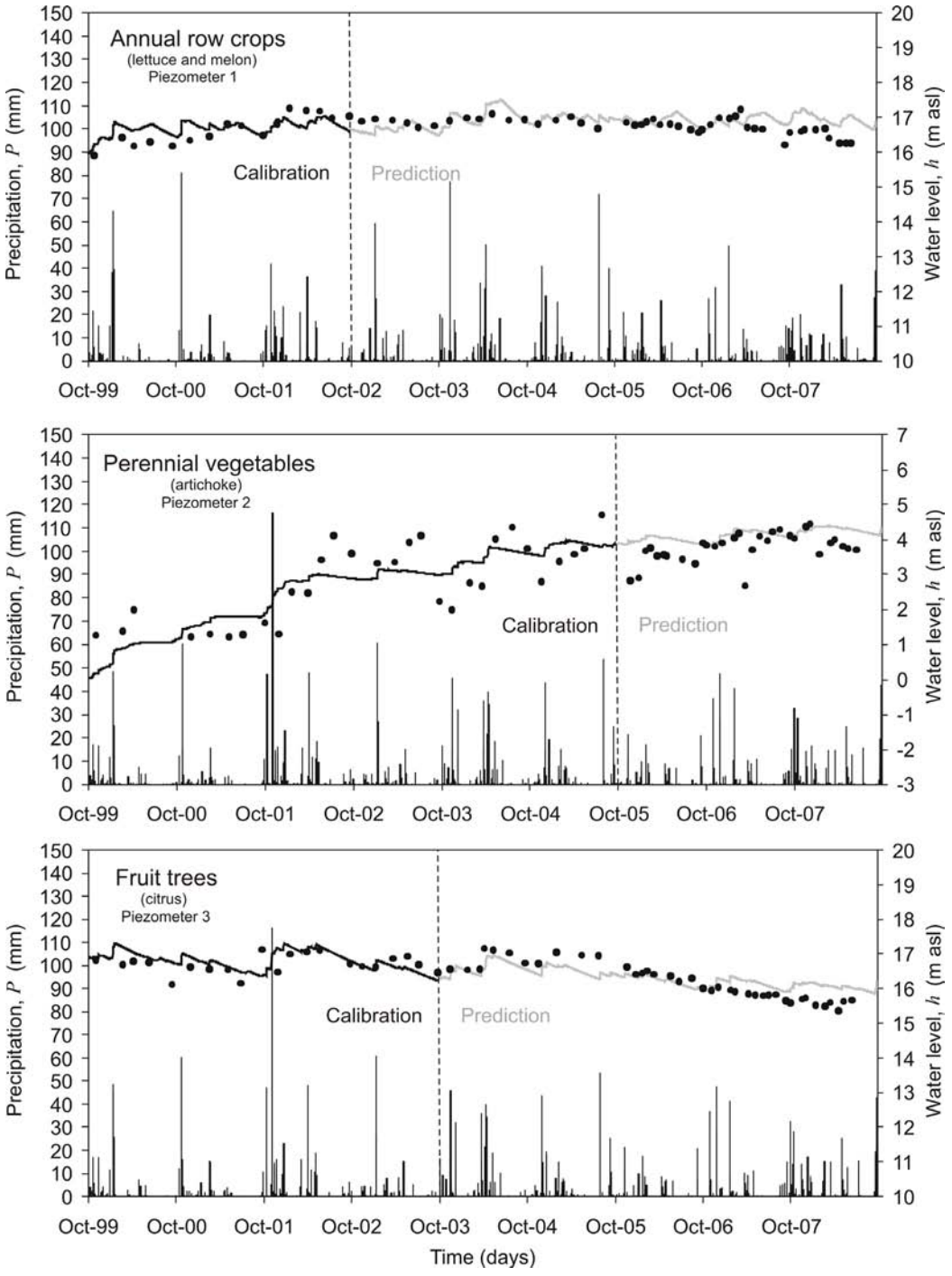

Figure 6.4: Simulated (calibration: black line; prediction: grey line) and observed (dots) water level for the piezometers 1, 2 and 3 located in each experimental plot (see Figure 2.3). Daily precipitation is shown as black bars.

is took, namely, fewer fitted parameters). Subsequently, the fitting was repeated using different initial estimates to ensure that the same fitted parameters were obtained. The best parameterization was found for eight of a total of fourteen parameters. Table 6.3 shows the initial value of the parameters, the prescribed value when not fitted, and the fitted parameter estimates. The final fitted parameter values were very similar for the three experimental plots, which confirmed the homogeneity of soil type in the study area (*Ramírez et al.*, 1999).

Calibration for each crop type was carried out for a given number of years (annual row crops 3 yr; perennial vegetables 6 yr; fruit trees 4 yr); once fitted parameterization was attained, it was used to predict at the site (Figure 6.4) the water level for the rest of the period (annual row crops 6 yr; perennial vegetables 3 yr; fruit trees 5 yr), in order to evaluate the model's reliability. Figure 6.5 shows for each crop type the root mean square error (*RMSE*) for a selected calibration period. As it can be observed, the *RMSE* reaches a sill and remains more or less constant after a certain number of years. Obtained results were used to assess the optimum number of years for model calibration in the area. In the annual row crops (set lettuce and melon) and perennial vegetables (artichoke) the *RMSE* value was stabilized after three years (≈ 0.3 and ≈ 0.65, respectively), while for the fruit trees (citrus) it stabilized after two years of calibration (≈ 0.3). Figure 6.4 shows observed and simulated water level measurements, while Table 6.4 presents the goodness-of-fit for the calibrated and predicted periods shown in Figure 6.4. Good agreement was obtained for annual row crops and fruit trees. However, this was not the case for perennial vegetables, which has been related to pumping near of this experimental plot

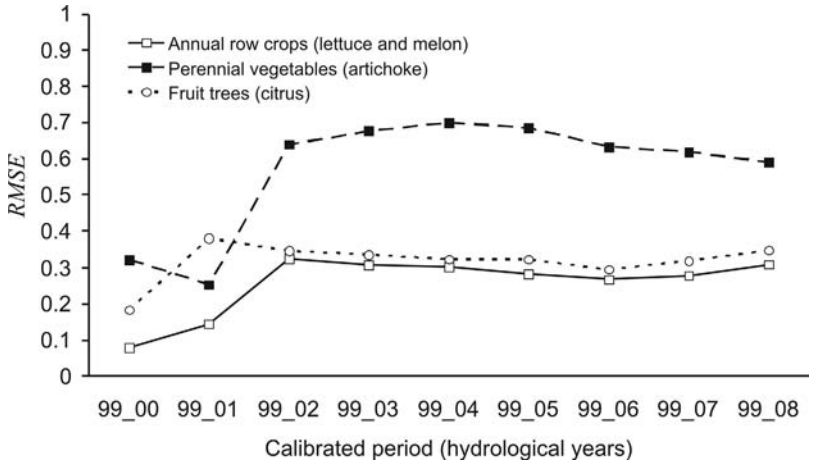

Figure 6.5: Root mean square error (*RMSE*) for the calibrated periods and the three crop types.

Table 6.4: Model performance assessment by fitting experimental data (water level, *h*) for calibrated and predicted periods shown in figure 6.4.

Simulation	Calibration period		Prediction period	
	RMSE[a]	*MAE*[b]	*RMSE*[a]	*MAE*[b]
Annual row crops (lettuce and melon)	0.324	0.276	0.312	0.246
Perennial vegetables (artichoke)	0.686	0.607	0.529	0.397
Fruit trees (citrus)	0.337	0.260	0.352	0.306

[a] Root mean square error, $RMSE = \sqrt{\frac{1}{n}\sum_{i=1}^{n}(x_i - y_i)^2}$ [b] Mean absolute error, $MAE = \frac{1}{n}\sum_{i=1}^{n}|x_i - y_i|$

6.4.2 Water balance and recharge estimation

Figure 6.6 shows the recharge evolution for each crop during the October 1999–September 2008 period. Considering that irrigation has remained more or less constant throughout the study period, the annual recharge variation has to be related to changes in precipitation. For the study period, mean recharge was 397 ± 70 mm for annual row crops (set lettuce and melon), 201 ± 64 mm for perennial vegetables (artichoke) and 194 ± 75 mm for fruit trees (citrus). Values were consistent with data for this type of crops provided by different authors (e.g. *Castel et al.*, 1987; *Hanson et al.*, 1997; *Lidón et al.*, 1999).

Due to the high irrigation dose and frequency of application, recharge dramatically increases when intensive precipitation events occur. As shown in Figure 6.4, the groundwater level increase correlates with the heaviest precipitation events. This rapid water level response is due to the relative narrowness of the vadose zone in the study area, with thickness of 3, 11 and 8 m in *LM*, *A* and *C* plot, respectively. Moreover, continuous and relatively high water content in the soil facilitates the infiltration process during intensive precipitation events. The pie diagrams of Figure 6.6 present the average value (%) of the different water balance components for each crop and study period (October 1999–September 2008). A higher value of interception for perennial vegetables and fruit trees than for the annual row crops is observed. The amount of hypodermic flow and runoff is very low.

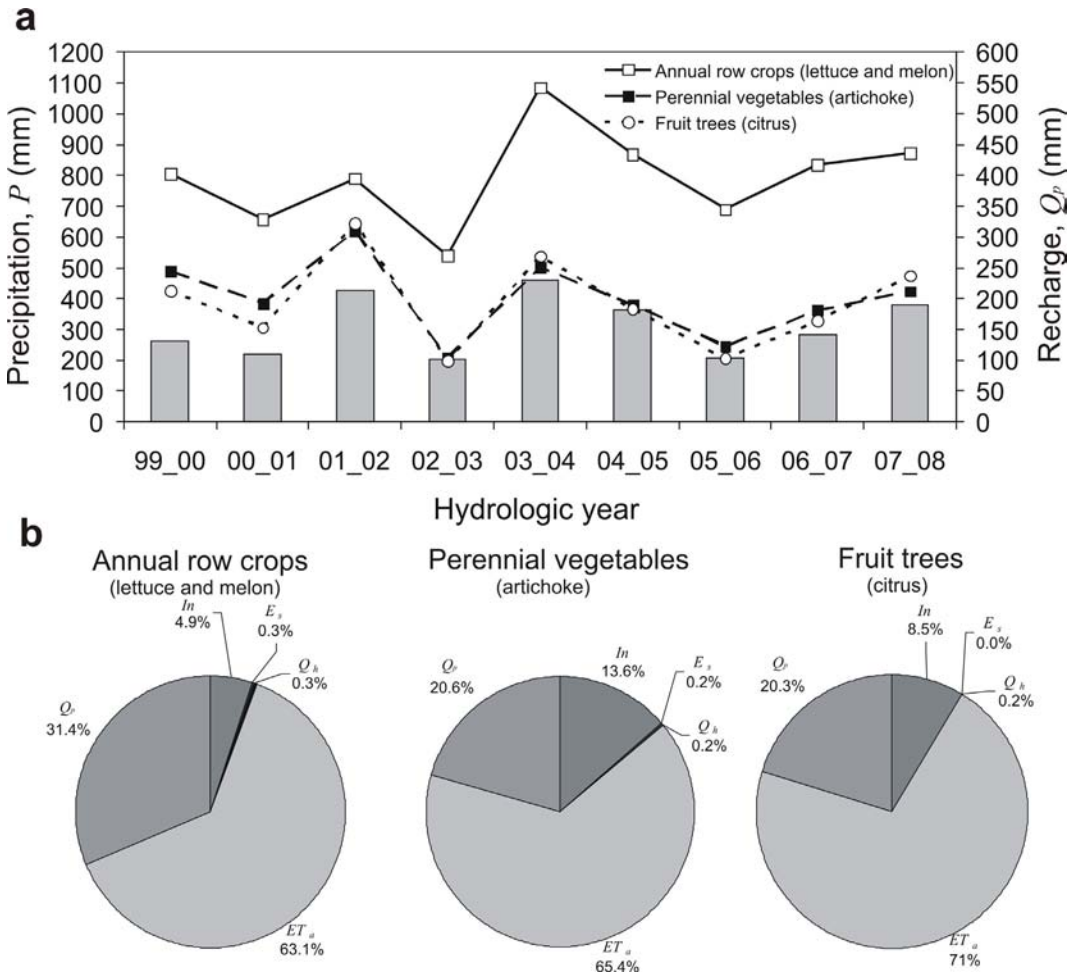

Figure 6.6: a) Annual recharge evolution (annual row crops: dashed line; perennial vegetables: solid line; fruit trees: doted line) and annual precipitation (grey bars) for each crop and studied period (Oct 1999-Sept 2008). b) Pie diagrams present average value (%) of the different water balance components for each crop. *In*: canopy interception; E_s: runoff; Q_h: hypodermic flow; ET_a: *actual* evapotranspiration; Q_p: aquifer recharge.

Figure 6.7 shows ET_p, ET_a and recharge cumulative values for the last simulated hydrological year (October 2007–September 2008) and the three crop types. The ET_a rate was frequently lower than the ET_p, as soil moisture at various times failed to sustain the *potential* transpiration T_p. This is particularly important for perennial vegetables, due to the lack of irrigation during June and July. Regarding recharge process, it could be divided into three stages for each experimental plot. Groundwater recharge mainly occurred between October and December, the rate decreased between January and May, and there was no recharge between June and September.

Note that the plastic cover on summer crops had a major impact on the annual row crops recharge. Percentage of applied water (*P+I*) becoming recharge and irrigation efficiency for each crop and mentioned period are shown in Table 6.5.

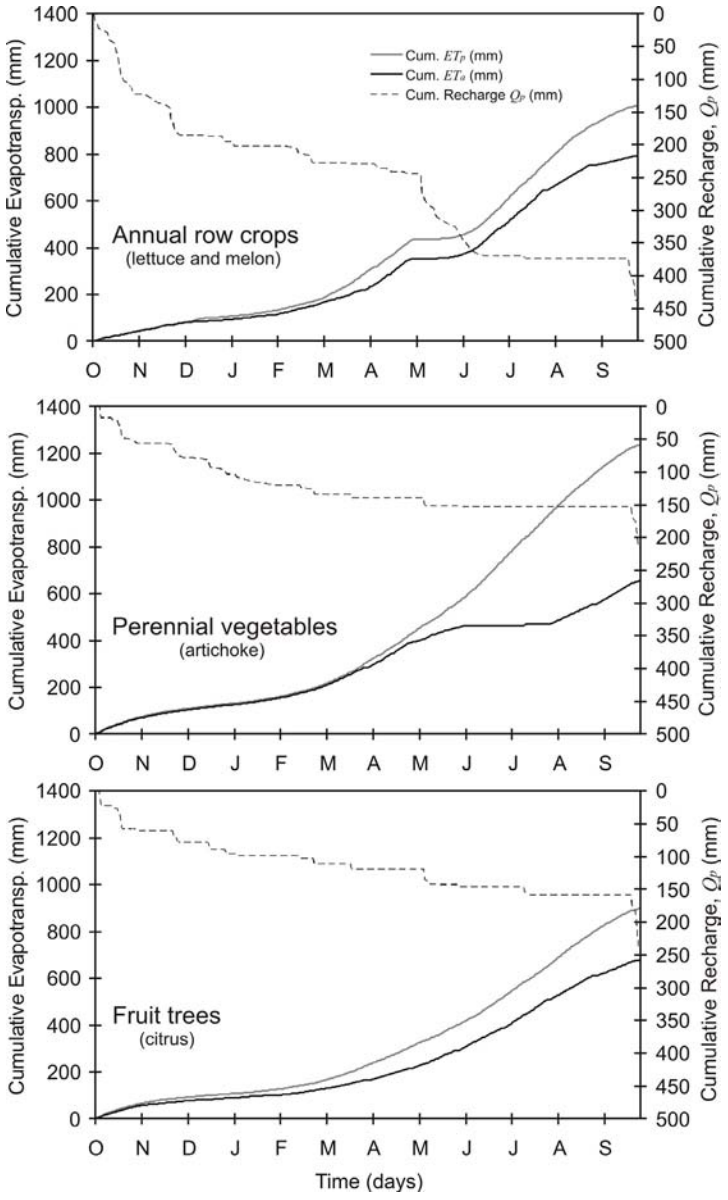

Figure 6.7: Cumulative *potential* evapotranspiration ET_p (grey line), *actual* evapotranspiration ET_a (black line) and aquifer recharge Q_p (dashed line) for the different crops, Oct 2007-Sept 2008 hydrological year.

Table 6.5: Simulated recharge according to applied water (*P*+*I*) for each crop type, 2007-2008 hydrological year. Irrigation efficiency calculated from *potential* and *actual* evaportranspiration (volume of irrigation water beneficially used).

Crop	*I* (mm)	*P* (mm)	*I*+*P* (mm)	Recharge		Irrigation Efficiency (%)†	
				(mm)	(%)	*Potential ET*	*Actual ET*
Annual row crops							
Lettuce (Sept-Dec)	206	189	395	209	52.9	91	66
Lettuce (Jan-Apr)	269	45	314	49	15.6	100	97
Melon (May-Aug) (with plastic cover)	471	81	552	194	35.1	73	63
Perennial vegetables (artichoke)	662	382	1044	212	20.3	100	99
Fruit trees (citrus)	641	382	1023	237	23.2	100	100

†Irrigation Efficiency from *Burt et al.* (1997).

6.4.3 Sensitivity analyses

Figure 6.8 shows the effect on the estimated recharge values of some parameters (set 1) and initial conditions (set 2). A series of simulations were performed in which individual parameters and initial condition values were perturbed into a range (shown in brackets, see Figure 6.8), while all other parameters and initial conditions were held at their baseline values (that is, the values used in our recharge calculations). The effect of perturbations on the estimated recharge (base run) was then evaluated.

The set 1 of sensitivity analysis involved evaluating a total of eleven parameters. The perturbation ranges of these parameters were sufficiently large and consistent with the scientific literature. Results of these calculations showed that recharge was most sensitive to six parameters in particular: field capacity θ_{fc}, wilting point θ_{wp}, θ_{ceme} (hydric deficit limit value, between θ_{fc} and θ_{wp}), curve number, and hypodermic flux depletion coefficient α_h (see Figure 6.8). For θ_{fc}, θ_{wp}, θ_{ceme} and α_h the three crop types (annual row crops; perennial vegetables; fruit trees) present the same trend of recharge change with respect to the perturbations. However, with respect to the curve number, such perturbations are only affecting changes in recharge for annual row crops and perennial vegetables. The set 2 of sensitivity analysis involved the evaluation of initial conditions: initial water content in soil $\theta(t_i)$ and initial water volume in vadose zone V_h. Recharge was only sensitive to $\theta(t_i)$, with a similar trend for all three crops.

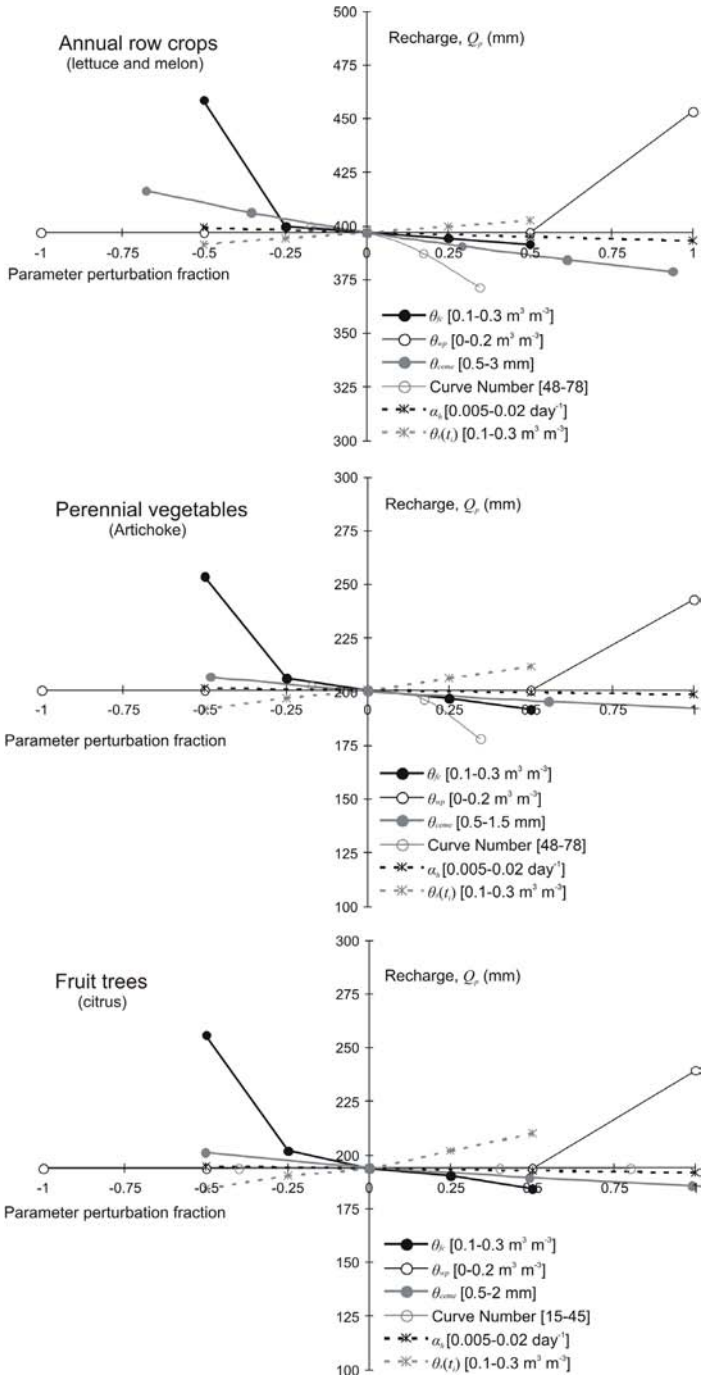

Figure 6.8: Effect of parameters and initial conditions (horizontal axes, expressed as a fraction of change) on the computed recharge (vertical axes). Horizontal axes cross at estimated recharge values (base run). Parameters considered for sensitivity analysis were: P_o; α_h; K_{vv}; α_p; θ_{ceme}; b_s; Φ_s; θ_{wp}; θ_{fc}; Curve Number; K_{vs}; $\theta(t_i)$; V_h. Only key parameters and initial conditions are plotted. Perturbation ranges are shown in brackets.

With regard to the sensitivity analysis for selected boundary conditions, effects due to temperature, number of daylight hours, wind velocity, air relative moisture or albedo appear to be included in ET_0. K_c causes a similar effect to ET_p according to Eq. [6.17], and it is not included in this analysis. The greatest change in the recharge is not always due to perturbations in the irrigation *Ir*, but also to variations in the precipitation *P* in the case of fruit trees (citrus) (Table 6.6).

Table 6.6: Summary of the relative sensitivity analysis performed for the selected boundary conditions.

Boundary Condition		Recharge					
		Annual row crops (lettuce and melon)		Perennial vegetables (artichoke)		Fruit trees (citrus)	
Name	*CP* (%)	*AS* (%)	*AS/CP*	*AS* (%)	*AS/CP*	*AS* (%)	*AS/CP*
Precipitation, *P*	+10	5.36	0.53	7.39	0.74	11.65	1.16
	-10	6	0.60	8.18	0.82	11.51	1.15
Reference evapotranspiration, ET_0	+10	9.04	0.90	10.03	1.00	5.57	0.56
	-10	10.79	1.08	14.36	1.44	9.22	0.92
Irrigation, *Ir*	+10	15.08	1.50	16.42	1.64	8.47	0.41
	-10	13.45	1.34	12.54	1.25	5.47	0.57
Height of the crop, *Z*	+30	4.01	0.13	15.37	0.51	-	-
	-30	4.03	0.13	16.17	0.54	-	-

CP: relative change (%) of a given variable or parameter; *AS*: relative change (%) in the output value; *AS/CP*: relative sensitivity

6.5 Conclusions

The daily water balance from water table fluctuations (WTF) used in this chapter is presented as a suitable method for estimating long-term groundwater recharge from farmland. This approach is valid under the next premises: (i) the rise in groundwater level is due to recharge water arriving to water table; (ii) the time lag span between the water application and the water arriving to the aquifer has to be short (hours or a few days); (iii) the water transport rate away from the water table has to be significantly slower than rate at which recharge water arrives at the water table. The presented analysis leads to the following main conclusions:

1. Water table fluctuations and recharge values for different crop types and irrigation regimes were successfully simulated with the presented approach. Good agreement was obtained for annual row crops and fruit trees, whereas not for perennial vegetables, which maybe related to a nearby pumping area. The best parameterization was found for eight of a total of fourteen parameters. The optimum number of years for model calibration for the study area and available data ranges between two and three years. Field observations suggest that hypodermic flow is negligible, confirmed by the fitted hypodermic flow depletion coefficient (α_h) and the estimated values for this water balance component. Higher values of vertical flow depletion coefficient (α_p) than groundwater discharge depletion coefficient (α_s) validate the premise (ii). The similar fitted parameters values obtained for the three experimental plots confirm the homogeneity of soil type for the study area (*Ramírez et al.*, 1999).

2. The mean recharge and standard deviation for the studied period (Oct 1999-Sept 2008) was 397 ± 70, 201 ± 64 and 194 ± 75 mm for annual row crops, perennial vegetables and fruit trees, respectively. Regarding annual row crops (lettuce and melon) the recharge for the hydrological year 2007-2008 was 452 mm for a water input $P+I$ = 1261 mm. Due to the high irrigation dose and frequency of application, a high recharge rate can be recognized when intensive precipitation events occur (mainly between September and December), as a consequence of constant high water content in the soil and the potentially preferential flow contribution.

3. The *actual* evapotranspiration rate was frequently lower than the *potential* rate, as soil moisture at various times failed to sustain the *potential* transpiration. This is particularly important for perennial vegetables, due to the lack of irrigation during June and July. The plastic cover on summer crops had a major impact on the annual row crops recharge.

4. The uncertainties associated with the high number of parameters that are employed, along with the particularities of the semi-arid climate and agricultural practices are associated difficulties with this type of method and environment. The highest sensitivity was found for the field capacity θ_{fc}, wilting point θ_{wp}, θ_{ceme}, curve number, and hypodermic flux depletion coefficient α_h parameter. With regard to the initial conditions, recharge was only sensitive to initial water content in soil $\theta(t_i)$. An intrinsic property of the presented approach (cascade model) is that parameters and initial conditions potentially concerning recharge (objective function) are included in soil and vadose zone. For boundary conditions, recharge was not always sensitive to the irrigation, also it was to the precipitation in the case of fruit trees (citrus).

5. Water balance approach based on water table fluctuations appears to be a promising method to estimate recharge from different crop types in intensively irrigated areas. It requires relatively low data density, generally available (meteorological and water level data), which can be estimated with reasonable accuracy, or obtained from literature with relative ease.

Notation

α	dimensionless constant (-)
α_h	hypodermic flow depletion coefficient (day^{-1})
α_p	vertical flow depletion coefficient (day^{-1})
α_s	groundwater discharge depletion coefficient (day^{-1})
β	extinction radiation coefficient (-)
b_s	soil thickness (m)
E_p	potential evaporation (mm)
E_s	amount of runoff (mm)
ET_a	actual evepotranspiration (mm)
ET_p	potential evepotranspiration (mm)
ET_0	reference evapotranspiration (mm)
f	ground cover sigmoid function (-)
Φ_e	drainable porosity (vadose zone) (m^3 m^{-3})
Φ_s	soil total porosity (m^3 m^{-3})
γ	empiric coefficient (depend of the vegetation type) (-)
h	groundwater level (m)
h_d	discharge single-cell aquifer water level (m)
h_i	initial single-cell aquifer water level (m)
h_0	reference base level in the aquifer (m)
i	mean slope in the hypodermic flow direction (m m^{-1})
I	Infiltration (mm)
In	interception (mm)
Ir	irrigation (mm)
K_c	crop-specific coefficient (-)
K_{hv}	horizontal permeability of vadose zone (mm day^{-1})
K_{vs}	vertical permeability of soil (mm day^{-1})
K_{vv}	vertical permeability of vadose zone (mm day^{-1})
L	length in the hypodermic flow direction (m)
LAI	leaf area index (m^2 m^{-2})
λ	characteristic length (m)
p	distance between waterfront and regional groundwater level (m)
P	precipitation (mm)
P_d	precipitation on the vegetation (mm)
P_e	potential recharge (mm)
P_o	precipitation limit (mm)
Q_h	hypodermic flow in vadose zone (mm day^{-1})
Q_p	vertical flow in vadose zone, recharge (mm day^{-1})
Q_s	groundwater discharge (mm day^{-1})

S	storage coefficient (-)
S_d	empiric coefficient (depend of the vegetation type)
S_y	specific yield (aquifer) (-)
t	time (day)
T	transmissivity (m^2 day^{-1})
T_p	potential transpiration (mm)
θ	volumetric soil water content (m^3 m^{-3})
θ_{ceme}	hydric deficit limit value (mm)
θ_{fc}	field capacity (m^3 m^{-3})
θ_{hd}	hydric deficit (mm)
θ_{wp}	wilting point (m^3 m^{-3})
V_a	water volume in aquifer (mm)
V_h	water volume in vadose zone (mm)
V_s	water volume in soil (mm)
W	input water (mm)
y_h	waterfront thickness (m)
Z	height crop (m)

References

Allen, R.G., Pereira, L.S., Raes, D., Smith, M., 1998. *Crop evapotranspiration. Guidelines for computing crop water requirements.* Irrigation and Drainage. Paper No. 56, FAO, Rome, Italy.

Burt, C.M., Clemmens, A.J., Strelkoff, T.S., Solomon, K.H., Hardy, L., Howell, T., Eisenhauer, D., Bleisner, R., 1997. Irrigation performance measures – Efficiency and uniformity. *J. Irrigation and Drainage Engineering* 123(6), 423-442.

Candela, L., von Igel, W., Elorza, F.J., Aronica, G., 2009. Impact assessment of combined climate and management scenarios on groundwater resources and associated wetland (Majorca, Spain). *J. Hydrol.* 376, 510-527.

CARM, 2007. *El Agua y la Agricultura en la Región de Murcia. Un Modelo de Eficiencia.* Consejería de Agricultura y Agua de la Región de Murcia. 111 pp.

Carrica, J. C. and Lexow, C., 2004. Evaluación de la recarga natural al acuífero de la cuenca superior del arroyo Napostá Grande, Provincia de Buenos Aires. *Revista de la Asociación Geológica Argentina* 39 (2), 281-290.

Castañeda, C. and García-Vera, M.A., 2008. Water balance in the playa-lakes of an arid environment, Monegros, NE Spain. *Hydrogeol. J.* 16, 87-102.

Castel, J.R., 2001. Consumo de agua para plantaciones de cítricos en Valencia. *Fruticultura profesional* 123, 27-32.

Castel, J.R., Bautista, I., Ramos, C., Cruz, G., 1987. Evapotranspiration and irrigation efficiency of mature orange orchards in Valencia (Spain). *Irrig. Drain. Syst.* 3, 205-217.

CSIRO, 2008. *TOPOG software*. CSIRO Land and Water and the Cooperative Research Centre for Catchment Hydrology. Available from: <http://www.per.clw.csiro.au/topog>.

Gracía-Santos, G., Mazol, V., Morales, D., Gómez, L. A., Pisani, B, Samper, J., 2005. Groundwater recharge in a mountain cloud laurel forest at Garajonay National Park (Spain). Geophysical Research Abstract 7, 00942.

Hanson, B.R., Schwankl, L.J., Schulbach, K.F., Pettygrove, G. S., 1997. A comparison of furrow, surface drip irrigation on lettuce yield and applied water. *Agric. Water Manage.* 33, 139-157.

Healy, R.W. and Cook, P.G., 2002. Using groundwater levels to estimate recharge. *Hydrogeol. J.* 10, 91–109.

Horton, R.E., 1919. Rainfall interception. *Mon. Weather Rev*. 47, 603–623.

ILRI, 2005. *SahysMod Version 1.7. Spatial Agro-Hydro-Salinity Model. Description of Principles, User Manual, and Case Studies*. International Institute for Land Reclamation and Improvement, Wageningen, Netherlands.

Jiménez, J., García, G., Queralt, I., Aragón, R., García-Arostegui, J. L., Solano, F., Candela, L., 2007. Vadose zone characterization in an experimental plot under intensive agriculture. Preliminary results. In: Candela et al. (Eds.), International conference WAter POllution in natural POrous media at different scales (WAPO2). IGME Book series: Hidrogeología y Aguas Subterráneas 22, 143-148.

Jiménez-Martínez, J., Skaggs, T.H., van Genuchten, M.Th., Candela, L., 2009. A root zone modelling approach to estimating groundwater recharge from irrigated areas. *J. Hydrol.* 367 (1-2), 138-149.

Kroes, J.G. and Van Damm, J.C., 2003. *Reference manual SWAP: Version 3.0.3*. Rep. 773. Alterra Green World Res., Wageningen, the Netherlands.

Lidón, A., Ramos, C., Rodrigo, A., 1999. Comparison of drainage estimation methods in irrigated citrus orchards. *Irrig. Sci.* 19, 25-36.

López Rodríguez, J.J. and Giráldez Cervera, J.V., 1997. Evaluación de la modificación de la recarga por cambios en la cobertura vegetal. In: Custodio, E., Llamas, R., Samper, J. (Eds.), La evaluación de la recarga a los acuíferos en la Planificación Hidrológica. AIH-GE, 209-227.

Pachepsky, Y.A., Smettem, K.R.J., Vanderborght, J., Herbst, M., Vereecken, H., Wosten, J.H.M., 2004. Reality and fiction of models and data in soil hydrology. In: Feddes R.A. et al. (Eds.), Unsaturated-zone modeling. Kluwer Academic Publishers, Dordrecht, the Netherlands.

Poulavassilis, A., Anadanistakis, M., Liakatas, A., Alexandris, S., Kerkides, P., 2001. Semi-empirical approach for estimating actual evapotrasnpiration in Greece. *Agric. Water Manage.* 51, 143-152.

Press, W.H., Flannery, B.P., Teukolsky, S. A., Vetterling, W.T., 1989. *Numerical recipes in pascal. The Art of Scientific Computing.* Cambridge University Press. 709 pp.

Ramírez, I., Vicente, M., García, J., Vaquero, A., 1999. *Mapa digital de suelos de la Región de Murcia.* Consejería de Agricultura, Agua y Medio Ambiente. Handbook and CD-ROM. 78 pp.

Samper, J., García-Vera, M. A., Pisani, B., Varela, A., Losada, J. A., Alvares, D., Espinha Marques, J., 2007. Using hydrological models and Geographic Information Systems for water resources evaluation: GIS-VISUAL-BALAN and its application to Atlantic basins in Spain (Valiñas) and Portugal (Serra da Estrela). In: Lobo Ferreira J. P., Vieira J. M. P. (Eds.), Water in Celtic Countries: Quantity, Quality and Climate Variability. IAHS 310, 259-266.

Samper, J., Huguet, Ll., Ares, J., García-Vera, M.A., 2005. User's guide (in Spanish) *VisualBALAN v.2.0: Código interactivo para la realización de balances hidrológicos y la estimación de la recarga.* 150 pp.

Sena, C. and Molinero, J., 2009. Water resources assessment and hydrogeological modelling as tool for the feasibility study of a closure plan for a open pit mine (La Respina Mine, Spain). *Mine. Water. Environ.* 28, 94-101.

Soil Conservation Service, 1975. *Engineering field manual conservation practices.* U. S. Department of Agriculture.

USGS, 2008. *Documentation of computer program INFIL3.0—A distributed-parameter watershed model to estimate net infiltration below the root zone*: U.S. Geological Survey Scientific Investigations Report 2008–5006, 98 pp.

Chapter 7

Conclusions and future research

7.1 General conclusions

In (semi-)arid regions surface water resources are generally scarce and highly unreliable, being groundwater the primary source of water. Therefore, accurate estimation of aquifer recharge appears to be essential for sustainable water resource management, even more if intensive agriculture is practiced. Aquifer recharge estimation from intensively irrigated farmland is not easy task since there are many interrelated factors included in atmosphere (rainfall amount, evaporation rate), crop (root depth, transpiration rate, interception), soil and vadose zone (infiltration capacity), aquifer (water table position), but overall agriculture management (water requirements, crop rotation, irrigation method, etc).

This chapter offers a summary of the main findings of this research. Main contributions of this thesis are:

1. An improvement of the understanding of the processes controlling aquifer recharge from intensively irrigated agriculture, usually carried out in semi-arid climate, by using different approaches: a) unsaturated water flow assessment; b) multiphase transport through a tritium tracer test; and c) water balance in soil, vadose zone and aquifer.

2. Consistent aquifer recharge values derived from the most common crops cultivated in the Mediterranean context have been provided. A deeper knowledge of aquifer recharge under mentioned conditions should prove helpful in upgrading water resources management and assessing aquifer vulnerability to contaminants.

With regard to the first contribution of the thesis, development of methodologies and field observations in both saturated and unsaturated media, along with the numerical modelling reveal the processes that govern recharge from different crop types (vegetables and fruit trees) and agricultural management. The specific contributions of each developed methodology can be summarized as follows:

a) Unsaturated flow approach for the root zone (Chapter 4) shows a suitable behaviour of the Richards' equation and van Genuchten-Mualem constitutive relationships, with an important influence of K_s on the root water uptake reduction. In spite of the lower frequency of θ measurements from TDR compared to h measurements from tensiometers, water content data are highly representative. The use of pedotransfer functions to specify the hydraulic parameters allowed to reduce the laboratory tests and provided reliable results, although refinements of some parameters based on model fitting to a subset of data are necessary.

b) Multiphase transport approach of tritium tracer test (Chapter 5) provides a suitable method to estimate recharge by irrigation return flow from a relatively low field sampling density. However, preferential tritium transport can be recognised due to soil tillage in the top soil. Richards' equation and Campbell constitutive relationships (only one water retention and hydraulic conductivity curves for the total soil profile) permitted to successfully reproduce tritium transport in soil, in spite of that (i) Campbell's power law does not fully reproduce water content values close to saturation, and (ii) tritium concentration varies sharply and is very sensitive to many interrelated factors (soil-plant-atmosphere). Advection and dispersion processes controlled transport of tritium in liquid phase, whereas in vapour phase only molecular diffusion process was considered. Effective molecular diffusion (*pore diffusion*) in liquid phase was approximately half of the obtained in clay soils. The main sinks of tritium were evaporation and transpiration. The tritium mass decay in soil took place in an exponential way, a loss of 95% occurred after 83 days, after 429 days tritium background concentration in soil was practically attained.

c) The long-term experiment water balance in soil, vadose zone and aquifer (Chapter 6), based on water table fluctuations (WFT), permitted to asses obtained recharge from the two other short-term methodologies (unsaturated flow and multiphase tritium transport) for annual row crops. Water balance approach permitted to reproduce successfully water table fluctuations, based on a linear function for solving drainage from soil to vadose zone, due to time step employed, days. For an improvement of obtained results and smaller time steps application, continuous unsaturated hydraulic conductivity function in soil and vadose zone should be necessary. The main advantage of this technique is relatively low data density requirements, generally available (e.g. water level data). On the other hand, it requires specific hydrodynamic conditions of the unconfined aquifer such as short time lag span between the water application and the water arriving to the aquifer, also groundwater level increase should be only due to water arriving. Considering recharge as the objective function, it only was sensitive to parameters included in soil and vadose zone, which is an intrinsic property of the presented water balance approach, a cascade model.

Common conclusions obtained from the three procedures are: (i) similar recharge values are obtained, although for unsaturated flow approach it is slightly overestimated; (ii) *actual* evapotranspiration was always lower than *potential* evapotranspiration, because soil moisture was insufficient to sustain the potential plant uptake, despite high irrigation frequency; (iii) although the agricultural practices from farmers are sound (high irrigation efficiency), high recharge values are achieved. Rainfall is unevenly distributed into a few intensive events highly variable in space and time, likewise very common in semi-arid regions, because soil water content is consistently high thus it meaningfully contributes to deep percolation; (iv) many of the involved parameters for model simulations can be estimated with reasonable accuracy or obtained from literature with relative ease.

As for the second contribution of the thesis, recharge values for the most common intensively irrigated crops in a Mediterranean context are provided. Results indicate that irrigation return flow accounts for a substantial portion of the total aquifer recharge, in spite of the current irrigation efficiency, as occur on the Campo de Cartagena. Improved irrigation scheduling based on soil moisture status and weather conditions could significantly reduce irrigation return flow. However, this is not an easy task, due to rainfall regime.

Many other crops (Table 4.3) have similar cultivation period and water requirement as the crops of the experiment, and they are grown for the same climate and soil conditions across the

Campo de Cartagena region. Therefore, in a first approximation, it may be assumed that irrigation return flow results are representative for other crops. Row crops in the region cover about 128.1 km^2. Approximately 19.3% of the crops are cultivated between January and April, 25.3% between May and August, while 55.4% are between September and December. Using the obtained recharge values for each of these periods, the recharge to the top unconfined aquifer from irrigation of annual row crops during hydrological year 2007-2008 was 22.4 hm^3. From irrigated perennial crops (34.1 km^2) and citrus (136.8 km^2) the recharge for the same period was 7.2 and 32.4 hm^3, respectively.

Obtained recharge, 62 $hm^3\ yr^{-1}$, is almost three times greater than value estimated by the Spanish Geological Survey (*IGME*, 1994), 23 $hm^3\ yr^{-1}$. The different estimation methods applied by *IGME* (1994), depending on available data, were based in the assumption that crop water use was at the potential rate. As indicated above, this fact tends to overestimate water use and hence, underestimates recharge.

Reliable recharge estimates are critical for management of water resources. Long-term average recharge rates are beneficial to groundwater management because management plans are generally developed at decadal timescales. Understanding factors controlling groundwater recharge shown in this thesis can be used to assess potential impacts by agrochemicals, climate variability and land use/land cover on aquifer.

7.2 Future research

Further work on this subject may be developed along the following lines of research:

- Specifically for the approaches presented in this thesis, parameter calibration for multiphase tritium transport model (Chapter 5) was carried out manually. However, this process is very time consuming. In order to carry out an automatic calibration, algorithms for parameter optimization need to be implemented.

- Numerical model restrictions condense or simplify the details contained in groundwater recharge process. To achieve greater reliability of model predictions, parameter

uncertainty and correlation structure at multiple levels should be quantified to establish confidence intervals.

- Recharge estimates of this thesis assumes equilibrium basis (uniform flow); however a non-equilibrium analysis (preferential flow) should be necessary in order to distinguish between preferential and non-preferential flow and transport and its quantification.

Future simulations should consider a distributed modelling approach and the intensity of precipitation for accurate recharge simulation in irrigated regions. The most fundamental conceptual aspect should be addressed to simulate vegetation dynamics (ground cover and root growth).